


2001

Photophysics and light induced photobiology of antiviral and antitumor agents, hypericin and hypocrellin

Jaehun Park
Iowa State University

Follow this and additional works at: <https://lib.dr.iastate.edu/rtd>

 Part of the [Biochemistry Commons](#), [Biophysics Commons](#), and the [Physical Chemistry Commons](#)

Recommended Citation

Park, Jaehun, "Photophysics and light induced photobiology of antiviral and antitumor agents, hypericin and hypocrellin " (2001). *Retrospective Theses and Dissertations*. 444.
<https://lib.dr.iastate.edu/rtd/444>

This Dissertation is brought to you for free and open access by the Iowa State University Capstones, Theses and Dissertations at Iowa State University Digital Repository. It has been accepted for inclusion in Retrospective Theses and Dissertations by an authorized administrator of Iowa State University Digital Repository. For more information, please contact digirep@iastate.edu.

INFORMATION TO USERS

This manuscript has been reproduced from the microfilm master. UMI films the text directly from the original or copy submitted. Thus, some thesis and dissertation copies are in typewriter face, while others may be from any type of computer printer.

The quality of this reproduction is dependent upon the quality of the copy submitted. Broken or indistinct print, colored or poor quality illustrations and photographs, print bleedthrough, substandard margins, and improper alignment can adversely affect reproduction.

In the unlikely event that the author did not send UMI a complete manuscript and there are missing pages, these will be noted. Also, if unauthorized copyright material had to be removed, a note will indicate the deletion.

Oversize materials (e.g., maps, drawings, charts) are reproduced by sectioning the original, beginning at the upper left-hand corner and continuing from left to right in equal sections with small overlaps.

Photographs included in the original manuscript have been reproduced xerographically in this copy. Higher quality 6" x 9" black and white photographic prints are available for any photographs or illustrations appearing in this copy for an additional charge. Contact UMI directly to order.

Bell & Howell Information and Learning
300 North Zeeb Road, Ann Arbor, MI 48106-1346 USA
800-521-0600

UMI[®]

**Photophysics and light induced photobiology of
antiviral and antitumor agents, hypericin and hypocrellin**

by

Jaehun Park

**A dissertation submitted to the graduate faculty
in partial fulfillment of the requirements for the degree of**

DOCTOR OF PHILOSOPHY

Major: Physical Chemistry

Major Professor: Jacob W. Petrich

Iowa State University

Ames, Iowa

2001

UMI Number: 3003259

UMI[®]

UMI Microform 3003259

Copyright 2001 by Bell & Howell Information and Learning Company.

All rights reserved. This microform edition is protected against
unauthorized copying under Title 17, United States Code.

Bell & Howell Information and Learning Company
300 North Zeeb Road
P.O. Box 1346
Ann Arbor, MI 48106-1346

**Graduate College
Iowa State University**

This is to certify that the Doctoral dissertation of

Jaehun Park

has met the dissertation requirements of Iowa State University

Signature was redacted for privacy.

Major Professor

Signature was redacted for privacy.

For the Major Program

Signature was redacted for privacy.

For the Graduate College

To my parents for their love, support and care.

TABLE OF CONTENTS

ABSTRACT	vi
CHAPTER 1. GENERAL INTRODUCTION	1
1.1 OVERVIEW	1
1.2 HYPERICIN AND HYPOCRELLIN.....	1
1.3 PHOTODYNAMIC THERAPY	4
1.4 ANTIVIRAL ACTIVITY OF HYPERICIN AND ITS ANALOGS	9
1.5 DISSERTATION ORGANIZATION	10
REFERENCES	10
CHAPTER 2. EXPERIMENTAL APPARATUS	20
2.1 INTRODUCTION	20
2.2 REGENERATIVE CHIRPED PULSE AMPLIFIER SYSTEM.....	22
2.2.1 OVERVIEW	22
2.2.2 MILLENIA V.....	23
2.2.3 TI:SAPPHIRE OSCILLATOR.....	23
2.2.4 CHIRPED PULSE AMPLIFICATION	28
2.3 OPTICAL PARAMETRIC AMPLIFIERS.....	34
2.3.1 BACKGROUND	34
2.3.2 NONCOLINEAR PARAMETRIC AMPLIFICATION.....	44
2.3.3 DESIGN AND OPERATION	45
2.4 PUMP-PROBE EXPERIMENT	48
2.5 THE FLUORESCENCE UPCONVERSION SPECTROMETER	50
REFERENCES.....	52
CHAPTER 3. CONFIRMATION OF EXCITED-STATE PROTON TRANSFER AND GROUND-STATE HETEROGENEITY IN HYPERICIN BY FLUORESCENCE UPCONVERSION	57
ABSTRACT.....	57
INTRODUCTION.....	58

EXPERIMENTAL.....	61
RESULTS AND DISCUSSION	64
CONCLUSIONS.....	71
ACKNOWLEDGEMENTS	73
REFERENCES.....	73
CHAPTER 4. IS THE EXCITED-STATE H-ATOM TRANSFER IN HYPERICIN CONCERTED?	78
ABSTRACT	78
INTRODUCTION.....	78
MATERIALS AND METHODS.....	81
RESULTS AND DISCUSSION.....	83
CONCLUSIONS.....	87
ACKNOWLEDGEMENTS.....	89
REFERENCES	89
CHAPTER 5. IDENTIFICATION OF A VIBRATIONAL FREQUENCY CORRESPONDING TO H-ATOM TRANSLOCATION IN HYPERICIN	95
ABSTRACT	95
INTRODUCTION.....	95
MATERIALS AND METHODS.....	99
RESULTS AND DISCUSSION.....	101
CONCLUSIONS.....	107
ACKNOWLEDGEMENTS.....	110
REFERENCES	110
CHAPTER 6. THE ROLE OF OXYGEN IN THE ANTIVIRAL ACTIVITY OF HYPERICIN AND HYPOCRELLIN	118
ABSTRACT	118
INTRODUCTION.....	118
MATERIALS AND METHODS.....	120
RESULTS AND DISCUSSION.....	123
CONCLUSIONS.....	127

ACKNOWLEDGEMENTS.....	128
REFERENCES	129
CHAPTER 7. TUMOR CELL TOXICITY OF HYPERICIN AND RELATED ANALOGS.....	136
ABSTRACT	136
INTRODUCTION.....	136
MATERIALS AND METHODS.....	138
RESULTS	143
DISCUSSION.....	148
CONCLUSIONS.....	150
ACKNOWLEDGEMENTS.....	150
REFERENCES	150
CHAPTER 8. CONCLUSIONS	155
GENERAL CONCLUSIONS.....	155
REFERENCES	157

ABSTRACT

The dissertation mainly focuses on the excited-state photophysics and the light-induced biological activity of hypericin and its analogs.

Femtosecond laser technology has provided the opportunity to investigate the rapid dynamics of these molecules. Fluorescence upconversion measurements, which monitor only emission from the fluorescent singlet state, demonstrate that hexamethoxy hypericin, which possesses no labile protons, has an instantaneous rise time for its transient response. On the other hand, hypericin shows a clear 10-ps rise time. This confirms excited-state H-atom transfer as the primary photophysical process in hypericin.

Femtosecond transient absorption spectroscopy technique is used to determine if excited state H-atom transfer is concerted. Previous studies using human serum albumin (HSA) and hypericin suggested that excited state H-atom transfer is concerted, but the results from the hypericin in reverse micelles show no evidence for a concerted hydrogen atom transfer mechanism. We are, however, unable to conclude if only one hydrogen atom is transferred or if two are transferred in a stepwise fashion.

By means of time-resolved infrared spectroscopy, *ab initio* quantum mechanical calculations, and synthetic organic chemistry, a region in the infrared spectrum, between 1400 and 1500 cm^{-1} , of triplet hypericin has been found corresponding to translocation of the hydrogen atom between the enol and the keto oxygens, $\text{O}\cdots\text{H}\cdots\text{O}$. This result is discussed in the context of the photophysics of hypericin and of eventual measurements to observe directly the excited-state H-atom transfer.

Light-induced antiviral activity of hypericin and hypocrellin is compared in

normoxic and hypoxic conditions. Although both molecules require oxygen to show full virucidal effects, hypericin is still effective at low oxygen level where hypocrellin is not. Since the singlet oxygen yield of hypericin is about half of that of hypocrellin, this result cannot be explained by a traditional Type II mechanism. We propose that the ejected proton upon illumination might enhance the activity of activated oxygen species.

A series of hypericin analogs were found to differ in their cytotoxic activity induced by ambient light levels. These analogs vary in their ability to partition into cells, to generate singlet oxygen as well as in other photophysical properties. The percent distribution of hypericin and its analogs in cells are measured using a steady state absorption technique. We attempt to find a relationship between those results and the exact localization of the drug at subcellular level.

CHAPTER 1. GENERAL INTRODUCTION

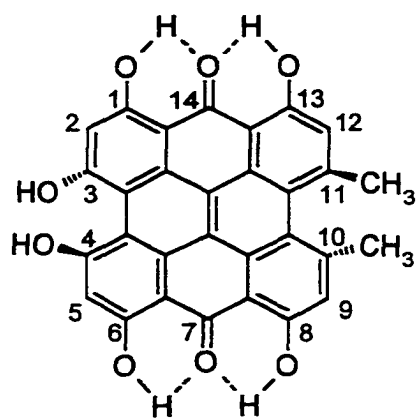
1.1 OVERVIEW

Due to the reliability and sophistication of laser based systems, especially ultrafast spectroscopic methods, we are able to study condensed-phase reaction dynamics. In recent years many applications of pulsed laser techniques have been developed in chemistry [1] and biology [2]. Current laser technology provides pulses as short as 4.5 fs at selected wavelengths [3] and widely tunable pulses with a duration less than 8 fs [4].

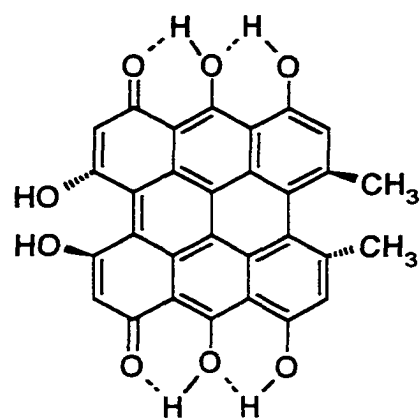
Using this technology we have investigated the primary photoprocesses of the light activated antiviral and antitumor agents, hypericin and hypocrellin (figure 1.1a and 1.1 c) In the following chapters, photophysical processes and photobiology of hypericin and hypocrellin are discussed.

1.2 HYPERICIN AND HYPOCRELLIN

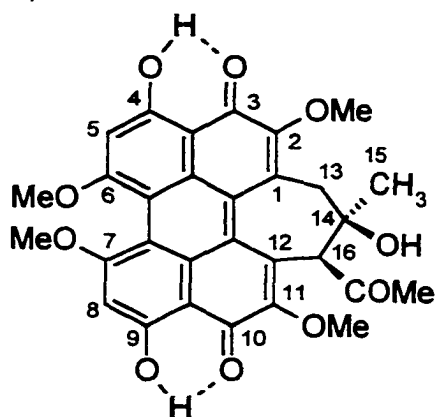
Hypericin, 1,3,4,6,8,13-hexahydroxy-10,11-dimethylphenanthro[1,10,9,8-*opgra*]perylene-7,14-dione (Figure 1a), derives its name from *hypericum*, a genus of plants which biosynthesize the pigment and its analog pseudohypericin. Hypericin forms up to 0.05 % of the plant substances in some species of genus [5]. St. John's Wort (*Hypericum perforatum* or other members of genus *Hypericum*) might be the richest hypericin source [6] and is widely distributed in Europe [7], North America, China [8] and the Middle East (Armenia, Jordan)[9, 10]. Hypericin extracts have been used as a folk medicine to treat headache, rheumatism, inflammation, wounds and diarrhea. The



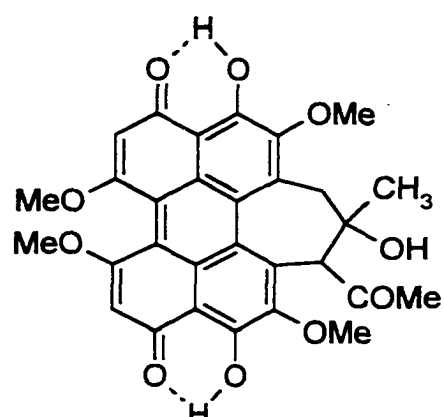
(a)



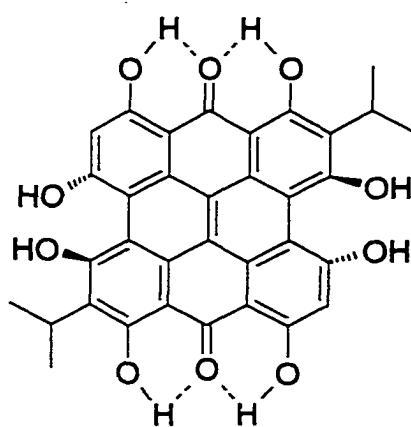
(b)



(c)



(d)



(e)

Figure 1.1 Structures of (a) normal form of hypericin, (b) possible hypericin double tautomer (c) normal form of hypocrellin (d) possible hypocrellin double tautomer (e) stentorin.

structure and spectra of hypericin is closely related or nearly identical to those of the stentorin (Figure 1.1e) and blepharismine chromophores [11, 12]. There is a growing interest in elucidating the roles of stentorin and blepharismine in the photosensory transduction of *Stentor coeruleus* [13, 14] and *blepharisma japonicum* [15, 16], the hypericin-like pigment-containing microorganisms. Song and coworkers have discovered light induced pH decrease across the cell membranes of *S. coeruleus* [11].

A systematic study of hypericin photophysics has been carried out by Jardon and coworkers since 1986 [17, 18, 19, 20]. They measured the triplet quantum yield of hypericin to be 0.71. Further studies have been carried out to reveal the kinetics of triplet hypericin [21, 22].

Hypocrellin derives its name from *Hypocrella bambuasa*, a parasitic fungus of *Sinarudinaria* sp. that grows only in southwestern region of Tibet in the People's Republic of China, and certain parts of Sri Lanka [23]. Like other similar perylene quinoids, this compound has traditionally been used as a folk medicine for many years in China, especially for skin lesions.

Both hypericin and hypocrellin are peri-hydroxylated polycyclic quinones, and have some common chemical and biological properties. Recently, they have gained great interest owing to their light induced biological activities [11, 24, 25, 26]. They have virucidal activity against several types of enveloped viruses including human immunodeficiency virus (HIV) [27, 28, 29, 30], and also antiproliferative and cytotoxic effects on tumor cells [31, 32, 33]. Hypericin also shows an antidepressant activity [34], light-dependent inhibition of protein kinase C [35, 36, 37], and induces apoptosis [32, 36,

38].

Owing to this biological activity, we have been studying the photophysics of hypericin and hypocrellin [39-58]. Based on deuterium isotope effects, the study of O-methylated analogues, and complementary studies using transient absorption and fluorescence upconversion techniques, we have argued that excited state hydrogen atom transfer is the primary photophysical mechanism in hypericin and hypocrellin in organic solvents.

Hypericin and hypocrellin A acidify their surroundings upon light absorption. The role of photogenerated protons takes on significance in the context of the growing body of literature implicating changes in pH with inhibition of virus replication [59], antitumor activity [60], and apoptosis (programmed cell death) [61, 62].

1.3 PHOTODYNAMIC THERAPY

Photodynamic therapy (PDT) is based on the dye-sensitized photooxidation of biological matter in the target tissue [63]. For PDT to be effective, a dye (sensitizer) needs to be present in the tissue. As the first step of PDT, the sensitizers are introduced into the organism, and are then illuminated. It is believed that some oxygenated species, which are harmful to cell function, are produced through various photophysical pathways, and finally the tissue is destroyed.

The delivery of the photosensitizer to the target tissue is the first step toward PDT tumor treatment. Bellnier *et al.* [64] did detailed preclinical studies of pharmacokinetics and tissue distribution for Photofrin II (PII) by radiolabeling sensitizers while maintaining

their photophysical, photochemical and biological characteristics. Most sensitizers studied to date do not accumulate selectively in neoplastic tissues. Some of the studies for the subcellular distribution of sensitizers have been done in *in vitro* systems. Roberts *et al* [65] found that PII initially binds to the plasma membrane, then redistributes to other lipophilic membrane sites, but another sensitizer mono-L-aspartyl chlorin e6 (Npe6) preferentially localizes in lysosomes while both are keeping PDT effects for tumor tissues. Based on the overview by Moan *et al.* [66], lipophilic, anionic dyes generally localize in membrane structures including plasma, nuclear membranes, mitochondria and endoplasmic reticulum, however hydrophilic materials accumulate in lysosomes. Certain cationic sensitizers can be found in mitochondria mainly due to electrical potential gradients across the mitochondrial membrane [67]. Research on subcellular distribution of hypericin also has been done by Sureau *et al.* [68], Vandenberghe *et al.* [37], Miskovsky *et al.* [69], and English *et al.* [70]. Also, *in vivo* studies have shown that although the tissue distribution pattern of hypocrellin is qualitatively similar to that of PII, hypocrellin shows much faster intracellular uptake kinetics [71, 72].

The second component for PDT tumor treatment is to deliver the light which can be absorbed by photosensitizer to the target tissue. Light fluence in tissue decreases exponentially with the distance. The effective penetration depth is inversely proportional to the effective attenuation coefficient ($\alpha = 1/\epsilon \cdot \text{depth}$). The latter is influenced by the optical absorption due to the tissue chromophore, and optical scattering within the tissue. The average α is about 1-3 mm at 630 nm [73], while penetration is approximately twice that at 700-850 nm [74].

PDT has the limitation of obtaining the proper levels of excitation light within the body. An interesting experiment using chemiluminescence has been done by Carpenter *et al.* [40]. They found the chemiluminescent oxidation of luciferin by the luciferase from the North American firefly generates the emission sufficiently intense and long lived enough to induce antiviral activity of hypericin. Light-induced virucidal activity of hypericin was shown against equine infectious anemia virus (EIAV). Some research on fluence rate effect in photodynamic therapy also have been carried out [75, 76, 77, 78].

The current study indicates that hypericin and hypocrellin have good properties for PDT application. They are as follows [79]:

- 1) The aminated hypocrellins which have high phototoxicity and minimal dark cytotoxicity have a strong absorption at the phototherapeutic window range (600-1000 nm).
- 2) The compounds show the selectivity for certain tumor cell-killing in the primary tests both *in vivo* and *in vitro* [12, 23, 72, 80, 81, 82, 83].
- 3) Hypocrellins have a much higher clearance rate from the host body than porphyrins, which reduces their delayed skin photosensitivity [23, 72, 81, 82] a side effect involved in the PDT of porphyrins.
- 4) Since hypericins and hypocrellins are different from porphyrin in structure, photophysics, photochemistry and biodistribution, a combination phototherapy might be possible, using the respective responses of hypericins/hypocrellins and porphyrins, to gain synergistic benefits of the different localization photophysics of the different photosensitizers.

- 5) Many animal and clinical experiments already have been done with both hypericin and hypocrellin [12, 84, 85, 86, 87].

Similar to ionizing radiation, the damage-inducing interactions of PDT occur within a very short time. Photodynamic interactions can take place wherever sensitizer, appropriate light and oxygen are present at the same time. A photosensitizer is first excited into the short-lived singlet state, then this excited singlet state photosensitizer converted into the long-lived (10^{-3} -10 s) triplet state via an intersystem crossing (ISC) process. Since photosensitization usually occurs only in the triplet state, a high triplet yield upon light absorption is required for efficient photosensitizers. Generally it is believed that the triplet photosensitizers can undergo two kinds of photochemical reactions, *i.e.* Type I and Type II (figure 1.2). In Type I, the triplet photosensitizer directly reacts either with substrate or solvent by hydrogen atom or electron transfer to form radicals or radical ions, which can produce reactive oxygenated species after interacting with oxygen. Type I is dependent on the concentrations of the sensitizer and the substrate, and is favored when the sensitizer is bound to or associated with the substrate. In Type II, the triplet photosensitizer can transfer its energy to the ground state of oxygen to produce singlet oxygen ($^1\text{O}_2$, lifetimes 4×10^{-6} s in water, $50\text{-}100 \times 10^{-6}$ s in lipid, 0.6×10^{-6} s in cellular environment), a highly reactive, oxidative species, which can mediate a variety of photosensitization processes. [64, 88] It is evident that Type II is an oxygen dependent process. Oxygen dependence was used to distinguish Type I and Type II reactions. Thomas *et al.* [80] observed that hypericin-photoinduced cell killing was mediated by an oxygen dependent Type II mechanism rather than the oxygen independent

Type I mechanism. However, Fehr *et al.* [41] observed that hypericin is equally toxic against equine infectious anemia virus (EIAV) under oxygenated and hypoxic conditions.

Type I and Type II reactions may occur simultaneously, and the ratio between the two processes is dependent upon the properties and concentrations of the sensitizer and substrate, and oxygen concentration, light intensity as well as the binding of the sensitizer to substrate. Several studies about this issue in the photosensitization of hypericin and hypocrellin also have been done by Diwu *et al.* [89, 90]. Chapter 4 will discuss the importance of oxygen in the antiviral activity based on these mechanisms and suggest another possible mechanism to explain our experimental results.

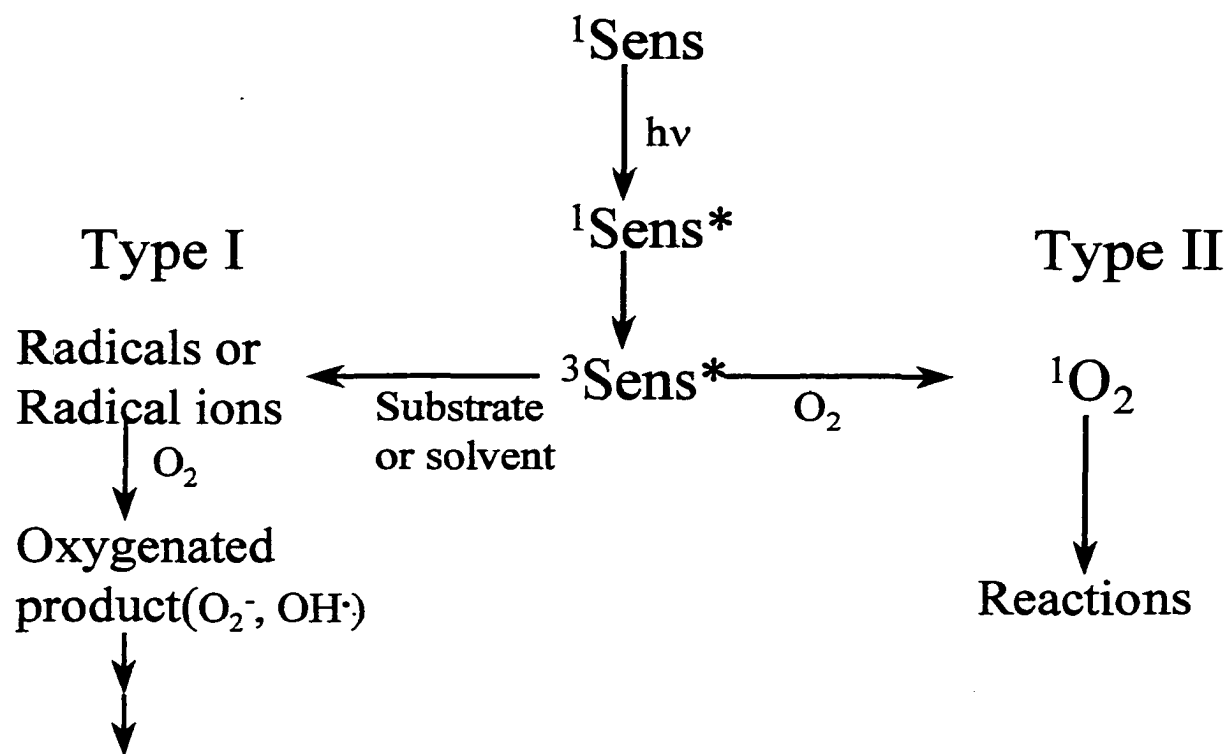


Figure 1.2. Mechanisms for photosensitized oxygenation.

1.4 ANTIVIRAL ACTIVITY OF HYPERICIN AND ITS ANALOGS

The antiviral activities of hypericin and its analogs have been studied since 1988 [27], and Carpenter *et al.* demonstrated that hypericin possesses light induced antiviral activity in 1991 [91]. There are two common features for the antiviral activities of the hypericin-like compounds. One feature is these compounds have good antiviral activity against enveloped viruses, but not against nonenveloped viruses [92]. The other feature is light enhances the virucidal activity of hypericin compounds against certain enveloped viruses [91, 93, 94, 95].

Several research results suggest that the virucidal activity of hypericin against enveloped viruses is different from the well-characterized antiviral nucleosides [28,96]. Hypericin is reported to inactivate viruses by altering viral proteins rather than nucleic acids [97]. It is suggested that a principal target for the light induced antiviral activity of hypericin-like compounds might be membranes [98, 99, 100, 101].

Light induced viral inactivation of hypericin against enveloped viruses is also attributed to the inhibition of fusion, which is a required membrane specific process for virus life cycle, by Lenard *et al.* and Stevenson *et al.* [28, 98]. Loss of the fusion function may explain why only enveloped viruses are inactivated by light activated hypericin. They suggest oxygen dependent Type II mechanism as a major process for the light induced antiviral activity of hypericin due to the resemblance of the virucidal activity between hypericin and rose bengal which is a good $^1\text{O}_2$ photosensitizer. However comparative studies for nine perylenequinones, including hypericin and hypocrellin, provide strong evidence that the singlet oxygen quantum yield is not sufficient to explain the reported

antiviral activities of these molecules and that other structural features of perylene quinones are involved [102]. This topic is also discussed in Chapter 6.

1.5 DISSERTATION ORGANIZATION

This dissertation includes five separate journal papers (Chapter 3-7) and is organized as follows.

1. Experimental apparatus including chirped pulse regenerative amplifier system, fluorescence upconversion system, and optical parametric amplifier (OPA) are described in Chapter 2.
2. Confirming the excited state H-atom transfer in hypericin is discussed in Chapter 3.
3. Concertedness of the excited state H-atom transfer is presented in Chapter 4.
4. Identification of a vibrational frequency corresponding to H-atom translocation in hypericin is discussed in Chapter 5.
5. The role of oxygen in hypericin's antiviral activity against equine infectious anemia virus (EIAV) is presented in Chapter 6
6. The relationship between the cytotoxic activity and the ability to cell partition and the singlet oxygen yields of a series of hypericin analogs is discussed in Chapter 7.
7. General summary is described in Chapter 8.

REFERENCES

1. Fleming, G. R., Chemical Applications of Ultrafast Spectroscopy (Oxford University Press, Oxford, 1986)

2. Kaiser, W., ed. *Ultrashort Laser Pulses and Applications* (Springer, Berlin, 1986)
3. Nisoli, M., S. De Silvestri, O. Svelto, R. Szipocs, K. Ferencz, Ch. Spielmann, S. Sartania and F. Krausz, *Opt. Lett.* **22**, 522 (1997)
4. Cerullo, G., M. Nisoli, S. Stagira and S. De Silvestri *Opt. Lett.* **23**, 1283 (1998)
5. Netien, G., D. Lebreton, *Ann. Pharm. Franc.* **22**, 69 (1964)
6. Giese, A. C., *Photochem. Photobiol. Rev.* **5**, 229 (1980), Vanhaelen, M. and R. Vanhaelen-Fastre, *J. Chromatogr.* **81**, 263 (1983)
7. Bueter, B.; C. Orlacchio, A. Soldati, K. Berger, *Planta Med.*, **64**, 431 (1998)
8. Bremness, L., *Herbs* (Dorling Kindersley: New York, 1994)
9. Al-Khalil, S. *Acta Technol. Legis Med.*, **8**, 97 (1997)
10. Melikian, E.; R. Boroyan, A. Karaguezian, A. Charchoghlian, E. Gabrielian, A. Panossian, *Pharm. Pharmacol. Lett.*, **8**, 101 (1998)
11. Duran, N. and P. S. Song, *Photochem. Photobiol.* **43**, 677 (1986)
12. Diwu, Z. and J. W. Lown, *Pharmacol. Ther.* **63**, 1 (1994)
13. Tao, N.; M. Orlando, J. S. Hyon, M. Gross, P. S. Song, *J. Am. Chem. Soc.* **115**, 2526.(1993)
14. Yang, K. C.; R. K. Prusti, E. B. Walker, P. S. Song, M. Watanabe, M. Furuya, *Photochem. Photobiol.* **43**, 305 (1986)
15. Song, P. S. *Kagaku to Kogyo (Tokyo)*, **48**, 1222 (1995)

16. Cubbedu, R.; F. Ghetti, F. Lenci, R. Ramponi, P. Taroni, *Photochem. Photobiol.* **52**, 567 (1990)
17. Jardon, P., N. Lazorchak and R. Gautron *J. Chim. Phys.* **83**, 311 (1986)
18. Jardon, P. and R. Gautron *J. Chim. Phys.* **86**, 2173 (1989)
19. Nafis, M. and P. Jardon *J. Chim. Phys.* **91**, 99 (1994)
20. Arabei, S. M.; J. P. Galaup, P. Jardon, *Chem. Phys. Lett.*, **270**, 31 (1997)
21. Michaeli, A., A. Regev, Y. Mazur, J. Feitelson and H. Levanon *J. Phys. Chem.* **97**, 9154 (1993)
22. Malkin, J. and Y. Mazur *J. Photochem. Photobiol. B Biol.* **20**, 133 (1993)
23. Diwu, Z. And J. W. Lown *Photochem. Photobiol.* **52**, 609 (1990)
24. Lown, J. W. *Can. J. Chem.* **75**, 99 (1997)
25. Kraus, G. A., W. Zhang, M. J. Fehr, J. W. Petrich, Y. Wannemuehler and S. Carpenter *Chem. Rev.* **96**, 523 (1996)
26. Falk, H. *Angew. Chem. Int. Ed.*, **38**, 3116 (1999)
27. Meruelo, D., G. Lavie and D. Lavie, *Proc. Natl. Acad. Sci. USA* **85**, 9729 (1988)
28. Lenard, J. A. Rabson, and R. Vanderoef *Proc. Natl. Acad. Sci. USA* **90**, 158 (1993)

29. Hudson, J. B., J. Zhou, J. chen, L. Harris, L. Yip, and G. H. N. Towers *Photochem. Photobiol.* **60**, 253 (1994)
30. Tobin, G. J.; W. H Ennis, D. J. Clanton and M. A Gonda *Antiviral Res*, **33**, 21 (1996)
31. Couldwell, W. T., R. Gopalakrishna, D. R. Hinton, S. He, M. H. Weiss, R. E. Law and M. L. Apuzzo *Neurosurgery* **35**, 705 (1994)
32. Anker, L., R. Gopalakrishna, K. D. Jones, R. E. Law and W. T. Couldwell *Drugs of the Future*, **20**, 511 (1995)
33. Zhang, W., R. E. Law, D. R. Hinton and W. T. Couldwell *Cancer Lett.* (Shannon, Irel.), **120**, 31 (1997)
34. Linde, K., G. Ramirez, C. D. Mulrow, A. Pauls, W. Weidenhammer and D. Melchart *Br. Med. J.* **313**, 253 (1996)
35. Kil, K.-S.; Y.-N. Yum, S.-H. Seo, and K.-T. Lee *Arch. Pharmacal Res.* **19**, 490 (1996)
36. Weller, M., M. Trepel, C. Grimmel, M. Schabet, D. Bremen, S. Krajewski and J. C. Reed *Neurol. Res.* **19**, 459 (1997)
37. Vandenbogaerde, A. L., E. M. Delaey, A. M Vantieghem, B. E. Himpens, W. J. Merlevede, P. A. De Witte *Photochem. Photobiol.* **67**, 119 (1998)
38. Mirossay, L. M., E. Kocisova, I. Radvakova, P. Miskovsky and J. Mojzis *Physiol. Res.* **48**, 135 (1999)

39. Gai, F., M. J. Fehr and J. W. Petrich *J. Am. Chem. Soc.* **115**, 3384 (1993)
40. Carpenter, S., M. J. Fehr, G. A. Kraus and J. W. Petrich *Proc. Natl. Acad. Sci. U. S. A.* **91**, 12273 (1994)
41. Fehr, M. J.; S. L. Carpenter, and J. W. Petrich *Bioorg. Med. Chem. Lett.*, **4**, 1339 (1994)
42. Fehr, M. J., F. Gai and J. W. Petrich. *Springer Ser. Chem. Phys.* **60**, 462 (1994)
43. Gai, F, M. J Fehr and J. W. Petrich *J. Phys. Chem.*, **98**, 8352 (1994)
44. Gai, F, M. J Fehr and J. W. Petrich *J. Phys. Chem.* **98**, 5784 (1994)
45. Fehr, M. J, S. L. Carpenter, Y. Wannemuehler and J. W. Petrich *Biochemistry*, **34**, 15845 (1995)
46. Fehr, M. J., M. A. McCloskey and J. W. Petrich. *J. Am. Chem. Soc.* **117**, 1833 (1995)
47. Petrich, J. W. *Excited-state proton transfer in hypericin and other polycyclic quinones.*; American Chemical Society: Chicago, IL, August 20-24, 1995, pp PHYS-085
48. Das, K.; D. S. English, M. J. Fehr, A. V. Smirnov and J. W. Petrich *J. Phys. Chem.*, **100**, 18275 (1996)
49. Das, K, D. S. English and J. W. Petrich *J. Phys. Chem. A* **101**, 3241 (1997)
50. Das, K, D. S. English and J. W. Petrich *J. Am. Chem. Soc.*, **119**, 2763 (1997)

51. English, D. S., K. Das and J. W. Petrich *Hypericin, hypocrellin and model compounds: Primary photoprocesses of light-induced antiviral agents.*; American Chemical Society, Washington, D. C., 1997, pp PHYS-405
52. English, D. S., K. Das., K. D. Ashby, J., J. W. Petrich and E. W. Castner, J. *J. Am. Chem. Soc.* **119**, 11585 (1997)
53. English, D. S.; K. Das, J. M. Zenner, W. Zhang, G. A. Kraus, R. C Larock and J. W. Petrich *J. Phys. Chem. A*, **101**, 3235 (1997)
54. English, D. S., W Zhang, G. A. Kraus and J. W. Petrich *J. Am. Chem. Soc.* **119**, 2980 (1997)
55. Das, K.; E. Dertz, E., J. Paterson, W. Zhang, G. A. Kraus and J. W. Petrich *J. Phys. Chem. B*, **102**, 1479 (1998)
56. Kraus, G. A., S. L. Carpenter and J. W. Petrich *Photoactivated antiviral and antitumor compositions using a photosensitizing chemical and an energy donating chemical, optionally linked by a chemical tether*: U.S., 1998
57. Park, J., D. S. English, Y. Wannemuehler, S. L. Carpenter, and J. W. Petrich *Photochem. Photobiol.*, **68**, 593 (1998)
58. Petrich, J. W., M. S. Gordon, M. Cagle *J. Phys. Chem. A*, **102**, 1647 (1998)
59. Pinto, L. H., L. J. Holsinger and R. A. Lamb *Cell*, **69**, 517 (1992)
60. Newell, K. J. and I. F. Tannock, *Cancer Res.* **49**, 4447 (1989)

61. Gottlieb, R. A. N., E. Skowronski and B. M. Babior *Proc. Natl. Acad. Sci. U. S. A.* **93**, 654 (1996)
62. Li, J. E., *J. Biol. Chem.* **270**, 3203 (1995)
63. Foot, C. S., "Chemical mechanisms of photodynamic action," *Proc. SPIE Institute Advanced Optical Technologies on Photodynamic Therapy*, IS **6**, 115 (1990)
64. Bellnier, D., K. Ho, R. K. Pandey, J. Missert and T. J. Dougherty, *Photochem. Photobiol.* **50**, 221 (1989)
65. Roberts, W. B., G.-Y. Shiau, J. S. Nelson, K. M. Smith and M. W. Berns, *J. Natl. Cancer Inst.* **80**, 330 (1988)
66. Moan, J., K. Berg, E. Kvam, A. Western, Z. Malik, A. Ruck and H. Schneckenburger, *Photosensitizing Compounds: Their Chemistry, Biology and Clinical Use*, (Wiley, Chichester, UK, 1989) pp. 95-107
67. Oseroff, A. R., D. Ohuoha, G. Ara, D. McAuliffe, J. Foley and L. Cincotta, *Proc. Natl. Acad. Sci. USA* **83**, 9729 (1986)
68. Sureau, F., P. Miskovsky, L. Chinsky, P. Y. Turpin, *J. Am. Chem. Soc.* **118**, 9484 (1996)
69. Miskovsky, P., F. Sureau, L. Chinsky, P. Y. Turpin, *Photochem. Photobiol.*, **62**, 546 (1995)
70. English, D. S., R. T. Doyle, J. W. Petrich, and P. G. Haydon, *Photochemistry and Photobiology*, **69**, 301 (1999)

71. Liu, J., G. G. Miller, L. Huang, Z. Diwu, J. W. Lown, K. Brown, R. B. Moore, J. Tulip, M. S. McPhee, *J. Labelled Compd. Radiopharm.* **36**, 815 (1995)
72. Miller, G. G., K. Brown, R. B. Moore, Z. Diwu, J. Liu, L. Huang, J. W. Lown, D. A. Begg, V. Chlumecky, J. Tulip and M. S. McPhee, *Photochem. Photobiol.* **61**, 632 (1995)
73. Henderson, B. W., and T. J. Dougherty, *Photochem. Photobiol.* **55**, 145 (1992)
74. Wilson, B. C., W. P. Jeeves and D. M. Lowe, *Photochem. Photobiol.* **42**, 153 (1985)
75. Blant, S. A., A. Woodtli, G. Wagnieres, C. Fontollet, H. Van den Bergh and P. Monnier, *Photochem. Photobiol.* **64**, 963 (1996)
76. Sitnik, T. M., B. W. Henderson, *Photochem. Photobiol.* **67**, 462 (1998)
77. Gibson, S. L., K. R. Van der Meid, R. S. Murant, R. F. Raubertas and R. Hilf, *Cancer Res.* **50**, 7236 (1990)
78. Foster, T. H., D. F. Hartley, M. G. Nichols and R. Hilf, *Cancer Res.* **53**, 1249 (1993)
79. Diwu, Z., *Photochem. Photobiol.* **61**, 529 (1995)
80. Thomas, C and R. Pardini, *Photochem. Photobiol.* **55**, 831 (1992)
81. Estey, E. P., K. Brown, Z. Diwu, J. Liu, J. W. Lown, G. G. Miller, R. B. Moore, J. Tulip, M. S. McPhee, *Cancer Chemother. Pharmacol.* **37**, 343 (1996)

82. Androni A., A. Colasanti, P. Colasanti, M. Mastrocinque, P. Riccio and G. Robert, *Photochem. Photobiol.* **59**, 529 (1994)
83. Wang, Z. J., Y. Y. He, J. S. Huang, Y. C. Huang, J. Y. An, Y. Gu and L. J. Jiang, *Photochem. Photobiol.* **70**, 773 (1999)
84. Hruza, L. L., N. Kollias, H. Lui, R. Gulick and T. J. Flotte, *Clin. Res.* **41**, 502 (1993)
85. Hruza, L. L., N. Kollias, H. Lui, R. Gulick and T. J. Flotte, *Invest. Dermatol.* **100**, 600 (1993)
86. Duffey, S. S. and J. M. Pasteels, *Physiol. Entomol.* **18**, 119 (1993)
87. Roots, I., R. Kerb, B. Staffeldt, M. Ploch, V. Schuz and J. Brockoller, *Clin. Pharmacol. & Ther.* **55**, 197 (1994)
88. Moan, J., *J. Photochem. Photobiol., B: Biol.* **6**, 343 (1990)
89. Diwu, Z. And J. W. Lown, *J. Photochem. Photobiol., B: Biol.* **18**, 131 (1993)
90. Diwu, Z. And J. W. Lown, *Free radical Biol. & Med.* **14**, 209 (1993)
91. Carpenter, S. and G. A. Kraus, *Photochem. Photobiol.* **53**, 169 (1991)
92. Hudson, J. B. and G. H. N. Towers, *Pharmacol. Ther.* **49**, 181 (1991)
93. Hudson, J. B., L. Harris and G. H. N. Towers, *Antiviral Res.* **20**, 173 (1993)
94. Hudson, J. B., E. A. Graham and G. H. N. Towers, *Planta Med.* **60**, 329 (1994)

95. Prince, A. M., D. Pascual, D. Meruelo, L. Liebes, Y. Mazur, E. Dubovi, M. Mandel and G. Lavie, *Photochem. Photobiol*, **71**, 188 (2000)
96. Lenard, J., A. Rabson, N. R. Stevenson and R. Vanderoef, *J. Cell. Biochem*, **17E-F**, 17 (1993)
97. Degar, S., A. M. Prince, D. Pascual, G. Lavie, B. Levin, Y. Mazur, D. Lavie, L. S. Ehrlich, C. Carter and D. Meruelo, *AIDS Res. Hum. Retroviruses* **8** 1929 (1992)
98. Stevenson, N. R., J. Lenard, *Antiviral Res.*, **21**, 119 (1993)
99. Weber, N. D., B. K. Murray, J. A. North and S. G. Wood, *Antiviral Chem. Chemother.* **5**, 83 (1994)
100. Chaloupka, R., T. Obsil, J. Plasek, F. Sureau, *Biochim. Biophys. Acta*, **1418**, 39 (1999)
101. Hirayama, J., K. Ikebuchi, H. Abe, K. W. Kwon, Y. Ohnishi, M. Horiuchi, M. Shinagawa, K. Ikuta, N. Kamo and S. Sekiguchi, *Photochem. Photobiol*, **66**, 697 (1997)
102. Hudson, J. B., V. Imperial, R. P. Haugland and Z. Diwu, *Photochem. Photobiol*, **65**, 352 (1997)

CHAPTER 2. EXPERIMENTAL APPARATUS

2.1 INTRODUCTION

We have built several experimental systems in our laboratory for the past few years in order to study the excited state dynamics of biologically active molecules. Among those instruments the most commonly used in our lab is a time-resolved spectrometer with sub-200 fs time resolution, based on chirped-pulse-amplification (Figure 2.1).

Amplified 800nm 1 kHz laser pulses are used to generate white light continuum as a probe and to be frequency doubled to make a pump pulse. We are currently building an optical parametric amplifier (OPA), which will give us a tunable light source. Now we only have 800 nm and 400 nm pump sources.

To measure the pump-induced absorbance change, pump and white light continuum pulse trains at certain wavelengths are generated. White light is split into probe and reference beams, then both are focused through the sample. The pump beam is also focused in the sample and overlap the probe beam. A mechanical chopper blocks every other 1 kHz pump pulse before it goes through the sample. Both probe and reference go through a monochromator onto two silicon photodiode and OP amp assemblies. The outputs are measured and averaged with gated integrator and boxcar averager modules (Stanford Research Systems SR 250), subsequent to an analog processor module (Stanford Research Systems SR 235) where the probe signal is divided by the reference to provide a shot-to shot normalization to eliminate the effect of probe pulse intensity fluctuations. The natural log of the quotient is calculated in the module, and sent to a third boxcar averager, which is operated in toggle mode to do an active baseline subtraction. ΔA is calculated using the

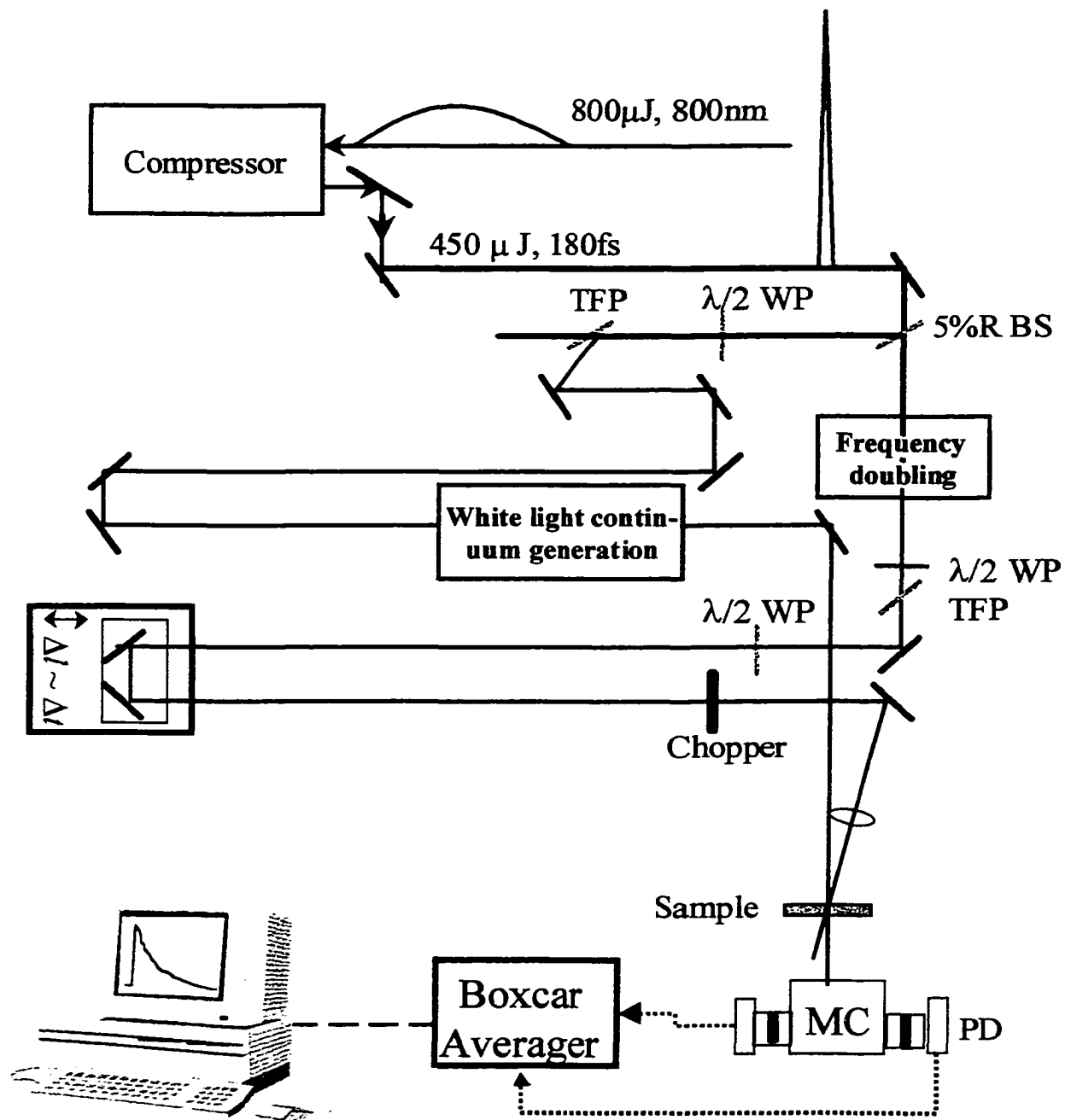


Figure 2.1 Schematic of the time-resolved absorption spectrometer. MC: monochromator, PD: photodiode, WP: wave plate, TFP: thin film polarizer, BS: beam splitter, HR: high reflector

difference between the probe/reference ratio when the pump is blocked and unblocked by chopper. Then averaged outputs are converted to digital signal in the A/D board, and sent to a personal computer. The change in absorbance is measured as a function of delay time between the pump and probe pulses and the probe wavelength.

2.2 REGENERATIVE CHIRPED PULSE AMPLIFIER SYSTEM

2.2.1 OVERVIEW

The recent progress in femtosecond laser technology has had a great impact on science and technology. Currently, the most widespread and convenient means to generate high intensity ultrashort pulses is by means of a technique called Chirped Pulse Amplification (CPA) [1]. CPA of femtosecond pulses using a Ti:sapphire laser was first demonstrated by Squier *et al.* [2].

Figure 2.2 shows a schematic of the Ti:sapphire chirped pulse amplifier system. Millennia V Diode pumped cw laser pumps a Ti:sapphire oscillator, and the output of the oscillator is a 100 MHz pulse train which has ~50 fs pulse duration and 2-4 nJ energy/pulse at 800 nm. Before going to the amplifier, these pulses are stretched to ~200 ps in the pulse stretcher to increase the pulse duration ~4,000 times, which reduces the peak intensity, so that they may be amplified without damaging the amplifier optics. Then, the stretched pulses are sent to a Ti:sapphire regenerative amplifier, which is pumped by a Nd:YLF laser firing at 1 kHz. The amplified pulse energy is ~800 μ J. The amplified pulses are sent to a pulse compressor to restore the pulses to the pulse duration of 150 fs with the final energy of ~450 μ J. Another instrument to protect our amplifier system is a missing pulse detector, which is an electronic timing circuit that checks for missing pulses in the synchronization pulse train.

A detailed description of the construction and operation procedure for CPA (Chirped Pulse Amplification) is given elsewhere [3] Here some important additional information and modifications of the system are described.

2.2.2 MILLENNIA V

Spectra physics Millennia V Diode-pumped cw visible laser is the pump source for our Ti: sapphire oscillator. It provides greater than 5 W of 532 nm output from a standard 110 or 220 Vac, single phase outlet. The laser offers beam quality, beam pointing and amplitude stability that are equal to or better than that of a conventional small frame ion laser. In addition, the optical noise is more than an order of magnitude lower than that of a comparable ion laser. This laser uses the neodymium yttrium vanadate (Nd:YVO₄) as a gain medium, and the lithium triborate (LBO) nonlinear crystal for the frequency doubling. The temperature of the Nd:YVO₄ crystal in the laser head is controlled by the compact recirculating chiller. The temperature is set at 18 °C to give an optimum performance. Because the Millennia V is a closed-loop system, it requires no facility water connections. Steamed distilled water should be used for the chiller. The noise level of the output power was measured less than 0.05 % rms. The output of the laser is vertically polarized to the table. By using a periscope the polarization has been rotated to horizontal and the beam goes to the Ti:sapphire oscillator.

2.2.3 TI: SAPPHIRE OSCILLATOR

After being developed by Spence *et al* [4], the self modelocked Ti:sapphire laser has been the principal workhorse in ultrafast science. This work is based on Kerr-lens modelocking (KLM) mechanism which uses self-focusing in the gain medium. For the laser material, the refractive index is given by $n = n_0 + n_2 I$, where I is the optical intensity, and n_2

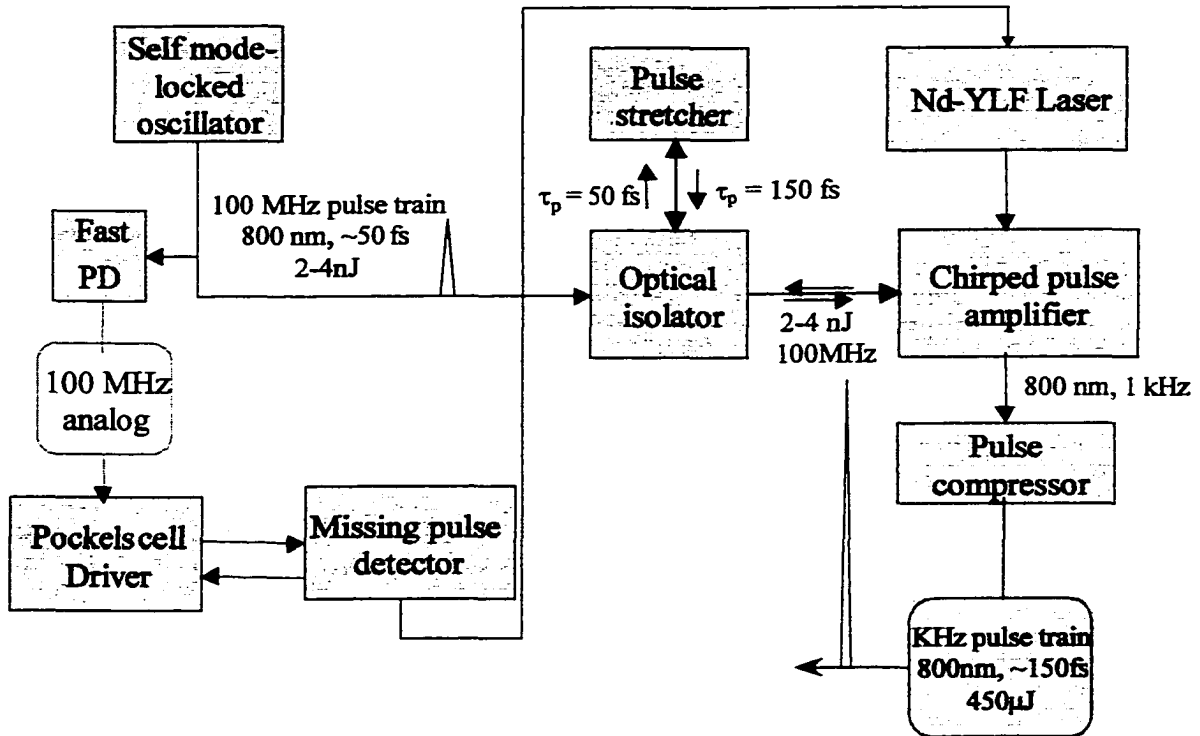


Figure 2.2 Schematic of the Ti:sapphire chirped pulse amplifier system. Solid arrows represent the paths of laser beams, and dashed arrows represent electronic connections. The pump laser for the oscillator is not shown.

is the nonlinear refractive index [5, 6]. Optical Kerr effect adds a nonlinear intensity dependent delay to the linear contribution because the phase delay experienced by the propagating optical signal is proportional to the index of refraction. The intensity of a Gaussian pulse varies across both its temporal and its spatial profile, so different parts of the profile will experience a different index of refraction. As a result, an index profile in the material, which is similar to that of a positive lens, will be produced, and this makes the beam focus itself (i.e. Kerr Lensing). Pulse shaping as well as pulse profile modulation by optical Kerr effect is continued until the pulse is compressed to its final steady-state value. Self-modelocking is achieved by these effects of self-phase-modulation (SPM) [7, 8], and

self-focusing. SPM occurs in the temporal domain. For a Gaussian pulse, the more intense center of the pulse experiences a higher index of refraction than the wings of the pulse, therefore there will be a phase change across the pulse profile during propagation. So, SPM produces a “chirp,” that is, the pulse develops a frequency sweep across itself because the derivative of phase with respect to time is equivalent to a frequency change.

The design of our self modelocked Ti:sapphire laser was first developed by Asaki *et al* [9]. This system is rather stable on daily bases. Stable room temperature is very important for the oscillator, so by experience a couple of hours of warm up time is needed before getting a stable modelocking. Also, the power supply of the other pump laser, which might generate heat, should be turned on to avoid subsequent temperature changes. There is no need for even minor adjustment for more than a week when everything is optimized and the temperature is stable. However, if the laser should become badly misaligned, it is usually necessary to realign the system “from scratch,” using the following procedure.

- 1) Start from the short cavity indicated in Figure 2.3: curved mirrors M1 and M2, the output coupler (OC), and the high reflector (HR).
 - a) Make the pump beam level along the center of the rail at 4” beam height. Make sure the pump beam goes through the center of M1. The M1 mount has $\sim 10^\circ$ angle with respect to normal. Make the position of M2 similar to that of M1 and check if the beam hits the center of the mirror.
 - b) Put the OC and HR close to M1 and M2. Pump at 5 W and try to get lasing by overlapping the fluorescence spots. Place a white card right in front of OC, and you will see a \odot image on the card if you put a red filter and block the green, then overlap the center of this image with the reflected image from HR. Once you got a good overlap on

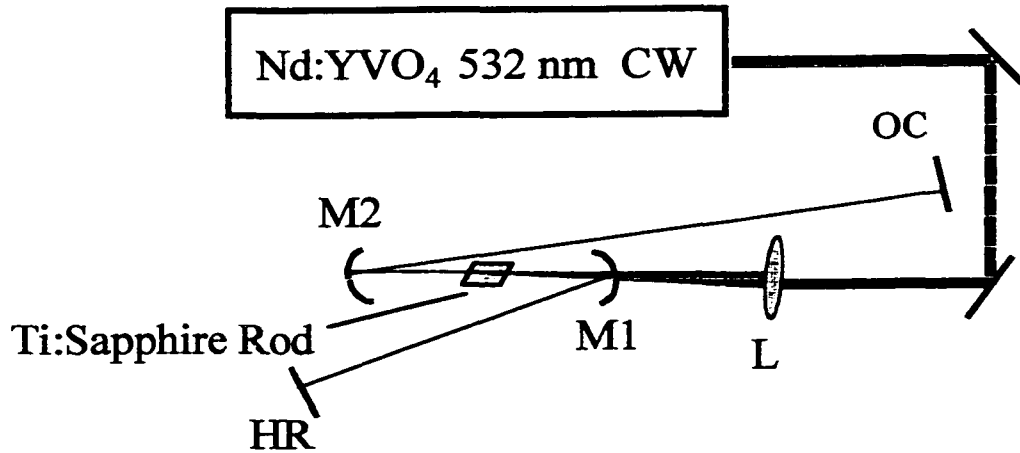


Figure 2.3. Short cavity of the Ti:sapphire oscillator. M1, M2: curved mirrors
L: lens, OC: output coupler, HR: high reflector

the OC, put the white card in front of the HR and make overlap again. If you do not obtain lasing, change the distance between M1 and M2. By translating either M1 or M2 or both you may see a brief flash of light. Set their position there, and optimize the power by alternatively tweaking vertical and horizontal knobs on the OC and HR, and translating the lens and curved mirrors.

2) Extend the cavity length. See Fig 2.4.

Replace OC with mirror 3 (M3) and rotate M3 to make reflected green beam parallel to the beam traveling between M1 and M2. Put OC close to M3. Put a white card which has a hole in it between M2 and M3, and overlap the incoming and reflected fluorescence from the OC to get lasing. To see this clearly use orange goggles and place the red filter between M2 and M3. If you don't get lasing after everything overlaps perfectly, move M1 forward to move the focus back. If you see lasing now, set the position there and optimize the power again. You should be able to obtain ~1 W of continuous wave lasing action at 5 W pump power. Extend the OC to the desired total length and optimize the power. Now move the HR back until it reaches the desired length, a distance from M1

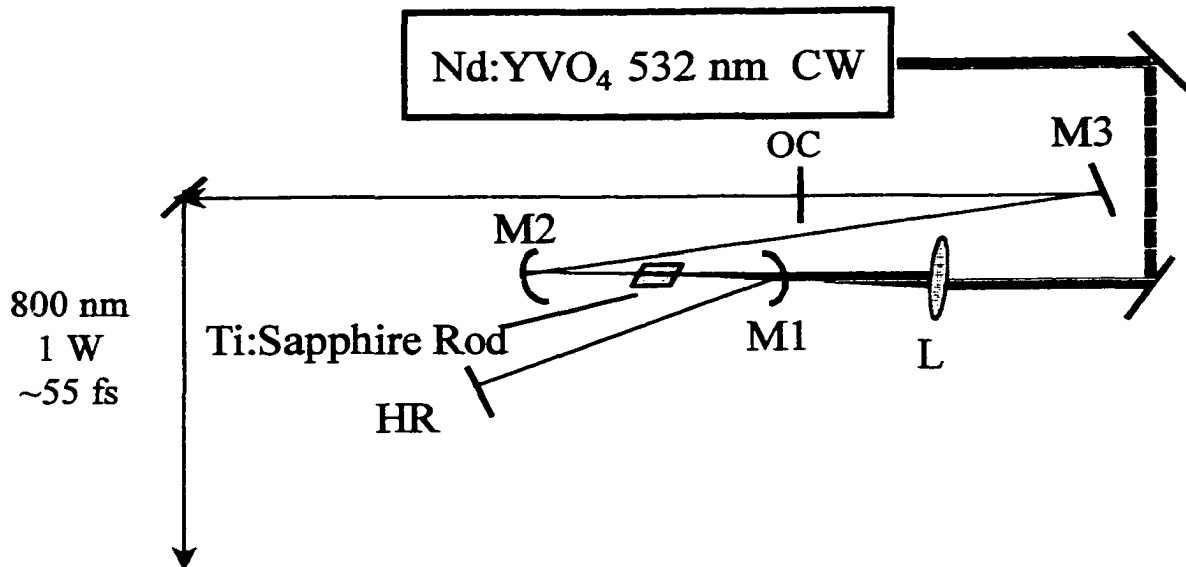


Figure 2.4. Short cavity of the Ti:sapphire oscillator. M1, M2: curved mirrors
M3: Mirror L: lens, OC: output coupler, HR: high reflector

roughly equivalent to its distance from M1 when the prisms are present, and maximize the power by tweaking horizontal and vertical controls on the HR and OC, and translating the curved mirrors, mainly M2.

- b) Insert the first prism by grazing a bit of the Ti:sapphire laser beam off the apex of the prism, and rotate it until you see minimum deviation of this light. Insert the second prism into this beam, and find minimum deviation position.

Place another high reflector after the second prism, and retroreflect this beam. Translate the prism into the beam until the laser is barely lasing, and optimize the power by moving M2 forward and tweaking the HR close to the second prism. Move the prism completely into the beam and optimize the power again. You should be able to obtain ~600 mW at 5 W pump power. See figure 2.5.

- 3) To obtain modelocking, first move out prism 1 until the power starts to drop while measuring the output lasing power. Repeat this for the prism 2. This way continuous wave lasing (cw) is suppressed and the modelocking mode is sustained. Then simply by

translating M1 or M2 towards the crystal by hand, and letting it back onto its original position is sufficient to establish modelocking. Sometimes slowly translating M2 forward after translating it back some distance needs to be accompanied with the action above.

The modelocking procedure is also given elsewhere [3].

2.2.4 CHIRPED PULSE AMPLIFICATION

Regenerative Amplifiers permit maximum energy ejection using a relatively simple cavity design. They are very well suited for seeding with low energy pulses. Having generated the short seed pulse, we need to be careful about the amplifier design.

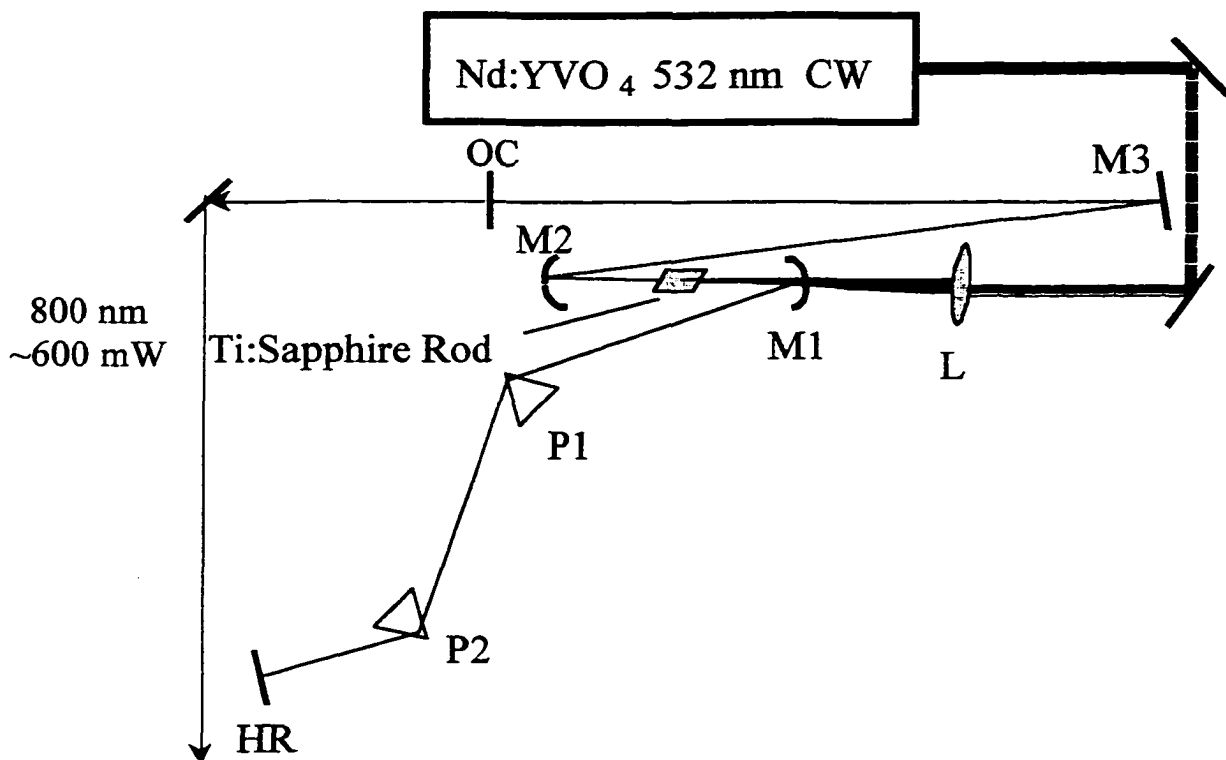


Figure 2.5. Full cavity of the Ti:sapphire oscillator. M1, M2: curved mirrors
M3: Mirror L: lens, OC: output coupler, HR: high reflector, P1, P2: glass
LAKL21 prisms

Although the nonlinear refractive index and the resulting self-focussing is useful for short pulse generation in the Ti:sapphire laser oscillator, they must be avoided in the amplification process. At very high pulse intensity, there is the possibility of the pulse distortion in the temporal and spatial domains. In amplification there is therefore a high risk of damaging the amplifier optics and gain medium when self-focusing is increased to a certain level. Hence, first we need to stretch the pulse duration by several orders of magnitude to reduce the peak pulse intensity. We then amplify the pulse. The pulse is subsequently compressed in the temporal domain.

2.2.4a Optical isolator

To avoid the amplified pulse following the reverse path of the seed pulse going back to the oscillator and disrupting the modelocking, we need a means to separate the incoming and outgoing pulses. This can be achieved by using an optical isolator, which is the combination of a thin film polarizer, a half wave plate, and a Faraday rotator. The schematic of the optical isolator is shown in Figure 2.6.

The Faraday rotator consists of a nonlinear magneto-optic material (such as yttrium-iron-garnet or terbium-garnet) [10] within a cylindrical ferromagnet. The Faraday rotator rotates the polarization of the linearly polarized beam, with a direction of rotation which depends on the magnetic field direction but not on the direction of travel of the beam. When a linearly polarized beam passes through the Faraday rotator, its polarization rotates by a certain angle α which depends on the medium length. And when it comes back, this beam obtains an additional rotation through an angle α , making a total rotation of 2α . Horizontally polarized laser pulses from the Ti:sapphire oscillator pass through the thin film polarizer, which transmits horizontal (p-polarized) beams and reflects vertical (s-polarized) beams, and

half wave plate, and then through a Faraday rotator ($\alpha=\lambda/4$) which preserves the polarization. The pulses chirped by the stretcher come back along the same path, and the Faraday rotator and half waveplate combination rotates the polarization from horizontal (p-polarized) to vertical (s-polarized), so the outgoing pulses are reflected by the thin film polarizer. Then, the vertically polarized chirped pulses are sent to the regenerative amplifier, passing through a 95% reflecting beam splitter. Since the grating has poor diffraction efficiency for vertical polarization, the 5% of the amplified pulse that comes back along this pass can be effectively filtered by the stretcher.

2.2.4b Pulse Stretcher

Although the energy of the pulses out of the Ti:sapphire oscillator is very low, due to the short pulse width, the peak powers of the pulses are high enough to give catastrophic damage to the optics of the regenerative amplifier. This can be avoided by introducing a chirp to the seed pulses by a pulse stretcher. Using our pulse stretcher (Figure 2.7), the pulse duration is increased (and the peak power is also reduced) by $\sim 4,000$ times.

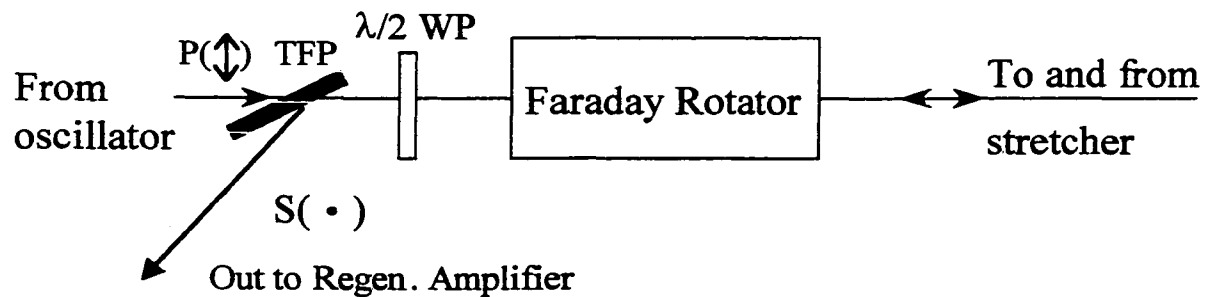


Figure 2.6 Schematic of the optical isolator. TFP: thin film polarizer, WP: wave plate

Dispersive elements like diffraction gratings or prisms can introduce a chirp by sending different wavelength or frequency components along different paths. The frequencies are separated by four dispersive elements, travel different path lengths, and are reunited collinearly. In this design each pulse makes four passes through the stretcher. The beam goes into the stretcher by passing above M3 and hits grating G1. The dispersed beam travels to a concave mirror M1, which is 0.5 m from G1, and then collimated. The concave mirror is used because it is achromatic, and unlike a lens it does not add material group velocity. The collimated beam goes little bit downward to M2, is retroreflected toward M1, continues back to G1, and then finally arrives at M3. The retroreflected beam from M3 is sent backwards along the original path, hitting the grating G1 two more times for a total of four.

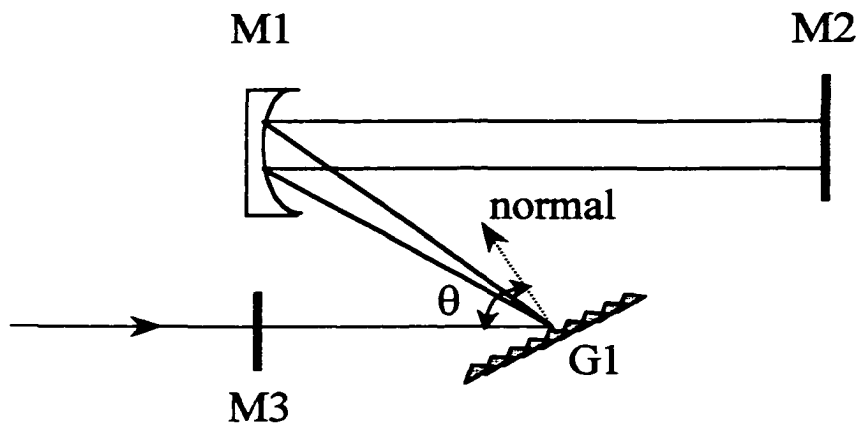


Figure 2.7 Optical schematic of the pulse stretcher. G1: 2000 g/mm gold coated grating, blazed for the near infrared, M1: silver coated curved mirror, $r=0.5\text{m}$, M2, M3: gold coated flat mirrors θ : an angle of incidence The beam from the isolator goes above mirror M3, parallel to the table and in the plane of diffraction. The dispersed beam propagates downward onto M2 via M1 and reflects back toward M1, then continues back to G1 and finally M3, which retroreflects the beam back along its original path, striking the grating total of four times.

2.2.4c Nd:YLF Laser

The pump source of our regenerative amplifier is a model 527DP-H 105CM Nd:YLF Laser. This Q-switched laser uses an intracavity LBO crystal to generate second harmonic at 527nm. A current of about 33A is sufficient to produce 15mJ pulses at 1 kHz, and the pulse duration is about 150 ns. The peak power instability is 4% p-p.

2.2.4d Ti:sapphire Regenerative Amplifier

The typical pulse energy emitted from a KLM oscillator is of the order of a few nanojoules (10^{-9} J), but this can be increased up to the Joule level in a series of amplifier stages. The use of regenerative amplification for short pulses has been demonstrated by Barty *et al.* [11], and Zhou *et al.* [12a, 12b]. Our amplifier cavity (Figure 2.8) is based on the design given by Squier *et al.* [13].

The seed pulse is injected into a laser cavity, allowed to make multiple passes through the amplifier medium, and then the amplified pulse is ejected. This regenerative system is very efficient because it is possible to trap the pulse in the amplifier until the gain saturates, thus ejecting all the available energy. To inject a weak pulse into the cavity, and to eject that pulse from the cavity after amplification, it is necessary to introduce an optical switch, which can quickly turn the beam polarization, together with a polarization sensitive element into the cavity. The s-polarized seed pulse is injected by reflecting the beam off an intracavity thin film polarizer, and a Pockels cell is used to rotate the polarization by 90° (p-polarized), so the pulse is kept in the cavity. The Pockels cell is an electro-optic crystal (KD_2PO_4) whose birefringence can be changed by applying a DC electric field. The Pockels cell assembly (Medox Electro-Optics) includes electronics which can switch ~ 3 kV across the crystal in ~ 4 ns to produce the electric field. Once the pulse has been amplified to the required level, the

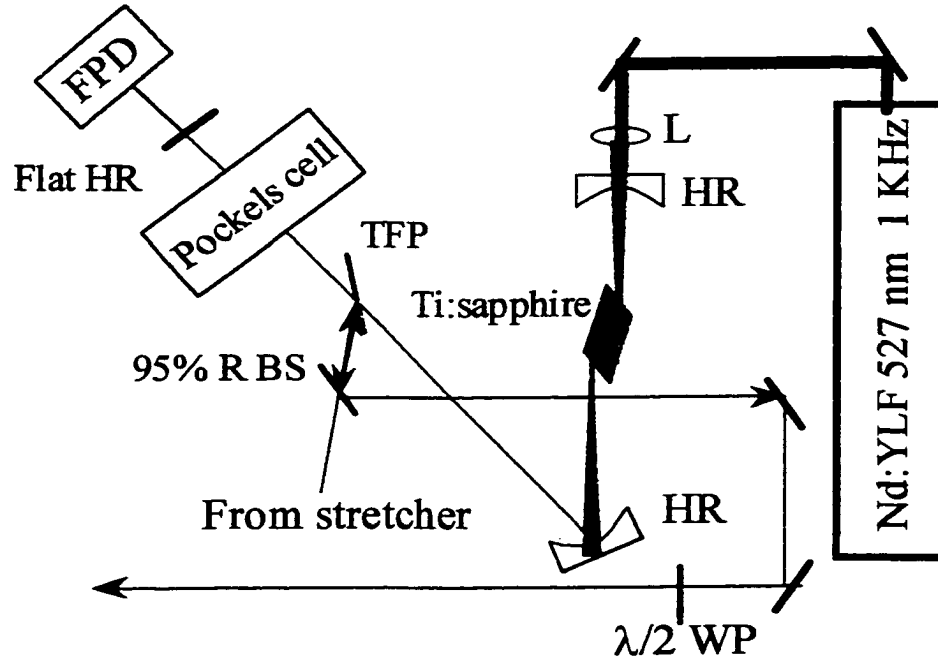


Figure 2.8 Diagram of the chirped pulse regenerative amplifier. HR: high reflector, TFP: thin film polarizer, BS: beam splitter, WP: wave plate, L: lens, FPD: fast photodiode. The seed pulse train and amplified pulse train enter and exit off of the same thin film polarizer. A pockels cell is used to switch pulses into and out of the amplifier cavity. A fast photodiode (FPD) placed at the flat high reflector monitors the growth of pulse energy.

beam polarization is again rotated 90° (s-polarized) by the Pockels cell, and the pulse is reflected by the thin film polarizer and ejected from the cavity.

A timing signal (must be ≥ 0.4 V) from the fast photodiode monitoring the oscillator is divided to produce a 1 kHz synchronized clock. The Q-switch of the Nd:YLF laser is activated upon this external “sync out” trigger, which is from the Pockels cell driver, and about $3.5\mu\text{s}$ later, the 527nm Nd:YLF laser pulse creates a population inversion in the Ti:sapphire rod. By first applying high voltage using “delay one” of the Pockels cell, which is set to follow the pump laser pulse by 200 ns, the pulse is trapped in the cavity and will be amplified. After 5-6 round trips, the gain begins to saturate. After that, the pulse energy begins to diminish, rather than increase, with each round trip. “Delay two,”

triggered by “delay one” is adjusted to eject the pulse when pulse build up is optimum, so maximum output energy is produced.

A missing pulse detector (MPD) is added to this amplifier. This, an electronic timing circuit, checks for missing pulses in the synchronization pulse train. So, when the oscillator and its synchronization signal become unstable, the whole amplifier system including Pockels cell and pump laser will be shut down. MPD prevents erratic Q- switching of the pump laser and the amplifier cavity, therefore it keeps the optical components such as the doubling crystal in the Nd:YLF laser and the Pockels cell safe.

2.2.4e Pulse Compressor

After being ejected from the amplifier cavity, the amplified pulse is sent to the compressor, and the chirp of the amplified pulse is removed after passing through the dual grating system twice, resulting in a short and high energy pulse which is near transform limited [14]. Figure 2.9 shows the layout of the pulse compressor.

2.3 OPTICAL PARAMETRIC AMPLIFIERS

2.3.1 BACKGROUND

The main purpose of optical parametric amplification is to generate frequency tunable ultrashort light pulses, so it can be a very good alternative to dye amplification. In a suitable nonlinear material, if a strong pump light wave is incident at frequency ω_3 , by parametric amplification and generation, the amplification and generation of two lower frequency light waves at frequencies ω_1 and ω_2 are observed. There is a relation between the pump and other generated or amplified waves.

$$\omega_3 = \omega_2 + \omega_1 \quad (\omega_3: \text{pump frequency, } \omega_2: \text{signal frequency, } \omega_1: \text{idler frequency}) \quad (2-1)$$

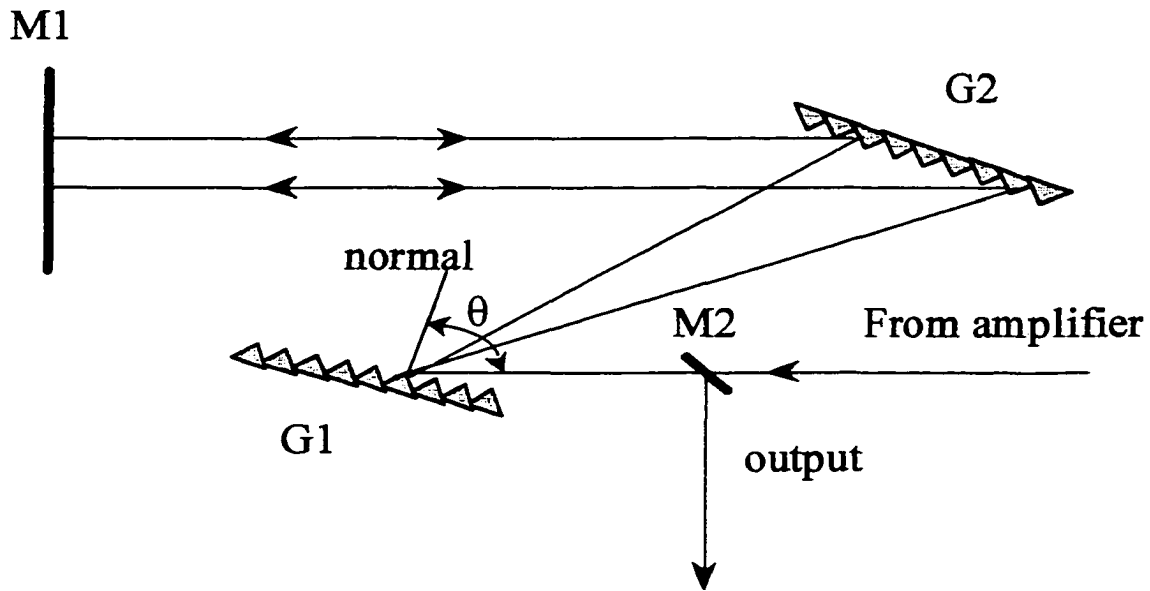


Figure 2.9 Diagram of pulse compressor. G1, G2: 2000 grooves/mm, gold coated grating, M1, M2: mirror, θ : an angle of incidence. The gratings are oriented with their faces parallel with angles of incidence and diffraction nearly the same as of that in the stretcher. The incoming beam from the amplifier, which is coming above M2, is diffracted at G1, collimated off of the second grating, and reflected back with M1. The reflected beam from M1 is vertically off so that it can be picked off with M2. The separation between two gratings can be adjusted by translating the G1 along the main axis.

This relation can be considered as the energy conservation equation. The efficiency of this conversion is very high when the phase matching condition between frequencies ω_2 , ω_1 and the pump frequency ω_3 is satisfied.

$$\Delta k = k(\omega_3) - k(\omega_2) - k(\omega_1) = 0 \quad (k_i \text{ is the wavevector of each field}) \quad (2-2)$$

In the case of collinear interaction, this reduces to the scalar relation

$$\Delta k = k(\omega_3) - k(\omega_2) - k(\omega_1) = 0 \quad (2-3)$$

The term “parametric process” is based on a periodic change of a parameter of a resonant circuit, usually of the capacity of the circuit [15]. Certain frequencies related to the changes of the system parameters are generated and amplified in this way. The nonlinear

crystal works as the circuit in optical parametric amplification, and the susceptibility of the nonlinear crystal can be changed with the radiated frequency by a strong pump wave.

When the intense pump wave ω_3 and a signal wave ω_2 interact with a nonlinear crystal, this system works as a parametric amplifier, and during the amplification process a third wave which has a frequency ω_1 is produced. This third wave is called the idler wave, and has the wave number vector $k(\omega_1) = k(\omega_3) - k(\omega_2)$. The parametric process can also occur without the signal input when a very intense pump wave is applied, this is because the photon noise can act as a signal, and the amplifier works as a generator. Although unseeded optical parametric amplifiers (OPA's) have broad tunability and efficient energy conversion of the pump into a signal wave, the amplified pulse width is limited to that of the pump pulse [16]. However, by compression of the pulse after the continuum amplification, dye amplifiers successfully produced pulses as short as 6 fs [17].

The frequencies ω_2 , ω_1 are determined by the phase matching condition and the interaction geometry. The tuning of the frequencies is achieved by changing the effective refractive indices in the nonlinear crystal by either rotating the crystal or altering its temperature.

OPA systems can be pumped by both the fundamental [18, 19, 20], and the second harmonic [21, 22,23] of amplified Ti:sapphire lasers. If one pumps with the fundamental, owing to higher pump energies and smaller group-velocity mismatches, one obtains higher energies; however, the blue tuning limit for this system is only 1.1-1.2 μm due to the absorption of the idler in the nonlinear crystal. Thus although frequency doubling can be done for the output of a fundamental pumped OPA, one loses a substantial part of the visible

spectrum. On the other hand, tunability into the blue-green can be achieved by pumping with the second harmonic of the Ti:sapphire laser system.

Two main advantages of optical parametric processes to amplify femtosecond pulses are high gain and broad amplification bandwidth. The intensity gain coefficient g is given by [24].

$$g = (\Gamma^2 - (\Delta k/2)^2)^{1/2}, \quad (2-4)$$

$$\Gamma^2 = \frac{2 \omega_s \omega_i |d_{\text{eff}}|^2 \Phi}{\epsilon_0 n_s n_i n_p c^3} = \frac{8 \pi^2 |d_{\text{eff}}|^2 \Phi}{\epsilon_0 n_s n_i n_p \lambda_s \lambda_i c} \quad (2-5)$$

$$\Delta k = k_2 + k_1 - k_3 \quad (2-6)$$

where $n_{s(i)}$ is the index of refraction of the signal (idler) wave, $\omega_{s(i)} = 2\pi c/\lambda_{s(i)}$, Φ is the pump intensity, ϵ_0 is the permittivity of the free space, $8.85 \times 10^{-12} \text{ C}^2 \text{ s}^2 / \text{kg m}^3$, d_{eff} is the effective nonlinear coefficient of the crystal, for type II phase matching in BBO, $d_{\text{eff}} = d_{22} \cos^2 \theta$, [25] with $d_{22} = 2.2 \text{ pm/V}$ [26], for type I phase matching $d_{\text{eff}} = d_{31} \sin \theta - d_{22} \cos \theta$ [27] with $d_{31} = \pm (0.07 \pm 0.03) d_{22}$ [28].

If there is any nonzero phase mismatch Δk , it will suppress the gain. When Δk is zero, the gain coefficient is only proportional to the square root of the pump intensity. So increasing gain coefficient has some limitation because the pump intensity is limited by the onset of self focusing, which results in continuum generation.

In general, there are two types of phase matching called type I (or parallel) and type II (or orthogonal) phase matching. The polarization vectors of the generated waves at ω_1 and ω_2

are parallel (and orthogonal to that of the pump at ω_3) in type I phase matching, whereas in the type II process the polarization vectors at ω_1 and ω_2 are perpendicular (with the pump polarization parallel to one of the generated waves) To satisfy the phase matching condition, the birefringence in the nonlinear optical crystal can be used. In uniaxial birefringent crystals the refractive index $n^e(\theta, \omega)$ for the wave of extraordinary polarization, which propagates at an angle θ to the optical crystal axis, is given by

$$\frac{1}{n^e(\theta, \omega)^2} = \frac{\cos^2 \theta}{[n^o(\omega)]^2} + \frac{\sin^2 \theta}{[n^e(\omega)]^2} \quad (2-7)$$

where $n^e(\omega)$ is the refractive index of an extraordinary wave, which propagates perpendicularly to the optical crystal axis. The phase matching angle for sum or difference frequency mixing can be calculated from

$$\omega_3 n^e(\theta, \omega_3) = \omega_2 n^o(\omega_2) + \omega_1 n^o(\omega_1) \quad (2-8)$$

for type I phase matching,

$$\omega_3 n^e(\theta, \omega_3) = \omega_2 n^o(\omega_2) + \omega_1 n^e(\theta, \omega_1) \quad (2-9)$$

for type II phase matching.

2.3.1a Walk-off effects

In addition to phase mismatch, spatial and temporal walk-off play an important role in the operation of parametric devices. Although the phase-matching condition is perfectly met, the maximum useful interaction length can be severely limited by walk-off effects, thus resulting in serious degradation in the nonlinear gain. This is from the reduction in the spatial or temporal overlap of the interacting beams like pump and signal with propagation through the nonlinear medium.

Spatial walk off arises from crystal double-refraction. In birefringent anisotropic material, the direction of the energy flow or the beam direction is not same as the direction of the wave-normal or the k -vector, which means that in a collinearly phase-matched interaction, though the k -vector of the interacting waves are in the same direction, the corresponding rays walk off from one another while propagating through the medium. This reduces the energy interchange between the pump and the generated field while propagating through the medium. So, after traveling a finite distance through the medium, the nonlinear interaction can become ineffective. In the presence of spatial walk-off, the maximum useful crystal length is limited by this distance, which is given by [29]

$$l_a = \frac{\sqrt{\pi} \omega_0}{\rho} \quad (2-10)$$

where ω_0 is the input beam waist radius, and ρ is the double refraction angle. So, by using large beam waists and small double refraction angle, the walk-off effect can be minimized. However, small double refraction angle, which is a consequence of birefringence, is not always desirable because it can restrain phase matching. By applying noncritical phase-matching geometries where the beams transmit along one of the principal index axes of the crystal, spatial walk-off effects can be removed. The crystal does not show double-refraction in these directions, so the wave-normal and beam directions become coincident and l_a becomes infinite. The nonlinear interaction is thus maximized, and high nonlinear gain can be achieved by using tightly focused beams and long interaction lengths. Other techniques for minimizing walk-off are the use of cylindrical focusing in the plane of walk-off [30], optimal mode-matching [31], and non-collinear interaction [32].

Temporal walk-off as well as spatial walk-off can give a strong influence on three wave interactions and reduce nonlinear gain by limiting the useful interaction length. This is important especially in the ultrafast regime where femtosecond and picosecond pulses are involved. When such pulses propagate in dispersive media, usually group velocities are used to describe the interaction because this is the speed of pulse envelope (or the pulse energy) in the medium. The group velocity mismatch between the interacting pulses induces temporal walk-off, which results in the reduced nonlinear coupling and energy transfer between the pump and parametric pulses while propagating through the crystal. Temporal walk-off can be described by pulse-splitting length, the distance after which they separate by a path equal to their pulse width, and is given by

$$l_{12}^g = \Delta\tau \left(\frac{1}{v_1^g} - \frac{1}{v_2^g} \right)^{-1} \quad (2-11)$$

where $\Delta\tau$ is the full-width at half-maximum pulse width, and v^g is the group velocity. From this equation temporal-walk-off is getting increased with shorter pulse duration and larger group velocity mismatch. Group velocity is defined by

$$v^g = \frac{\partial\omega}{\partial k} = \frac{c}{n} \left[1 + \lambda \frac{\partial n}{\partial \lambda} \right] \quad (2-12)$$

where n is index of refraction, ω is $2\pi f = 2\pi c/\lambda$.

Then, group velocity mismatch is given by

$$\frac{1}{\Delta v^g} = \frac{1}{\Delta v_{2,1}} = \left(\frac{1}{v_2} - \frac{1}{v_1} \right) \quad (2-13)$$

Temporal walk-off can be reduced by using materials with small group velocity mismatch or by employing noncollinear geometries [33]

2.3.1b Material requirements

The choice of the nonlinear crystal is critical in the design of parametric devices. The main criteria for the nonlinear crystal are broad tunability range, large effective nonlinear coefficient for efficient conversion, and high optical damage tolerance which is most important. Based on equation 2-5, parametric gain is dependent on the input pump intensity, Φ . At the higher input intensity the larger nonlinear gain and the stronger parametric interaction can be achieved. If the material damage threshold is too low, although all other design criteria is satisfied, parametric generation will be suppressed by the onset of damage and threshold will not be reached. The crystal β -BaB₂O₄ (BBO) meets all these condition. Most OPA systems are employing type I phase matching for the nonlinear crystal. Although type I phase matching has a higher nonlinear coefficient, all type I crystals have a problem of exploding bandwidth as approaching to degeneracy (when $\omega_s = \omega_i$). However type II phase matching does not have that problem. The parametric gain band width can be estimated by use of the following formula [16].

$$\Delta\nu = \frac{0.53}{c |1/\nu_s - 1/\nu_i|} \sqrt{\Gamma_0/L}, \quad (2-14)$$

where L is the length of the crystal, c is the speed of light, and $\nu_{s(i)}$ is the group velocity of the signal(idler). Γ_0 is related to the parametric gain, and defined in equation 2-5. The index of refraction is calculated based on the Sellmeier equation using parameters given by Kato [25],

$$n_o^2 = 2.7359 + \frac{0.01878}{\lambda^2 - 0.01822} - 0.01354 \lambda^2 \quad (2-15)$$

$$n_e^2 = 2.3753 + \frac{0.01224}{\lambda^2 - 0.01667} - 0.01516 \lambda^2 \quad (2-16)$$

where λ is in microns.

In type I phase matching ($e \rightarrow o + o$), both signal and idler have same polarization, so since group velocity mismatch goes to zero as the wavelengths approach to degeneracy, there is a bandwidth explosion problem (Figure 2.10).

In type II phase matching ($e \rightarrow o + e$), the polarization of the signal is perpendicular to that of the idler, so group velocities are not the same even at degeneracy. The bandwidth for type II phase matching is narrower than for type I at all wavelengths.

The bandwidth for type II phase matching remains essentially flat from 500nm to degeneracy (Figure 2.11). The calculated group velocity mismatch between pump (412nm) and signal waves for type II phase matching based on eq. 2-12 and 2-13 is in figure 2.12.

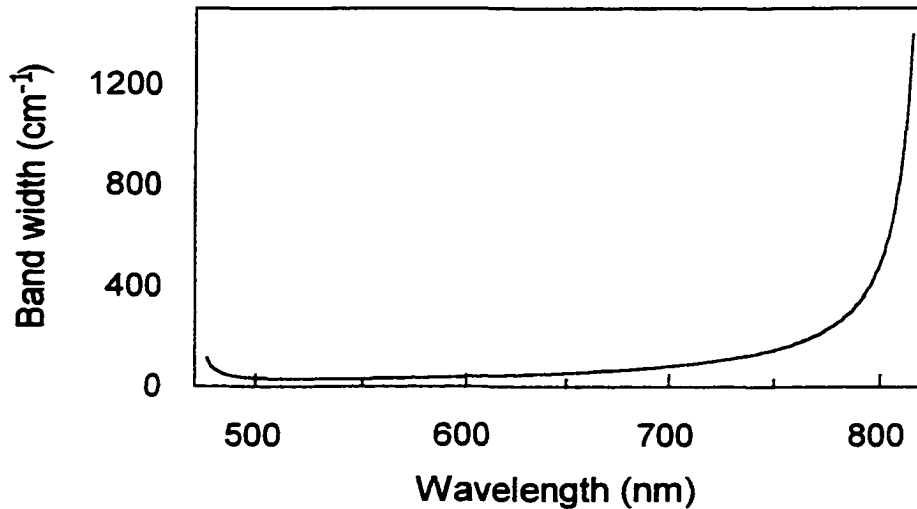


Figure 2.10 Calculated bandwidths based on eq. 2-14 for type I phase matching in a BBO crystal. Actual parameters are $\Phi = 140 \text{ GW/cm}^2$, $L = 3 \text{ mm}$. Pumped at 412nm. θ is at 27.6° .

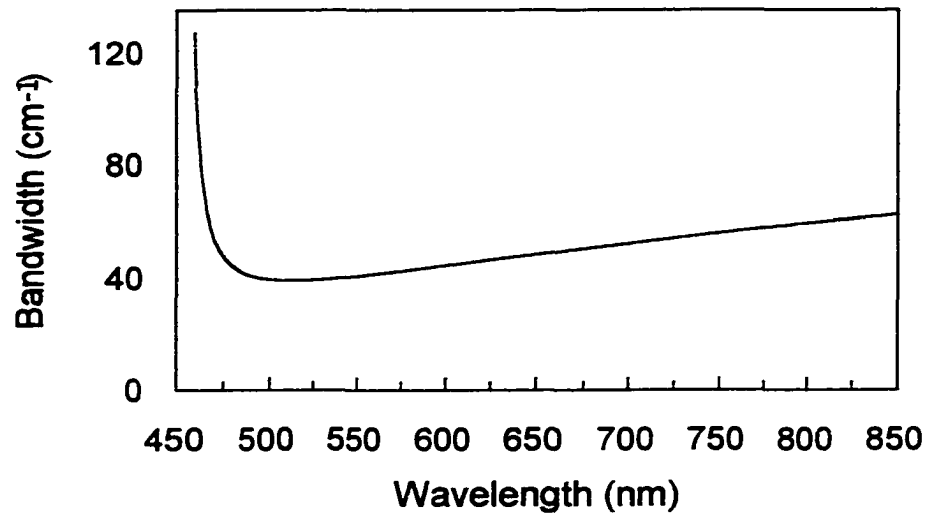


Figure 2.11 The calculated bandwidths for the first stage OPA (type II BBO). The experimental parameters are $\Phi = 140 \text{ GW/cm}^2$, $L = 3 \text{ mm}$. Pumped at 412 nm . θ is at 32° .

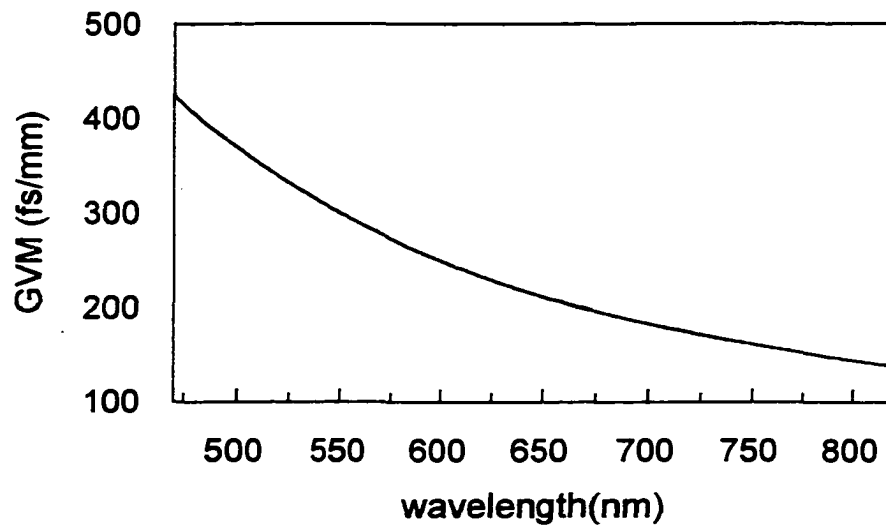


Figure 2.12 Group velocity mismatch between pump (412 nm) and signal waves for type II phase matching in a BBO crystal.

2.3.2 NONCOLLINEAR PARAMETRIC AMPLIFICATION

Optical parametric generation and optical parametric amplification are widely used for giving tunable intense light sources. Some of the common nonlinear crystals such as BBO, LBO, and LiIO_3 have the interesting birefringence and dispersion properties, which allow phase matching between pump beam wave vectors and the signal (idler) wave vectors to be achieved for collinear as well as for noncollinear propagation directions. For the picosecond or nanosecond pulses, usually the efficiency of the collinear parametric process is higher than that of the noncollinear process. This higher efficiency occurs because parallel beams have the longer overlapping interaction length of pump and parametric waves inside the crystal than the beams crossing at an angle. So, for picosecond and nanosecond pulses, efficient conversion of the pump energy into signal and idler can be achieved in long nonlinear crystals.

When high intensity ultrashort pump pulses were employed, high efficiency was observed for both collinear and noncollinear parametric processes [34, 35, 36] This is because high parametric gain can be achieved by strong femtosecond pulses in nonlinear crystal within a few millimeters which is relatively short interaction length. And also when the phase matching condition as well as the group velocity matching condition are met, the highest conversion can be achieved. The group velocity matching becomes very important when nonlinear crystals have large dispersion, pulse duration is very short like tens of femtosecond, and pump pulse wavelengths are in UV spectral ranges (shorter than 400-500 nm) [46, 47]. In this case noncollinear parametric process is more efficient.

An interesting property of β -barium borate (BBO) was found in optical parametric generation [37, 38, 39]. When using nonlinear phase matching, the angle between a pump

and signal is set to be around 3.7° , the phase matching angle becomes independent of wavelength over most of the visible, so very large gain bandwidths can be achieved. And also there is another factor to provide high gain. There is an angle (4°) that spatial walk-off between pump and signal is compensated, and this angle is very close to the angle described above. Recently broad band OPA's seeded by the white light continuum were built based on this concept and those were tunable across the visible [40, 41]. Amplified pulses with a FWHM band width extending from 790nm to 535nm, and pulse duration as short as 8 fs have been reported.

The use of noncollinear amplification appears to be necessary if one wants to run the OPA with very short pump pulses (like a few tens of femtoseconds), or in the UV spectral range, where large collinear group velocity mismatch occurs. For our experiment we built a collinear optical parametric amplifier because this collinear approach is simpler and gives efficient amplification with the 180fs, 400nm pump pulse. Also, spectral resolution is more important than temporal resolution for our case.

2.3.3 DESIGN AND OPERATION

Our OPA system employs the two-stage configuration based on the design of Greenfield *et al.* [42] (Figure 2. 13). The pulse energy out of the amplified Ti:sapphire pulse is $\sim 480 \mu\text{J}/\text{pulse}$ following compression. The preamplifier stage uses a 3-mm long BBO type II crystal, which is cut at $\theta = 32^\circ$. For the amplifier stage the 2mm type I BBO crystal, which is cut at $\theta = 27.6^\circ$ is employed. The tuning range of the OPA only depends on the first stage.

Five percent of the recompressed beam is split off using a beam splitter to generate white light. Its intensity is adjusted by a half waveplate and a thin film polarizer combination, and the pulses are focused with a 150 mm f.l. lens into a 3 mm thick sapphire disk. A stable

and a thin film polarizer combination, with approximately 20 μJ diverted to pump the preamplifier stage of the OPA. The white light continuum is focused with 25 mm f.l. lens into a 3 mm type II β -Barium Borate (BBO) crystal, and the blue light is reduced with a 3x telescope, and combined with white light continuum seed by a dichroic beam splitter. Spot sizes for the seed and the pump beams are 1.4 mm and 0.45 mm at the first crystal. The pump intensity is 70 GW/cm^2 (You can see weak off-axis parametric superfluorescence at this intensity). The amplified output energy out of the first stage is ~ 300 nJ (both signal and idler). By carefully adjusting a variable delay line and direction of the beams, spatial and temporal overlap of the beams is achieved.

The blue light transmitted through the thin film polarizer is used to pump the amplifier stage after changing the polarization to vertical by using a half-wave plate. This makes the pump polarization extraordinary. Parametric light from the preamplifier stage is amplified by overlapping the beam from the preamplifier stage with the remaining 70 μJ of blue light reduced with a 2x telescope in a 2 mm type I BBO crystal. In the preamplifier stage, type II process is undergoing, so the polarizations of the signal (o) and idler (e) are different. Although both the signal and idler are transmitted amplifier stage at which type I process ($e \rightarrow o + o$) is undergoing, only the signal is amplified since the polarization of the idler generated in the preamplifier stage is orthogonal to that generated in the amplifier stage. Spot sizes are 1.2 mm and 1.4 mm for the pump and the output of the preamplifier stage, respectively. The pump intensity for the amplifier stage is 25 GW/cm^2 . The signal is separated from the idler by use of a dichroic beam splitter. The signal output energy is typically 2-3 $\mu\text{J}/\text{pulse}$, with a wavelength tuning range of 475-820 nm. Tuning can be done

easily by adjusting the timing and the crystal angle of the preamplifier stage, and minor timing adjustment is needed for the amplifier stage.

2.4 PUMP-PROBE EXPERIMENT

A mechanical chopper synchronized to one half the repetition rate of the laser is used to block every other pump pulse. The pump beams are focused onto the sample using a 150 mm f.l. lens, and the probe beam is focused using a 500 mm f.l. lens. The pump energy is adjusted by using a half waveplate and a thin film polarizer combination. The probe and reference beams are vertically displaced, and sent into a monochromator (ISA HR-320) with a grating blazed at 1200 g/mm. The probe and reference beams are detected with Hamamatsu S1336-5BQ photodiodes, and amplified with Analog devices op467 precision high-speed OP amps. The outputs are measured and averaged with gated integrator and boxcar averager modules (Stanford Research Systems SR 250), subsequently to an analog processor module (Stanford Research Systems SR 235) where the probe signal is divided by the reference to provide a shot-to shot normalization. The natural log of the quotient is calculated in the module, and sent to a third boxcar averager, which is operated in toggle mode to do an active baseline subtraction. Then averaged outputs are converted to digital signal in the A/D board, and sent to a personal computer (Figure 2.14). Data sets are typically the average of twenty scans, with each point in the scan being an average of five hundred shots. Optical densities of the samples for the transient absorption experiments are 0.2-0.7 (concentration $< 10^{-4}$ M) at the excitation wavelength for 1-mm pathlength cells. Samples are stored in the 1 mm pathlength spinning cells, and rotated during the experiment to prevent thermal lensing and sample degradation.

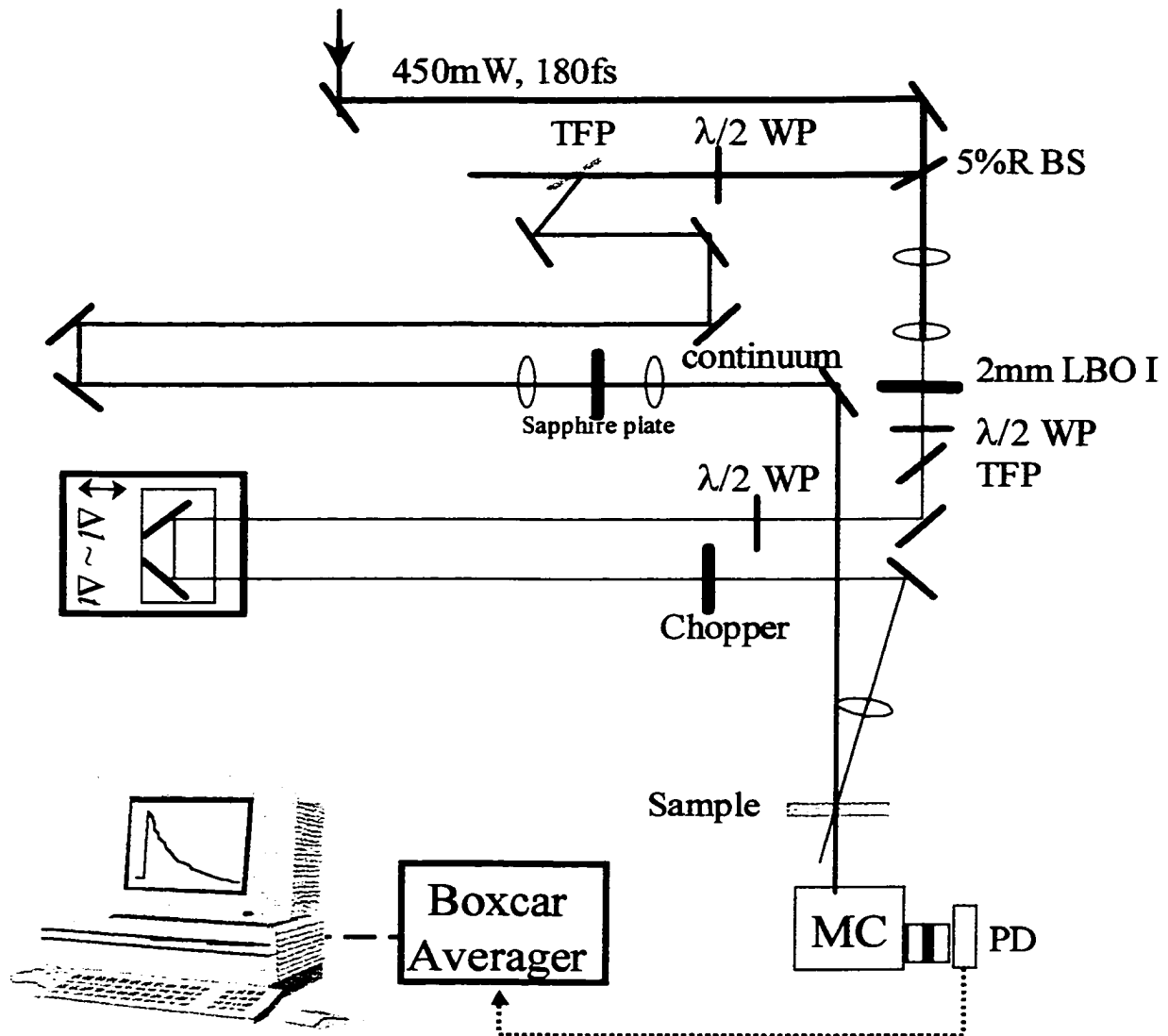


Figure 2.14 Schematic diagram of pump-probe experiment. $\lambda/2$ WP: half wave plate, TFP: thin film polarizer, MC: monochromator, PD: photodiode, LBO I: type I lithium triborate crystal

2.5 THE FLUORESCENCE UPCONVERSION SPECTROMETER

Fluorescence upconversion is a powerful technique that is complementary to transient absorption. Transient absorption monitors all absorbing and emitting species (via stimulated emission), given an adequate signal-to-noise ratio. In transient absorption, it is hard to distinguish ground-state bleaching from stimulated emission in regions where the emission spectrum overlaps the absorption spectrum. Also, the spectrum from emitting species may often be obfuscated by the presence of absorbing species (singlets and triplets) present in higher concentration or with a larger extinction coefficient. Because the upconversion technique detects only emission from the excited state, the potential ambiguities in the transient absorption experiment referred to above can be eliminated.

The fluorescence upconversion apparatus is described in detail elsewhere [43, 44, 45], and is based on a Ti:sapphire oscillator, producing tunable (750-900 nm) 50-65-fs pulses (Figure 2.15). Sample is excited by frequency-doubled pulses. The residual fundamental wavelength after frequency doubled is used as the gate pulse to upconvert the fluorescence, which is collected and focused into a 0.4-mm BBO crystal with an ellipsoidal reflector. After separation from the gate beam, from the second and third harmonic beams, and from the fluorescence, the upconverted signal is focused into a monochromator coupled to a Hamamatsu R760 photomultiplier selected for zero dark counts. The instrument response function is obtained by collecting a cross correlation function of the second harmonic and the fundamental: the resulting third harmonic is plotted against delay time. Cross correlation functions typically have a fwhm of 140-144 fs. All curves were fit and deconvoluted from the instrument function using an iterative convolute-and-compare nonlinear least-squares algorithm.

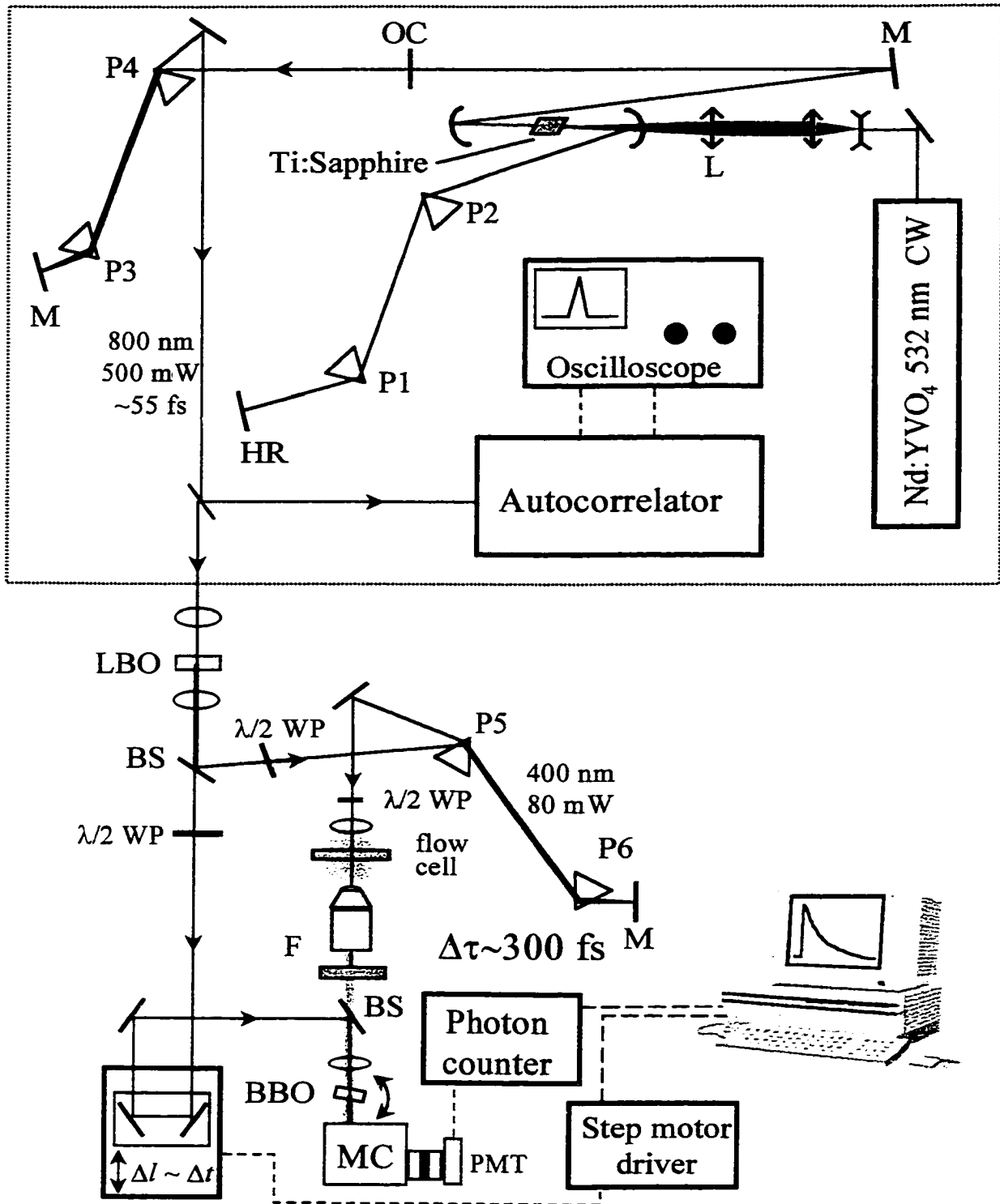


Figure 2.15 Schematic diagram of the fluorescence upconversion spectrometer. Ti:sapphire oscillator is located within the box region with GVD precompensator. BS: beam splitter, L:lens, M: mirror, OC: output coupler, HR: high reflector, MC: monochromator, P: prism. F: filter

REFERENCES

1. Maine, P.; D. Strickland, P. Bado, M. Pessot, G. Mourou, "Generation of ultrahigh peak power pulses by chirped pulse amplification," *IEEE J. Quantum Electron.* **QE-24**, 398 (1988)
2. Squier, J., G. Salin, G. Morou, and D. Harter, "100 fs pulse generation and amplification in Ti:Al₂O₃," *OPT. Lett.* **16**, 324 (1991)
3. English, D. S. *Elucidation of the primary photophysical processes in the light activated antiviral agents, hypericin and hypocrellin.*; Iowa State University: Ames, (1998)
4. Spence, D. E., P. N. Kean, and W. Sibbett, "60-fsec pulse generation from a self-modelocked Ti:sapphire laser," *Opt. Lett.* **16**, 42 (1991)
5. Miller, A. And D. M. Finlayson *Laser Sources and Applications*, (Scottish Universities Summer School in Physics & Institute of Physics Publishing, 1996)
6. Schreiber, E. *Femtosecond Real-Time Spectroscopy of Small Molecules and Clusters*, (Springer-Verlag, New York, 1998)
7. Shen, Y. R., "Self-Focusing: Experimental," *Prog. Quant. Electr.* **4**, 1 (1975)
8. Marburger, J. H., "Self-Focusing: Theory," *Prog. Quant. Electr.* **4**, 35 (1975)
9. Asaki, M. T., C-P Huang, D. Garvey, J. Zhou, H. C. Kapteyn and M. M. Murnane, "Generation of 11-fs pulses from a self-mode-locked Ti:sapphire laser," *Opt. Lett.* **18**, 977 (1993)
10. Saleh, B. E. A., and M. C. Teich *Fundamentals of Photonics* , (John Wiley & Sons, Inc., New York, 1991)
11. Barty, C. P. J., C. L. Gordon, and B. E. Lemoff, "Multiterawatt 30-fs Ti:sapphire laser system," *Opt. Lett.* **19**, 1442 (1994)

12. (a) Zhou, J., C. P. Huang, C. Shi, M. M. Murnane, and H. C. Kapteyn, "Generation of 21-fs millijoule-energy pulses by use of Ti:sapphire," *Opt Lett.* **19(2)**, 126 (1994), (b) Zhou, J., G. Taft, C. P. Huang, M. M. Murnane, and H. C. Kapteyn, "Pulse evolution in a broad bandwidth Ti:sapphire laser," *Opt Lett.* **19(15)**, 1149 (1994)
13. Squier, J., G. Korn, G. Morou, G. Vallincourt, M. Bouvier, "Amplification of femtosecond pulses at 10-kHz repetition rates in Ti:Al₂O₃," *Opt Lett.* **18(8)**, 625 (1993)
14. Shank, C. V., R. L. Fork, R. Yen, and R. H. Stolen, "Compression of femtosecond optical pulses," *Appl. Phys. Lett.* **40**, 761 (1982)
15. Herrmann, J., B. Wilhelmi *Lasers for Ultrashort Light Pulses*, (North-Holland, 1987)
16. Danielius, R.; A. Piskarskas, A. Stabinis; G. P. Banfi; P. Di Trapani; and R. Righini, "Traveling-wave parametric generation of widely tunable, highly coherent femtosecond light pulses," *J. Opt. Soc. Am. B* **10(11)**, 2222 (1993)
17. Cruz, C. H. Brito; R. L. Fork, W. H. Knox, and C. V. Shank, "Spectral hole burning in large molecules probed with 10-femtosecond optical pulses," *Chem. Phys. Lett.* **132(4-5)**, 341 (1986)
18. Petrov, V.; F. Seifert, and F. Noack, "High repetition rate traveling wave optical parametric generator producing nearly bandwidth limited 50 fs infrared light pulses," *Appl. Phys. Lett.* **65(3)**, 268 (1994)
19. Yakovlev, V. V., B. Kohler, and K. R. Wilson, "Broadly tunable 30-fs pulses produced by optical parametric amplification," *Opt. Lett.* **19**, 2000 (1994)
20. Nisoli, M., S. De Silvestry, V. Magni, O. Svelto, R. Danielius, A. Piskarskas, G. Valiulis, and A. Varanavicius, "Highly efficient parametric conversion of femtosecond Ti:sapphire laser pulses at 1 kHz," *Opt. Lett.* **19**, 1973 (1994)

21. Reed, Murray K.; M. K. Steiner-Shepard, D. K. Negus, "Widely tunable femtosecond optical parametric amplifier at 250 khz with a Ti:sapphire regenerative amplifier," *Opt. Lett.* **19**, 1855 (1994)
22. Petrov, V.; F. Seifert, F. Noack, "Visible optical parametric generator producing nearly bandwidth-limited femtosecond light pulses at 1-kHz repetition rate," *Appl. Opt.* **33**, 6988 (1994)
23. Greenfield, S. R., M. R. Wasielewski, "Optical parametric amplification of femtosecond pulses tunable from the blue to the infrared with microjoule energies," *Appl. Opt.* **34**, 2688 (1995)
24. Bayer, R. L., and R. L. Herbst *Nonlinear Infrared Generation*, Y. R. Shen, ed. (Springer-Verlag, New York, 1977)
25. Kato, K. "Second-Harmonic Generation to 2048 Å in β -BaB₂O₄," *IEEE J. Quantum Electron.* **QE-22**, 1013 (1986)
26. Eckardt, R. C., H. Masuda, Y. X. Fan, and R. L. Byer, "Absolute and Relative Nonlinear Optical Coefficients of KDP, KD*P, BaB₂O₄, LiIO₃, MgO:LiNb₃, and KTP Measured by Phase-Matched Second-Harmonic Generation," *IEEE J. Quantum Electron.* **26**, 922 (1990)
27. Armstrong, D. J., W. J. Alford, T. D. Raymond, and A. V. Smith, " Absolute measurement of the effective nonlinearities of KTP and BBO crystals by optical parametric amplification," *Appl. Opt.* **35**, 2032 (1996)
28. Chen, C., Y. X. Fan, R. C. Eckardt, and R. L. Byer, "Recent developments in barium borate," in *Laser and Nonlinear Optical Materials*, L. G. DeShazer, ed., Proc. SPIE, **681**, 12 (1986)

29. Ebrahimzadeh, M., in *Laser Sources and Applications*, A. Miller, and D. M. Finlayson, ed. (SUSSP Publications and Institute of Physics Publishing, 1996) p239
30. Kuizenga, D. J., "Optimum focusing conditions for parametric gain in crystals with double refraction," *Appl. Phys. Lett.* **21**, 570 (1972)
31. Boyd, G. D.; and D. A. Kleinman, "Parametric interaction of focused Gaussian light beams," *J. Appl. Phys.* **39**, 3597 (1968)
32. Watchman, E. S., W. S. Pelouch, and C. L. Tang, *J. Appl. Phys.* **70**, 1893 (1991)
33. Di Trapani, P., A. Andreoni, P. Foggi, C. Solcia, R. Danielius, A. Piskarskas, "Efficient conversion of femtosecond blue pulses by traveling-wave parametric generation in non-collinear phase matching," *Opt. Commun.* **119**, 327 (1995)
34. Petrov, V.; F. Noack, "Tunable femtosecond optical parametric amplifier in the mid-infrared with narrow-band seeding," *J. Opt. Soc. Am. B* **12**, 2214 (1995)
35. Reed, M. K.; M. K. Steiner-Shepard, M. S. Armas; D. K. Negus, "Microjoule-energy ultrafast optical parametric amplifiers," *J. Opt. Soc. Am. B* **12**, 2229 (1995)
36. Wilson, K. R.; V. V. Yakovlev, "Ultrafast rainbow: tunable ultrashort pulses from a solid-state kilohertz system," *J. Opt. Soc. Am. B* **14**, 444 (1997)
37. Driscoll, T. J.; G. M. Gale, F. Hache, "Ti : sapphire second-harmonic-pumped visible range femtosecond optical parametric oscillator," *Opt. Commun.* **110**, 638 (1994)
38. Gale, G. M.; M. Cavallari, T. J. Driscoll, F. Hache, "Sub-20-fs tunable pulses in the visible from an 82-MHz optical parametric oscillator," *Opt. Lett.* **20**, 1562 (1995)
39. Hache, F.; M. Cavallari; G. M. Gale, "Ultrafast visible optical parametric oscillators: a route to tunable sub-10-femtosecond pulses?" in *Ultrafast Phenomena X*, P. F. Barbara, J. G. Fujimoto, W. H. Knox, and W. Zinth ed., *Springer Ser. Chem. Phys.* **62**, 33 (1996)

40. Wilhelm, T., J. Piel, and E. Riedle, "Sub-20-fs pulses tunable across the visible from a blue-pumped single-pass noncollinear parametric converter," *Opt. Lett.* **22**, 1494 (1997)
41. Cerullo, G., M. Nisoli, S. Stagira, and S. De Silvestry, "Sub-8-fs pulses from an ultrabroadband optical parametric amplifier in the visible," *Opt. Lett.* **23**, 1283 (1998)
42. Greenfield, S. R., M. R. Wasielewski "Near-transform-limited visible and near-IR femtosecond pulses from optical parametric amplification using Type II β -barium borate," *Opt. Lett.* **20**, 1394 (1995)
43. Horng, M. L.; Gardecki, J. A.; Papazyan, A.; Maroncelli, M. *J. Phys. Chem.* **99**, 17311 (1995)
44. Rosenthal, S. J.; Jiminez, R.; Fleming, G. R.; Kumar, P. V.; Maroncelli, M., *Journal of Molecular Liquids* **60**, 25 (1994)
45. Smirnov, A.V. *Primary photoprocesses of light-activated antiviral and antitumor agents, hypericin and hypocrellin*; Iowa State University: Ames, IA, 1999, chapter 2.
46. Di Trapani, P., A. Andreoni, C. Solcia, P. Foggi, R. Danielius, A. Dubietis, and A. Piskaskas, "Matching of group velocities in three-wave parametric interaction with femtosecond pulses and application to traveling-wave generators," *J. Opt. Soc. Am. B*, **12**, 2237 (1995)
47. Krylov, V., O. Ollikainen, J. Gallus, U. Wild, A. Rebane and A. Kalintsev, "Efficient noncollinear parametric amplification of weak femtosecond pulses in the visible and near-infrared spectral range," *Opt. Lett.* **23**, 100 (1998)

**CHAPTER 3: CONFIRMATION OF EXCITED-STATE PROTON
TRANSFER AND GROUND-STATE HETEROGENEITY IN
HYPERICIN BY FLUORESCENCE UPCONVERSION**

A paper published in the Journal of the American Chemical Society¹

D. S. English², K. Das², K. D. Ashby², J. Park², J. W. Petrich ^{*2}, and E. W. Castner, Jr. ^{*3}

ABSTRACT

Fluorescence upconversion measurements of hypericin and its methylated analog, *O*-hexamethoxy hypericin, which possesses no labile protons, confirm excited-state proton (or hydrogen atom) transfer as the primary photophysical event in hypericin. The presence of a rising component in the time-resolved fluorescence of hypericin and the absence of such a component for the hexamethoxy analog are consistent with our assignment of excited-state proton or atom transfer as the primary photophysical process in the light activated antiviral compound, hypericin. The results using the fluorescence upconversion technique, *which detects only emission from the excited state*, are in good agreement with our previous transient absorbance measurements. The results are also consistent with a heterogeneous ground-state of hypericin.

¹Reprinted with permission from *The Journal of the American Chemical Society*, 1997, **119**, 11585. Copyright © 1997 American Chemical Society

²Department of Chemistry, Iowa State University, Ames, Iowa 50011-3111.

³Department of Chemistry, Brookhaven National Laboratory, Upton, New York 11973.

*Authors to whom correspondence should be addressed.

INTRODUCTION

Interest in the polycyclic quinone, hypericin (see ref. 1 for reviews, Figure 3.1a) was spawned by the discovery that it possesses extremely high toxicity towards certain viruses, including HIV, and toward tumors [2-4] and that this toxicity absolutely requires light [5]. The interaction of light with hypericin and hypericin-like chromophores is clearly of fundamental biological importance. Previously we have used ultrafast time-resolved transient absorption spectroscopy as a tool to understand the excited state processes of hypericin (and its analog hypocrellin) [6-13]. We have concluded that the primary nonradiative process [38] in hypericin is excited-state intramolecular proton (or atom) transfer.

In this work, we make use of a complementary technique, fluorescence upconversion, to measure the excited state dynamics. In fluorescence upconversion spectroscopy, an ultrashort laser pulse populates the excited state of the sample. The molecular emission is collected efficiently, and imaged into a nonlinear optical, or gating crystal. The spontaneous emission is gated, or “upconverted” by using a replica of the excitation pulse: the sum of the emission light frequency and the gating pulse is detected as a function of gate pulse delay time. The excited state dynamics, as manifested by the spontaneous emission transients, can be observed with <25 fs time resolution in this way. This technique provides the shortest possible time resolution for spontaneous emission dynamics, at least an order of magnitude better than available with direct detection techniques using streak cameras.

Our argument for intramolecular excited-state proton transfer in hypericin is as follows. The hypericin analog lacking labile protons, mesonaphthobianthrone [14] (Figure 3.1d), is significantly fluorescent and has optical spectra that resemble those of hypericin only

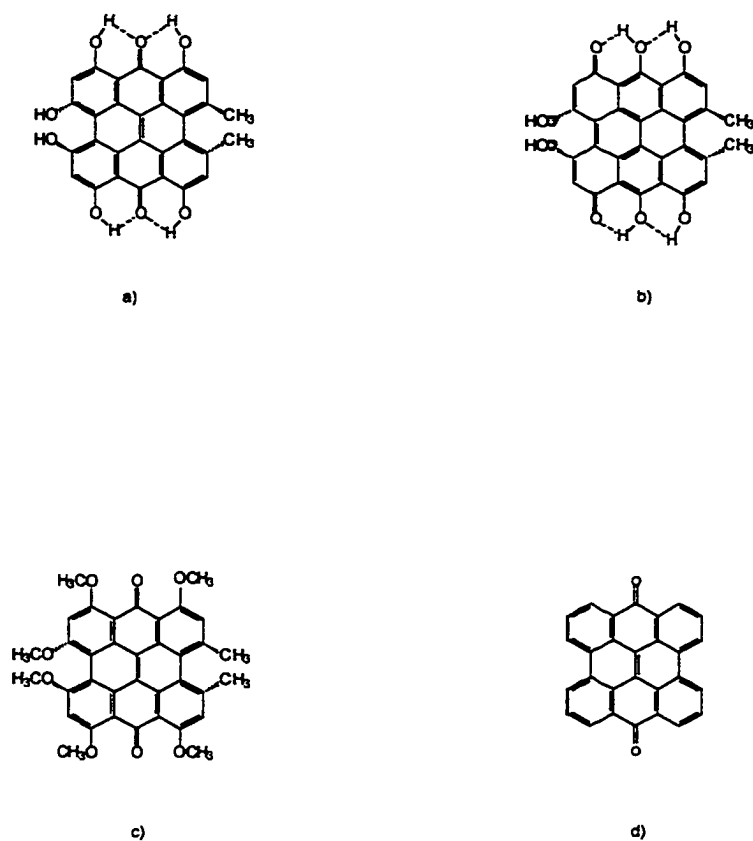


Figure 3.1 Structures of a) hypericin, b) one of the three possible hypericin double tautomers [7] (there are two possible monotautomers), c) *O*-hexamethoxy hypericin, and d) mesonaphthobianthrone.

when its carbonyl groups are protonated [6,7] (Figure 3.2). Previously, we have argued that the fluorescent state of hypericin grows in on a time scale of several picoseconds, based on transient absorption measurements interpreted in terms of the rise time of stimulated emission of one species and the concomitant decay of transient absorption of another species.

Therefore, the combined observations of the requirement of protonated carbonyls for strong hypericin-like fluorescence and the rise time of fluorescence in hypericin was taken as evidence for intramolecular excited-state proton transfer in hypericin [7,8]. This conclusion was further strengthened by a comparison of the transient absorbance of hypericin and its

methylated analog, *O*-hexamethoxy hypericin [9,10]. The assignment of proton transfer also was supported by the observation of a deuterium isotope effect of 1.4 in the excited-state transients of the hypericin analog, hypocrellin [13].

The interpretation of transient absorbance data, however, can be subject to complications because they measure ground-state bleaching, absorption of all excited states present (both singlet and triplet), and stimulated emission [9,10]. Because fluorescence upconversion monitors emission only from the fluorescent singlet state, it is not subject to these complications and hence provides complementary information not subject to the same ambiguities. The fluorescence upconversion measurements presented here clearly reveal a rising component of ~ 7 ps in the emission of hypericin and the absence of such a component in the emission of hexamethoxy hypericin, which cannot execute excited-state proton transfer.

Of special relevance to the role of labile protons for light-induced antiviral activity is the observation that hypericin acidifies its surroundings upon light absorption [15-17], and that it retains its toxicity in the absence of oxygen [18]. The retention of toxicity in the absence of oxygen excludes unique assignment of antiviral activity to the trivial generation of singlet oxygen--even though hypericin does generate triplets in high yield ($\sim 70\%$) [19-21]. Thus, the role of photogenerated protons takes on additional significance, especially in the context of the growing body of literature implicating pH decreases with pharmacologically important functions, such as virucidal activity [22], antitumor activity [23,24], apoptosis (a form of cell death associated with DNA fragmentation and chromatin condensation) [25-27], and the subcellular distribution of hexokinase [28]. We have proposed a chemiluminescent means of activating the pharmacological activity of hypericin and its analogs [1d, 29].

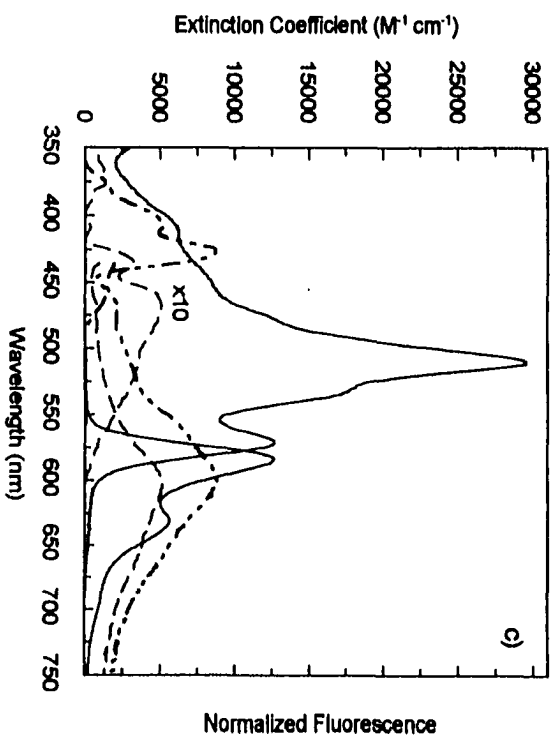
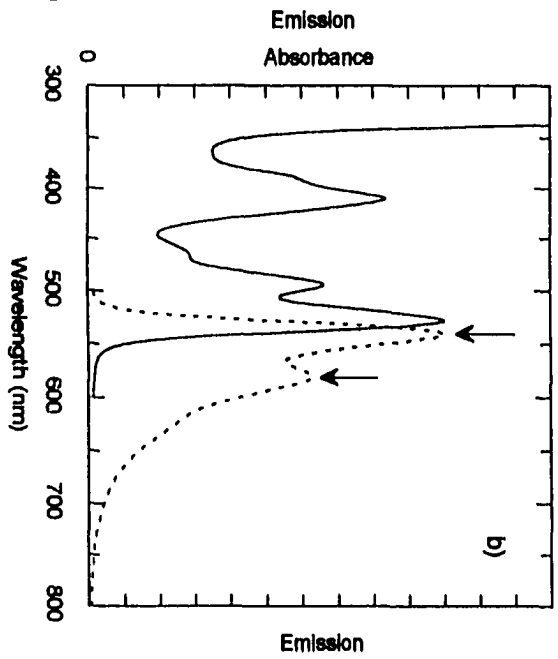
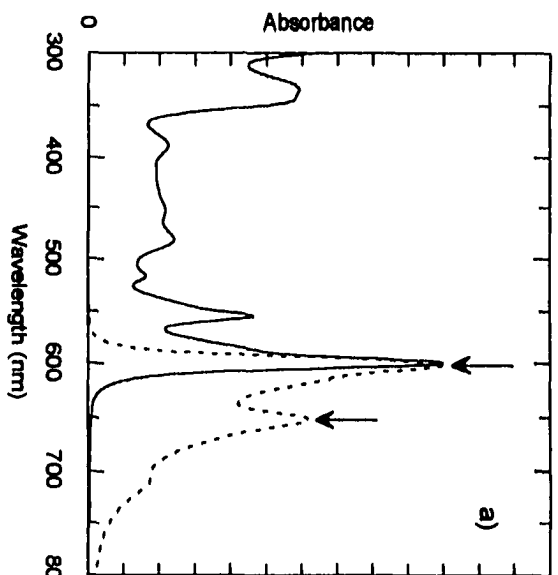
EXPERIMENTAL

Hypericin [Carl Roth GmbH (for transient absorption measurements) or Molecular Probes (for upconversion measurements)] was used as received. Anhydrous DMSO from Aldrich was used (freshly opened) without further purification. *O*-Hexamethoxy hypericin was prepared as described elsewhere [9], dissolved in DMSO, and kept under argon for both the upconversion and transient absorbance experiments. (Falk and Mayr have reported the synthesis of an *O*-hexamethoxy hypericin [30].) Storage under argon was necessary to prevent the hexamethoxy sample from degrading, possibly from singlet oxygen formation. Steady-state absorbance spectra were obtained on a Perkin Elmer Lambda 18 double-beam UV-vis spectrophotometer with 1-nm resolution. Steady state fluorescence spectra were obtained on a Spex Fluoromax with a 4-nm bandpass and corrected for detector response.

The apparatus for transient absorbance measurements is based on an amplified, homemade Ti:sapphire laser system producing pulses of less than 200 fs fwhm at a variable repetition rate as high as 10 kHz. This system is described in detail elsewhere [9].

The fluorescence upconversion apparatus is described in detail elsewhere [31,32] and is based on a Ti:sapphire oscillator (Spectra Physics, Tsunami) producing tunable (750-900 nm) 50-65-fs pulses. Frequency-doubled pulses are used to excite the sample. The residual fundamental wavelength is used as the gate pulse to upconvert the fluorescence, which is collected and focused into a 0.4-mm BBO crystal with an ellipsoidal reflector. The upconverted signal is separated from the gate beam, from the second and third harmonic beams, and from the fluorescence; and it is focused into a monochromator coupled to a Hamamatsu R760 photomultiplier selected for zero dark counts. The instrument response

Figure 3.2 Steady-state absorbance (—) and emission (—) spectra of (a) hypericin in DMSO and (b) *O*-hexamethoxyhypericin in DMSO. Also presented are emission and absorption spectra for mesonaphthobianthrone (mnb (c)) in DMSO (- - - -), methanol (—), and sulfuric acid (—). In panels a and b, the arrows denote the detection wavelengths selected for the transient absorbance and upconversion experiments. Mesonaphthobianthrone (mnb) was prepared (1d) according to the procedure of Koch *et al.* (39). A synthesis of this compound has also been reported by Falk and Vaisburg (14). The absorption spectra of mnb in DMSO and methanol are of higher quality than those presented earlier (1d,7) where the very weak features were hidden by scattering and other artifacts. Note, that the absorption spectra in these solvents are multiplied by a factor of 10 in order to compare them with those in sulfuric acid. In all cases, the emission spectra are normalized to have the same intensity as the corresponding absorption spectra. In order to compare the absorption and emission of hypericin with that of mnb, we cite their extinction coefficients and the fluorescence quantum yields of mnb *relative to that of hypericin in DMSO*. Hypericin/ethanol: $\epsilon(590 \text{ nm}) = 40\,000 \text{ cm}^{-1} \text{ M}^{-1}$ (40); $\phi_F = 1.00$ (the absolute value is conventionally taken as 0.3)(19). Mnb/DMSO: $\epsilon(428 \text{ nm}) = 850 \text{ cm}^{-1} \text{ M}^{-1}$; $\phi_F = 0.056$. Mnb/methanol: $\epsilon(468 \text{ nm}) = 510 \text{ cm}^{-1} \text{ M}^{-1}$; $\phi_F = 0.11$. Mnb/H₂SO₄: $\epsilon(510 \text{ nm}) = 3.0 \times 10^4 \text{ cm}^{-1} \text{ M}^{-1}$; $\phi_F = 1.5$. The extinction coefficients we have obtained for mnb in DMSO and methanol are subject to considerable uncertainty. Mnb is very insoluble in these solvents; light scattering from undissolved material, as well as the presence of impurities, contributes to the poor quality of the absorption spectra. Falk and Vaisburg (14) report $\epsilon(423 \text{ nm}) = 7000 \text{ cm}^{-1} \text{ M}^{-1}$ in DMSO. The spectra they obtain, especially in methanol, bear qualitative similarity to those presented here. The relative fluorescence quantum yields of mnb in DMSO and methanol must be considered to be upper limits, since even a small amount of highly fluorescent (i.e., long-lived) impurity can contribute to the measured value (10). The value obtained in H₂SO₄ is more certain than those obtained in DMSO or methanol, since in H₂SO₄ mnb is much more fluorescent and has a relatively long-lived fluorescence lifetime of 15 ns (7).



function is obtained by collecting a cross correlation function of the second harmonic and the fundamental: the resulting third harmonic is plotted against delay time. Cross correlation functions typically have a fwhm of 140-144 fs. All curves were fit and deconvoluted from the instrument function using an iterative convolute-and-compare nonlinear least-squares algorithm.

RESULTS AND DISCUSSION

Steady-state absorption and emission spectra for hypericin and *O*-hexamethoxy hypericin are given in Figure 3.2. Also included in Figure 3.2 are absorption and emission spectra for the simplest hypericin analog that we have investigated, mesonaphthobianthrone. As we note in the Introduction, this compound has played a pivotal role in our early investigation of the hypericin photophysics and in our identification of intramolecular proton (or atom) transfer as the primary photoprocess. The spectra presented here are of higher quality than those we have previously reported [7,1d]. Figure 3.3 presents a comparison of the fluorescence upconversion and transient absorption traces for hypericin and hexamethoxy hypericin in DMSO. The fluorescence upconversion signal for hypericin clearly shows a rising component (~ 7 ps), which is not present in hexamethoxy hypericin. (Preliminary data indicate an ~ 2.5 -ps rising component in ethanol). This result is consistent with results obtained using a pump wavelength of 588 nm, in which the rise time is fit to an ~ 11 -ps component.

The fluorescence upconversion signal of hypericin reveals significantly different kinetics in the first 40 picoseconds of the fluorescence decay at the two emission wavelengths investigated, 600 and 650 nm (compare Figure 3.3 and Figure 3.4). At 650 nm the ~ 7 ps

rising component is completely absent. As we discuss in the Conclusions section, these results support our previous suggestions that the ground state of hypericin is heterogeneous.

Figure 3.5 presents data collected on a shorter time scale. For both hypericin and hexamethoxy hypericin at both emission wavelengths, there is evidence of an ~100-fs rise time in the upconversion signal. These ultrafast 100-fs risetimes are not instrumental artifacts. The same upconversion spectrometer has been used to observe fluorescence decays for various photoinduced electron transfer systems with lifetimes of < 50 fs [32] as well as a series of subpicosecond to several-picosecond decays which have a definite risetime [31a]. In the case of risetimes observed for fluorescent coumarin excited singlet states being reductively quenched by aromatic amine solvents, there is good reason to assign these ~100-fs risetimes to inertial solvation dynamics, as the polar solvents librate about the very polar coumarin excited state [31b]. Solvation dynamics cannot, however, be invoked to explain the risetimes for the hypericins, as the emission displays only a small amount of solvatochromism, indicating a negligible difference between ground- and excited-state dipole moments for the hypericins. A likely assignment for the observed risetimes in the hypericins is internal conversion from a higher-lying singlet state, pumped by the ~415-nm laser pulses, to the lowest singlet excited state near 600 and 540 nm for hypericin and *O*-hexamethoxy hypericin, respectively. Chudoba et al. have also assigned such 100-fs transients to internal conversion for a different excited-state proton-transfer molecule, 2-(2'-hydroxy-5'-methylphenyl)benzotriazole [35]. Both in the Introduction and the Conclusion of this article, we note the potential ambiguities to which transient absorption measurements are subject. In this context, Figure 3.6 presents fits to previous transient absorption data in which the component previously described as a

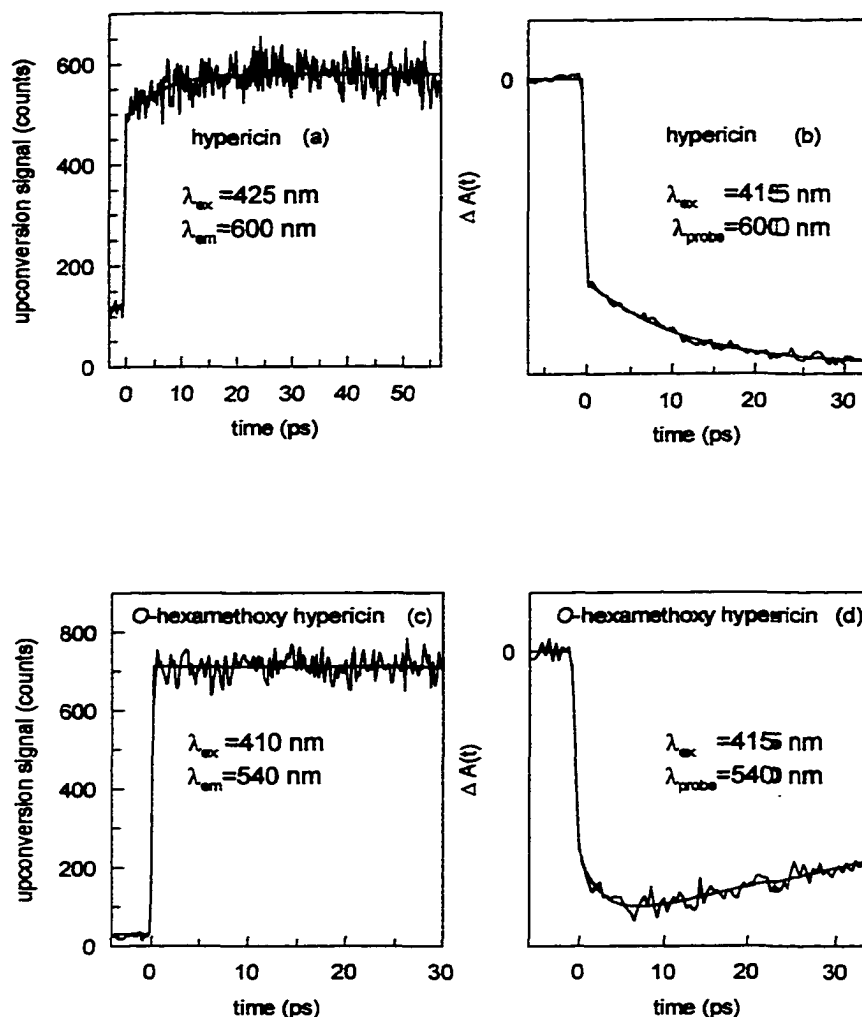


Figure 3.3 Comparison of fluorescence upconversion and transient absorbance traces for hypericin in DMSO at $\lambda_{em} = \lambda_{probe} = 600 \text{ nm}$ and for *O*-hexamethoxy hypericin in DMSO at $\lambda_{em} = \lambda_{probe} = 540 \text{ nm}$. These wavelengths correspond to the maxima in the steady state emission spectra of the respective compounds. In the absorption transients of *O*-hexamethoxy hypericin there is evidence for a rising component which is not present in the upconversion data. We have assigned this as a rise in the bleach that is attributed to a decay of excited state absorbance with a time constant of 2.6 ps. The data are fit to the following functions:

- $F(t) = -0.19 \exp(-t/7.3 \text{ ps}) + 1.0 \exp(-t/\infty)$
- $\Delta A(t) = 0.30 \exp(-t/11.6 \text{ ps}) - 1.00 \exp(-t/\infty)$
- $F(t) = 1.00 \exp(-t/\infty)$
- $\Delta A(t) = 0.11 \exp(-t/2.6 \text{ ps}) - 1.20 \exp(-t/480 \text{ ps}) + 0.89 \exp(-t/\infty)$

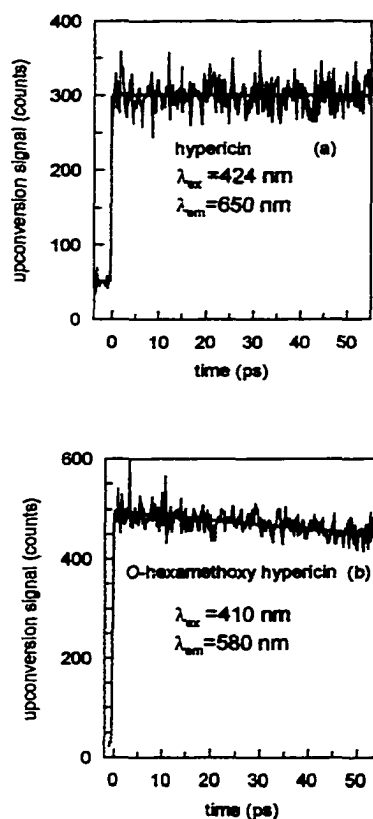


Figure 3.4 Fluorescence upconversion traces of hypericin at 650 nm and *O*-hexamethoxy hypericin at 580 nm. These wavelengths correspond to the second maxima (Figure 3.2) of the respective fluorescence spectra. The data are fit to the following functions:

- a) $F(t) = 1.00 \exp(-t/\infty)$
 b) $F(t) = 1.00 \exp(-t/503 \text{ ps})$

rise in stimulated emission is now attributed to a decay of one species whose excited-state absorption spectrum overlaps the emission spectrum of at least one other species.

Fluorescence anisotropy decays were constructed from upconversion signals polarized parallel and perpendicular to the excitation beam. These are displayed in Figure 3.7 for hypericin and hexamethoxy hypericin. Of significance is that excitation at 410 nm gives rises to a negative anisotropy, i.e., a negative prefactor, $r(0)$. Elsewhere [33] we have presented a

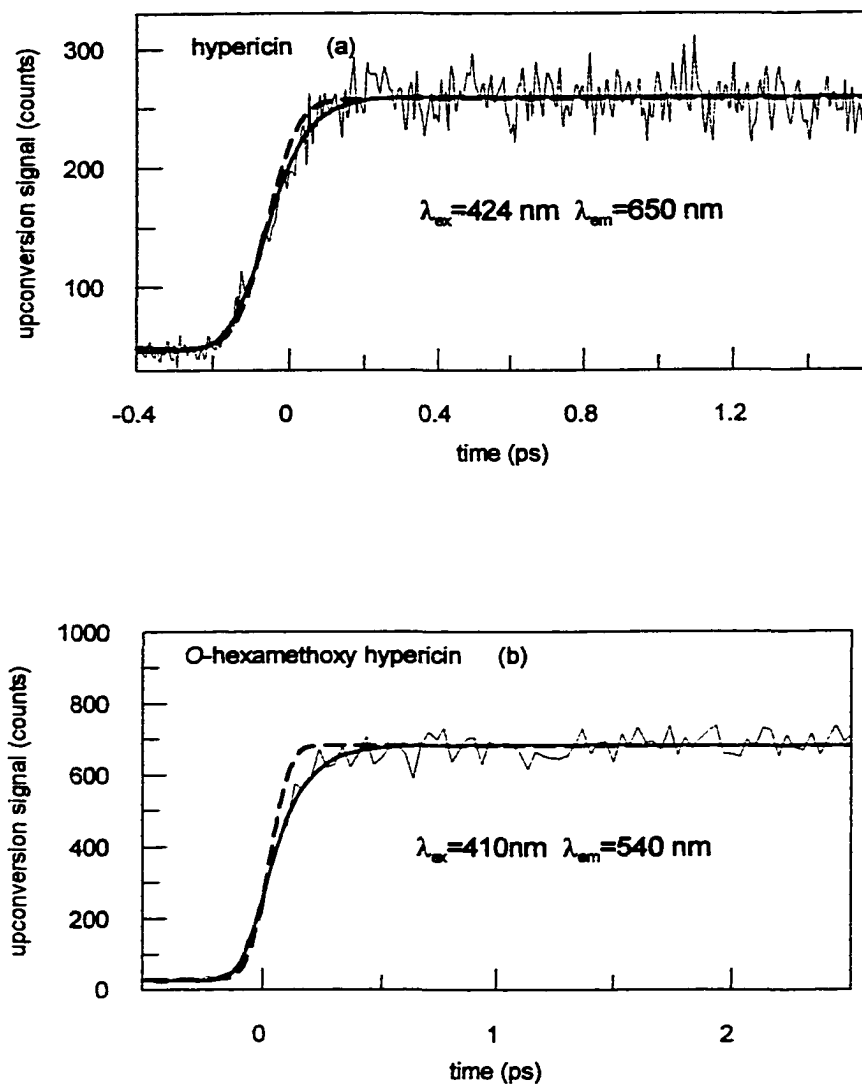


Figure 3.5 Observation of an ~ 100 -fs rise time in the fluorescence upconversion signal. The dashed lines are single exponential fits corresponding to an instantaneous risetime in the fluorescence signal. Fitting the rise of the fluorescence signal to a rise time yields (solid lines):
 (a) $F(t) = -0.91\exp(-t/64\text{ fs}) + 1.00\exp(-t/\infty)$
 (b) $F(t) = -0.83\exp(-t/114\text{ fs}) + 1.00\exp(-t/\infty)$

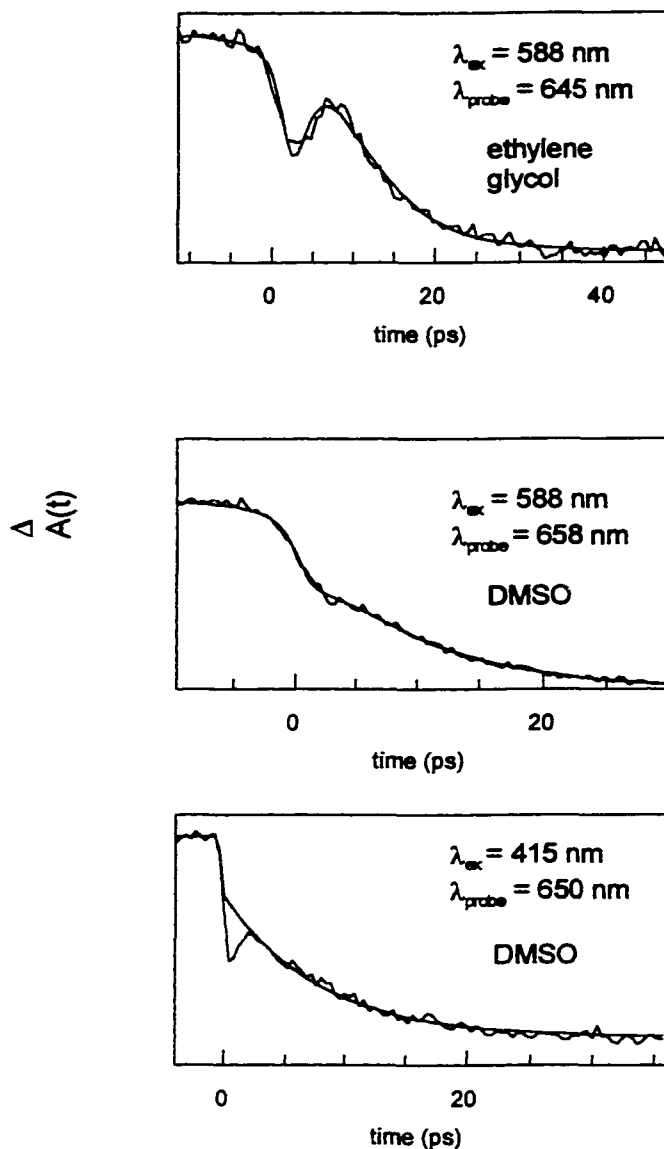


Figure 3.6 Reconsideration of previously obtained transient absorption signals for hypericin in the light of upconversion data presented here. Top: $\lambda_{ex} = 588$ nm, $\lambda_{probe} = 645$ nm, ethylene glycol (7,8); $\Delta A(t) = -0.56 \exp(-t/2.0 \text{ ps}) + 0.43 \exp(-t/6.4 \text{ ps}) - 0.19$. Middle: $\lambda_{ex} = 588$ nm, $\lambda_{probe} = 658$ nm, DMSO (7,8); $\Delta A(t) = -0.19 \exp(-t/2.0 \text{ ps}) + 0.27 \exp(-t/6.4 \text{ ps}) - 0.30$. Bottom: $\lambda_{ex} = 415$ nm, $\lambda_{probe} = 650$ nm, DMSO (9); $\Delta A(t) = 0.21 \exp(-t/8.0 \text{ ps}) - 0.29$. The spike at “zero time” is not considered in this fit because it is attributed to a cross-phase modulation artifact resulting from the ~ 150 fs pulses used in the experiment (9,10,41). It is unlikely that this is the case for the top trace, however, since the pulses used for this experiment were no shorter than 1 ps. In each case, the last term in the fit corresponds to a component that does not decay on the time scale of the experiment and that is attributed to the long-lived fluorescent species.

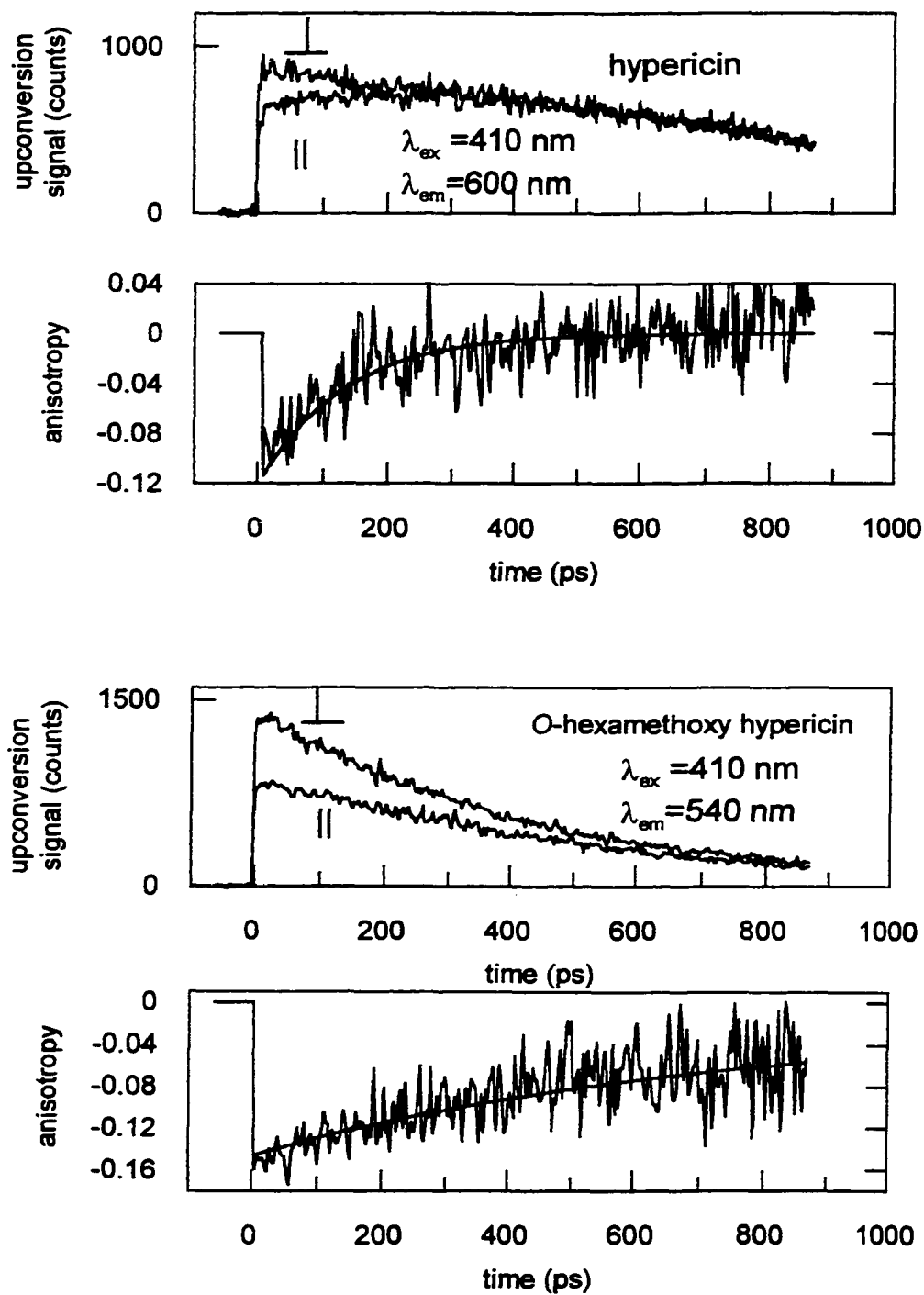


Figure 3.7 Polarized fluorescence traces and anisotropy curves.

Hypericin: $r(t) = -0.10 \exp(-t/192\text{ps})$.

O-hexamethoxy hypericin: $r(t) = -0.10 \exp(-t/621\text{ps}) - 0.05 \exp(-t/2.1\text{ns})$.

detailed investigation of the dependence of the steady-state fluorescence-excitation anisotropy and have observed similar behavior: depending on the excitation wavelength, the prefactor can be positive or negative. This results from the transition dipoles connecting the ground electronic state to the first two excited electronic states being at large angles to each other. If hypericin (which actually has a very twisted aromatic skeleton [13,34]) had C_{2v} symmetry, these transition dipoles would be orthogonal. Also of interest is that the time constant for the anisotropy decay for hexamethoxy hypericin is roughly three times greater than that for hypericin and does not decay to zero on the same time scale.

CONCLUSIONS

The fluorescence upconversion technique with 100-fs resolution was applied to hypericin and its synthetic analog, *O*-hexamethoxy hypericin. The results of these studies were compared with previous results obtained by means of transient absorption spectroscopy. Fluorescence upconversion is a powerful technique that is complementary to transient absorption. Transient absorption monitors all absorbing and emitting species (via stimulated emission), given an adequate signal-to-noise ratio. It is difficult, if not impossible, to distinguish ground-state bleaching from stimulated emission in regions where the emission spectrum overlaps the absorption spectrum. Also, emitting species may often be obscured by the presence of absorbing species (singlets and triplets) present in higher concentration or with a larger extinction coefficient. We have discussed and addressed these complications in previous work [7,9,10]. *Because the upconversion technique detects only emission from the excited state, the potential ambiguities in the transient absorption experiment referred to*

above are obviated. The fluorescence upconversion results presented here are in complete agreement with the major results and conclusions we have already presented: namely, that excited-state intramolecular proton (or atom) transfer is a primary photophysical event for hypericin and its analogs with labile protons. The upconversion results also validate the transient absorption technique as a means of monitoring proton or atom transfer rates in hypericin, assuming that the transient absorption spectrum is well understood.

In addition, the results presented here support our previous suggestions that the ground state of hypericin is heterogeneous [7,9,10], existing either as various tautomers or conformational isomers, and implies that the same argument can be made for hypocrellin and other hypericin analogs [11-13,33]. We originally suggested that the ground state of hypericin is heterogeneous in order to rationalize the mirror-image symmetry between its steady-state absorption and emission spectra [7,8]. Such symmetry is atypical of molecules whose excited states undergo nuclear rearrangements, such as proton or atom transfer. The archetypal excited-state proton-transfer system, 3-hydroxyflavone, provides a good example of the absence of such symmetry [36]. The transient absorption data obtained using different excitation wavelengths (415 and 588 nm) presented in Figure 3.6 yield different excited-state kinetics and are also suggestive of such heterogeneity. The upconversion results provide the most direct evidence to date for ground-state heterogeneity in hypericin at ambient temperatures [37]. Not only are the fluorescence profiles for hypericin different at the emission wavelengths of 600 and 650 nm, but even at 600 nm there are, in addition to the ~100-fs component, two components to the fluorescence risetime with 7-ps and

instantaneous" time constants. These may be attributed to untautomerized and tautomerized (or at least partially tautomerized) species.

ACKNOWLEDGMENTS

This work was supported in part by NSF grant CHE-9613962 to J. W. P. The fluorescence upconversion experiments were carried out at Brookhaven National Laboratory under contract DE-AC02-76CH00016 with the U. S. Department of Energy and supported by its Division of Chemical Sciences, Office of Basic Energy Sciences. We thank Professor H. Falk for comments regarding phenanthro[1,10,9,8,*o,p,q,r,a*]perylene-7-14-dione.

REFERENCES

1. a) Duran, N.; Song, P.-S. *Photochem. Photobiol.* **1995**, *61*, 529-539. b) Diwu, Z. *Photochem. Photobiol.* **1995**, *61*, 529-539. c) Lown, J. W. *Can. J. Chem.* **1997**, *75*, 99-119. d) Kraus, G. A.; Zhang, W.; Fehr, M. J.; Petrich, J. W.; Wannemuehler, Y.; Carpenter, S. *Chem. Rev.* **1996**, *96*, 523-535.
2. a) Meruelo, D.; Lavie, G.; Lavie, D. *Proc. Natl. Acad. Sci. USA* **1988**, *85*, 5230-5234. b) Degar, S.; Prince, A. M.; Pascual, D.; Lavie, G.; Levin, B.; Mazur, Y.; Lavie, D.; Ehrlich, L. S.; Carter, C.; Meruelo, D. *AIDS Res. Hum. Retroviruses* **1992**, *8*, 1929-1936. c) Lenard, J.; Rabson, A.; Vandroef, R. *Proc. Natl. Acad. Sci. USA* **1993**, *90*, 158-162. d) Meruelo, D., Degar, S., Nuria, A., Mazur, Y., Lavie, D., Levin B., and Lavie, G. In *Natural Products as Antiviral Agents*; Chu, C. K.; Cutler, H. G., Eds.; Plenum Press: New York, 1992; pp 91-119 and references therein.

3. Hudson, J. B.; Zhou, J.; Chen, J.; Harris, L.; Yip, L.; Towers, G. H. N. *Photochem. Photobiol.* **1994**, *60*, 248-254.
4. Thomas, C.; Pardini, R. S. *Photochem. Photobiol.* **1992**, *55*, 831-837.
5. Carpenter, S.; Kraus, G. A. *Photochem. Photobiol.* **1991**, *53*, 169-174.
6. Gai, F.; Fehr, M. J.; Petrich, J. W. *J. Am. Chem. Soc.* **1993**, *115*, 3384-3385.
7. Gai, F.; Fehr, M. J.; Petrich, J. W. *J. Phys. Chem.* **1994**, *98*, 5784-5795.
8. Gai, F.; Fehr, M. J.; Petrich, J. W. *J. Phys. Chem.* **1994**, *98*, 8352-8358.
9. English, D. S.; Zhang, W.; Kraus, G. A.; Petrich, J. W. *J. Am. Chem. Soc.* **1997**, *119*, 2980-2986.
10. English, D. S.; Das, K.; Zenner, J. M.; Zhang, W.; Kraus, G. A.; Larock, R. C.; Petrich, J. W. *J. Phys. Chem.* **1997**, *101A*, 3235-3240.
11. Das, K.; English, D. S.; Fehr, M. J.; Smirnov, A. V.; Petrich, J. W. *J. Phys. Chem.* **1996**, *100*, 18275-18281.
12. Das, K.; English, D. S.; Petrich, J. W. *J. Am. Chem. Soc.* **1997**, *119*, 2763-2764.
13. Das, K.; English, D. S.; Petrich, J. W. *J. Phys. Chem.* **1997**, *101A*, 3241-3245.
14. This compound is more correctly referred to as phenanthro[1,10,9,8,*o,p,q,r,a*]perylene-7-14-dione. Falk, H.; Vaisburg, A. F. *Monatshefte fhr Chemie* **1995**, *126*, 361-364.
15. Fehr, M. J.; McCloskey, M. A.; Petrich, J. W. *J. Am. Chem. Soc.* **1995**, *117*, 1833-1836.
16. Fehr, M. J.; Carpenter, S. L.; Wannemuehler, Y.; Petrich, J. W. *Biochemistry* **1995**, *34*, 15845-15848.

17. a) Sureau, F.; Miskovsky, P.; Chinsky, L.; Turpin, P. Y. *J. Am. Chem. Soc.* **1996**, *118*, 9484-9487. b) Chaloupka, R.; Sureau, F.; Kocisova, E.; Petrich, J. W. *J. Am. Chem. Soc.*, submitted.
18. Fehr, M. J.; Carpenter, S. L.; Petrich, J. W. *Bioorg. Med. Chem. Lett.* **1994**, *4*, 1339-1344.
19. Racinet, H.; Jardon, P.; Gautron, R. *J. Chim. Phys.* **1988**, *85*, 971-977.
20. Eloy, D.; Le Pellec, A.; Jardon, P. *J. Chim. Phys.* **1996**, *93*, 442-457.
21. Jardon, P.; Gautron, R. *J. Chim. Phys.* **1989**, *86*, 2173-2190.
22. Pinto, L. H.; Holsinger, L. J.; Lamb, R. A. *Cell* **1992**, *69*, 517-528.
23. Newell, K. J.; Tannock, I. F. *Cancer Res.* **1989**, *49*, 4447-4482.
24. Newell, K. J.; Wood, P.; Stratford, I.; Tannock, I. *Br. J. Cancer* **1992**, *66*, 311-317.
25. Barry, M. A.; Reynold, J. E.; Eastman, A. *Cancer Res.* **1993**, *53*, 2349-2357.
26. Li, J.; Eastman, A. *J. Biol. Chem.* **1995**, *270*, 3203-3211.
27. Gottlieb, R. A.; Nordberg, J.; Skowronski, E.; Babior, B. M. *Proc. Natl. Acad. Sci. USA.* **1996**, *93*, 654-658.
28. Miccoli, L.; Oudard, S.; Sureau, F.; Poirson, F.; Dutrillaux, B.; Poupon, M. F. *Biochem. J.* **1995**, *313*, 957-962.
29. Carpenter, S.; Fehr, M. J.; Kraus, G. A.; Petrich, J. W. *Proc. Natl. Acad. Sci. USA* **1994**, *91*, 12273-12277.
30. Falk, H.; Mayr, E. *Monatshefte für Chemie* **1995**, *126*, 699-710.
31. a) Castner, E. W., Jr. manuscript in preparation. b) Horng, M. L.; Gardecki, J. A.; Papazyan, A.; Maroncelli, M. *J. Phys. Chem.* **1995**, *99*, 17311-17337. c) Rosenthal,

- S. J.; Jiminez, R.; Fleming, G. R.; Kumar, P. V.; Maroncelli, M., *Journal of Molecular Liquids* **1994**, *60*, 25-56.
32. Murakoshi, K.; Yanagida, S.; Capel, M.; Castner, E. W., Jr. "Interfacial electron transfer dynamics of photosensitized zinc oxide nanoclusters," ACS Symposium Series 679: Nanostructured Materials-Clusters, Thin Films, and Composites. Shalaev, V. and Moskovits, M., Chapter 17, eds., 221-238 (American Chemical Society, 1997).
33. Das, K.; Dertz, E.; Paterson, J.; Zhang, W.; Kraus, G. A.; Petrich, J. W. *J. Phys. Chem. B* **1998**, *102*, 1479-1484
34. a) Etlzstorfer, C.; Falk, H.; Müller, N.; Schmitzberger, W.; Wagner, U. G. *Monatsh. Chem.* **1993**, *124*, 751-761. b) Falk, H., personal communication. c) Freeman, D.; Frolow, F.; Kapinus, E.; Lavie, D.; Lavie, G.; Meruelo, D.; Mazur, Y. *J. Chem. Soc., Chem. Commun.* **1994**, 891-892.
35. Chudoba, D.; Riedle, E.; Pfeiffer, M.; Elsaesser, T. *Chem. Phys. Lett.* **1996**, *263*, 622-628.
36. a) Brucker, G. A.; Swinney, T. C.; Kelley, D. F. *J. Phys. Chem.* **1991**, *95*, 3190-3195. b) Strandjord, A. J. G.; Barbara, P. F. *J. Phys. Chem.* **1985**, *89*, 2355-2361. c) McMorro, D.; Kasha, M. *J. Phys. Chem.* **1984**, *88*, 2235-2243. d) Brucker, G. A.; Kelley, D. F. *J. Phys. Chem.* **1987**, *91*, 2856-2861. e) Schwartz, B. J.; Peteanu, L. A.; Harris, C. B. *J. Phys. Chem.* **1992**, *96*, 3591-3598.
37. a) Arabei, S. M.; Galaup, J. P.; Jardon, P. *Chem. Phys. Lett.* **1995**, *232*, 127-134. b) Pschierer, H.; Friedrich, J.; Falk, H.; Schmitzberger, W. *J. Phys. Chem.* **1993**, *97*, 6902-6906.

38. Intramolecular proton or atom transfer is not, however, the only process of which excited-singlets of hypericin are capable. In addition to intersystem crossing [19-21], Song and coworkers have demonstrated the ability of *the long-lived fluorescent state* to transfer an electron to a series of acceptors. Wells, T. A.; Losi, A.; Dai, R.; Scott, P.; Park, S.-M.; Golbeck, J.; Song, P.-S. *J. Phys. Chem.* **1997**, *101A*, 366-372.
39. Koch, W.; Saito, T. Yoshida, Z. *Tetrahedron* **1972**, *28*, 3191.
40. Jardon, P.; Lazortchak, N.; Gautron, R. *J. Chim. Phys.* **1986**, *83*, 311-315.
41. Diels, J.-C.; Rudolph, W. *Ultrashort Laser Pulse Phenomena*; Academic Press: San Diego, 1996; p 142.

CHAPTER 4. IS THE EXCITED-STATE H-ATOM TRANSFER IN HYPERICIN CONCERTED?

A paper accepted in Photochemistry and Photobiology

J. Park, A. Datta, P. K. Chowdhury, and J. W. Petrich*

ABSTRACT

The excited-state intramolecular H-atom transfer of hypericin (Hyp) was investigated as a function of pH in monodispersed reverse micelles formed by sodium bis(2-ethylhexyl)sulfosuccinate/heptane/water and in complexes with Tb^{3+} under conditions in which one of the two carbonyl groups of Hyp is incapable of accepting a hydrogen atom. The results of pump-probe transient absorption experiments provide no evidence for a concerted H-atom transfer mechanism.

INTRODUCTION

Hypericin (Hyp) (Fig. 4.1) is one of many naturally and commonly occurring perylene quinone pigments that have stimulated great interest because of their broad spectrum of light-induced biological activities (1-5), among which are light-induced virucidal activity against several types of viruses, including the human immunodeficiency virus (HIV) (6-8), as well as antiproliferative and cytotoxic effects on tumor cells (9-11). Owing to this important biological activity, over the past few years we have been studying the photophysics of Hyp and its analogs (12-24). By means of H/D substitution, investigation of *O*-methylated

Department of Chemistry, Iowa State University, Ames, Iowa 50011-3111.

*Authors to whom correspondence should be addressed.

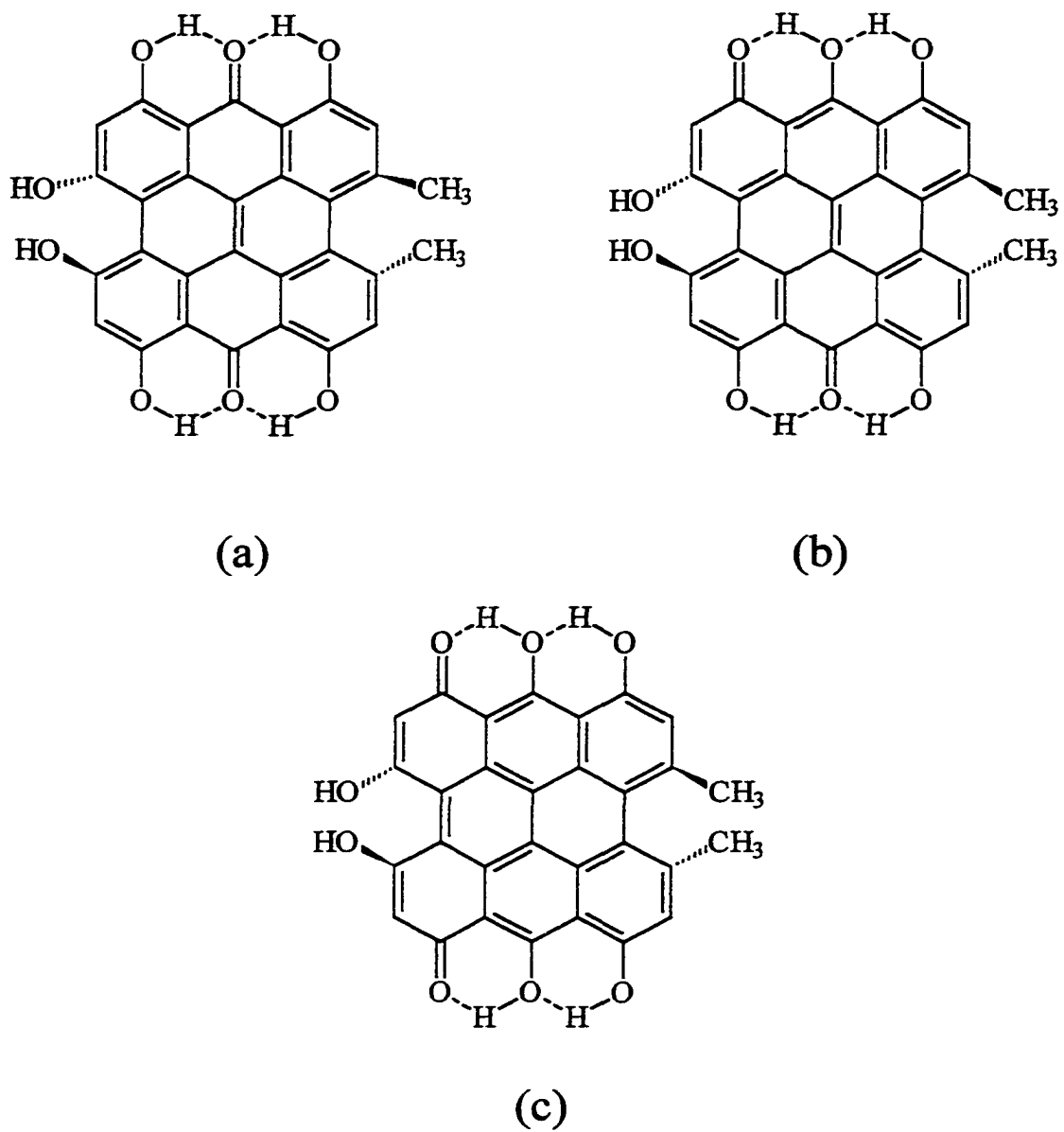


Figure 4.1 Structures of hypericin: (a) “normal” form (b) monotaomer form and (c) double tautomer form.

analogs, and complementary studies using both transient absorption and fluorescence upconversion spectroscopies, we have argued that the major primary photophysical process in organic solvents is excited-state hydrogen atom transfer.

Given the structure of hypericin, with two sets of two hydroxyl groups *peri* to a carbonyl, one is naturally inclined to inquire how many hydrogen atoms are transferred in the excited state and, if more than one is transferred, whether the process is stepwise or concerted. (It is useful to note the difference between a concerted and a synchronous reaction. A concerted reaction takes place in a single kinetic step, with no reaction intermediate, where some of the changes in bonding take place to different extents in different parts of the reaction. A synchronous reaction is one where all the bond-making and bond-breaking processes take place at the same time and proceed at the same extent during the reaction (25, 26). It is a common error to assume that concertedness implies synchrony.)

We have previously observed that when Hyp is bound to human serum albumin (HSA), it no longer undergoes an excited-state hydrogen atom transfer. Assuming that the binding occurs through the interaction of one of the two carbonyl groups of hypericin and the N₁-H of the single tryptophan residue (W214), which would necessarily impede H-atom transfer on this half of the Hyp molecule, we suggested that the absence of H-atom transfer in the complex was indicative of concerted, double H-atom transfer in the excited state of Hyp (20).

Here, we investigate the effects that are induced by impeding the excited-state H-atom transfer by protonating one of the carbonyl groups of Hyp, or by complexing it with a metal ion, such as Tb³⁺. Jordan and coworkers (27-32) have produced a large body of careful work on the steady state spectra and the triplet photophysics of Hyp in various conditions.

They were the first to study Hyp as a function of pH in Brij-35 micelles (27) and the triplet-state photophysics of Hyp/metal complexes (33).

MATERIALS AND METHODS

Hypericin was purchased from Molecular Probes and was used as received. Sodium bis(2-ethylhexyl)sulfosuccinate (AOT) purchased from Sigma Chemical Co. (St. Louis, MO), was purified by dissolving in methanol and stirring it overnight in the presence of activated charcoal. Subsequent filtration and removal of methanol by distillation under vacuum yielded AOT suitable for use. Spectrophotometric grade heptane (Hep) purchased from Aldrich was refluxed over calcium hydride and collected by distillation before use. $\text{TbCl}_3 \cdot 6\text{H}_2\text{O}$ was obtained from Aldrich.

Preparation of Sample: Reverse micelles formed by dissolving AOT in Hep provide an ideal system because their size and properties may be very well controlled. AOT/ H_2O reverse micelles are well characterized regarding their size, shape and the number of AOT molecules per aggregate, *i.e.* the aggregation number (34). Addition of water to AOT/alkane solutions produces systems that resemble small water pools in bioaggregates (34). The polarity of the AOT/alkane solutions increases with the fraction of water inside the pool, with the stability of the micelles being determined by the concentration ratio: $w_0 = [\text{H}_2\text{O}]/[\text{AOT}]$. The nature of the water present in reverse micelles, as well as the interactions between reverse micelles and small molecules, has been discussed in a recent review by Siber *et al.* (35). Eastoe *et al.* have shown that the microemulsion droplets are spherical for Na^+ and Ca^{2+} counterions, but become rod-shaped for Co^{2+} , Ni^{2+} , Cu^{2+} and Zn^{2+} counterions (36). At the very low probe to surfactant ratio used in our studies, it can be safely assumed

that the structure of the reverse micelles are not affected to any serious extent by the presence of Hyp or its ions. The solution of AOT in Hep was prepared in such a way that the concentration was 0.9 M. Hypericin is insoluble in Hep and dissolves very slowly in the AOT/Hep reverse micellar system. On addition of water, however, hypericin dissolves much more readily. The color of the reverse micellar system with hypericin was red at low pH and at intermediate pH values, while at a pH of 13, the solution had a dark green color. The basic solution, however, slowly reverts to the red color characteristic of Hyp in AOT/Hep, indicating a gradual shifting of the equilibrium towards the “normal” form (the 7,14 diketo tautomer, displayed in Figure 4.1a). The concentration of Hyp was kept at $\sim 10^{-4}$ M (such a concentration of Hyp was necessary to obtain a sufficiently large signal in pump-probe transient absorption experiments). The pH was maintained by HCl of appropriate molarity and its subsequent neutralization by 0.1 M NaOH solution. The pH was recorded by a manual Fisher-Accumet (955) Mini pH meter. All measurements were carried out at 298K.

To determine the stoichiometry of the Hyp/Tb³⁺ complexes, a Job plot was constructed using 5×10^{-5} M solutions of Hyp and TbCl₃·6H₂O, in varying proportions, keeping the total volume constant. The solutions were allowed to stabilize overnight before absorbance measurements of the complex were performed at 680 nm, a wavelength where free Hyp does not absorb. Absorption and emission spectra of the complex are given in Figure 3. In order to determine the binding constant for the complex, a Benesi Hildebrand plot was constructed, assuming a 1:1 stoichiometry obtained from the Job plot. The concentration of hypericin was 1×10^{-5} M. The concentration of TbCl₃ was varied from 2×10^{-4} M to 2×10^{-3} M. A large excess of the terbium salt was used in order to satisfy the condition that the equilibrium concentration of the metal ion was practically the same as the

initial concentration. Absorption measurements were performed at 640 nm. To prepare the Hyp /terbium complexes for the pump probe experiment, a solution of 5×10^{-4} M Hyp in ethanol was prepared and solid $\text{TbCl}_3 \cdot 6\text{H}_2\text{O}$ was added to make the solution 0.2 M in the salt. The Hyp: TbCl_3 ratio was maintained at 1:400 in order to make sure that practically all the hypericin molecules were in the chelated form and there was no signal from free Hyp.

Spectroscopic Measurements: Steady-state absorption spectra were recorded on a Perkin-Elmer Lambda-18 double-beam UV-visible spectrophotometer with 1-nm resolution. Steady-state fluorescence spectra (both excitation and emission), were obtained on a SPEX Fluoromax with a 4-nm bandpass (a smaller bandpass, up to 2-nm, was used in some cases to avoid saturating the detector to preserve linearity in response), and corrected for detector response. For both fluorescence and absorption measurements, a 1-cm path-length quartz cuvette was used.

The apparatus for pump-probe transient absorption measurements and the analysis of the kinetic data are described in detail elsewhere (23, 37).

RESULTS AND DISCUSSION

Effect of Protonating the Carbonyl Group

The effect of pH on the absorption and emission spectra of Hyp in AOT reverse micelles is given in Figure 4.2. The length of the hydrocarbon chain of AOT is 9 Å. Because the hydrocarbon chain is shorter than both dimensions of Hyp (major axis, 10.5 Å; minor axis, 9.6 Å), it is most likely that two *peri* hydroxyl and the intervening carbonyl groups of Hyp protrude into the polar core (38). It is very improbable that any significant amount of water permeates the extremely apolar and hydrophobic chains of the AOT (39, 40)

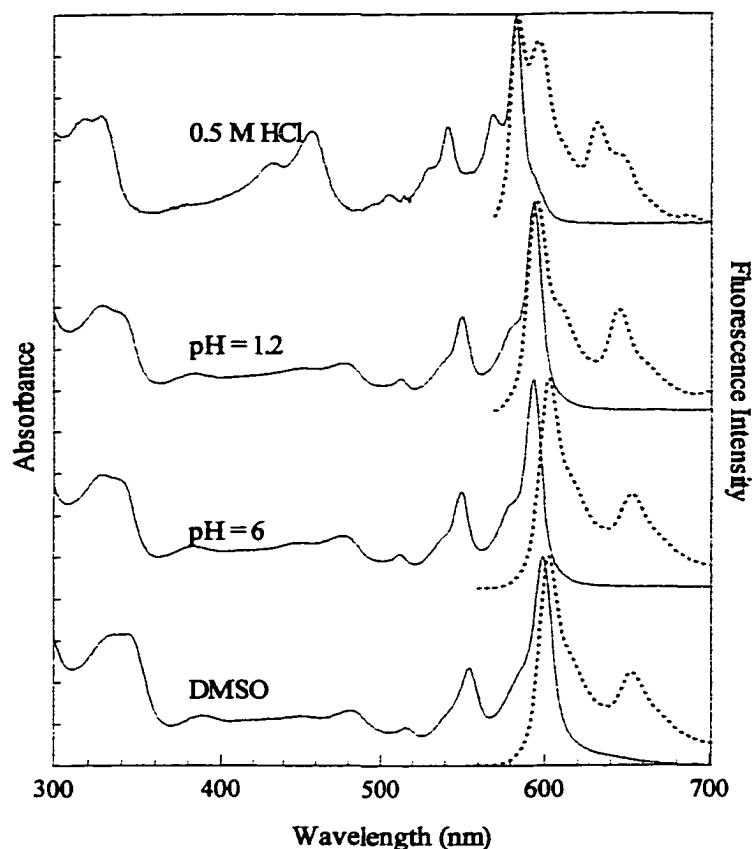


Figure 4.2. Absorption (—) and emission (----) spectra of hypericin (5×10^{-4} M) in dimethylsulfoxide and in AOT/water/*n*-heptane reverse micelle ($w_0 = 2$) at different concentrations of HCl (pH = 6, 1.2 and 0.5 M HCl). We were unable to probe more acidic environments due to the instability of the reverse micelles under such extreme conditions. The excitation wavelength for the emission spectra is 550 nm. For $[AOT] = 0.9$ M and $[Hyp] = 5 \times 10^{-4}$ M there are about 100 micelles for every Hyp molecule. It should be noted that we use the term “pH” to refer to the pH of the water prior to addition to the reverse micellar system. The effective pH within the reverse micelles is expected to be correlated, but not identical to these pH values. As pointed out by El Seoud (42), the apparent pK_a in the reverse micellar system differs from that in bulk water due to a combination of medium and electrostatic effects.

, and hence, this environment is very unlikely to accommodate H^+ or OH^- , or any charged species. We thus conclude that in AOT reverse micelles, the only groups of Hyp susceptible to titration are those protruding into the polar core.

From the results summarized in Table 4.1, a clear rise in the stimulated emission, with a time constant of 10 ps, is observed in the transient absorption kinetics of hypericin in AOT reverse micelles, both in 0.5 M HCl, where the exposed carbonyl groups are expected to be completely protonated, and at pH 6, where they remain fully unprotonated. Thus, protonation of the carbonyl group in the reverse micelles does not impede the H-atom transfer of the part of the molecule buried in the hydrophobic portion of the micelle. The complementary experiment of measuring the kinetics when the *peri* hydroxyls are deprotonated could not be performed because Hyp /AOT is unstable at pH > 12 (38).

Table 4.1. Global fitting parameters for hypericin in AOT/water/n-heptane reverse micelles ($w_0=2$)^{*}

0.5 M HCl	a_1	τ_1 (ps)	a_2
590 nm	0.01	10.5	-0.16
596 nm	0.05	10.5	-0.17
600 nm	0.03	10.5	-0.16
Neutral pH			
590 nm	0.04	10.3	-0.16
596 nm	0.04	10.3	-0.16
600 nm	0.02	10.3	-0.16

^{*}Transient absorption data are fit to the function: $\Delta A(t) = a_1 \exp(-t/\tau_1) + a_2 \exp(-t/\tau_2)$. The preexponential factors are all normalized and should not be interpreted in terms of absolute optical density changes owing to changes in pump intensities and gain settings on data acquisition hardware. In all cases, $\tau_2 = \infty$ since the time scale on which the experiment is performed does not permit its determination.

Effect of Chelating the Carbonyl Group to Tb^{3+}

The steady-state spectra of the Hyp/ Tb^{3+} complex are given in Figure 4.3. Its stoichiometry is 1:1 and its binding constant is 1.6×10^4 . The small peaks at 590 and 620 nm likely arise from the very few Hyp molecules that are not chelated. We have measured the quantum yield of the chelate to be 5×10^{-5} , approximately 600 times less than that of free Hyp; thus, even a very small amount of the free molecule is sufficient to give rise to a perceptible fluorescence intensity. Under our experimental conditions, only one carbonyl is chelated. Transients of 10 ps are observed in the traces obtained at probe wavelengths ranging from 520-650 nm (Table 4.2 and Figure 4.4); but it is unlikely that they result from excited-state H-atom transfer. This time constant reflects, rather, the lifetime of the first excited singlet state of the complex, which decays rapidly owing to intersystem crossing.

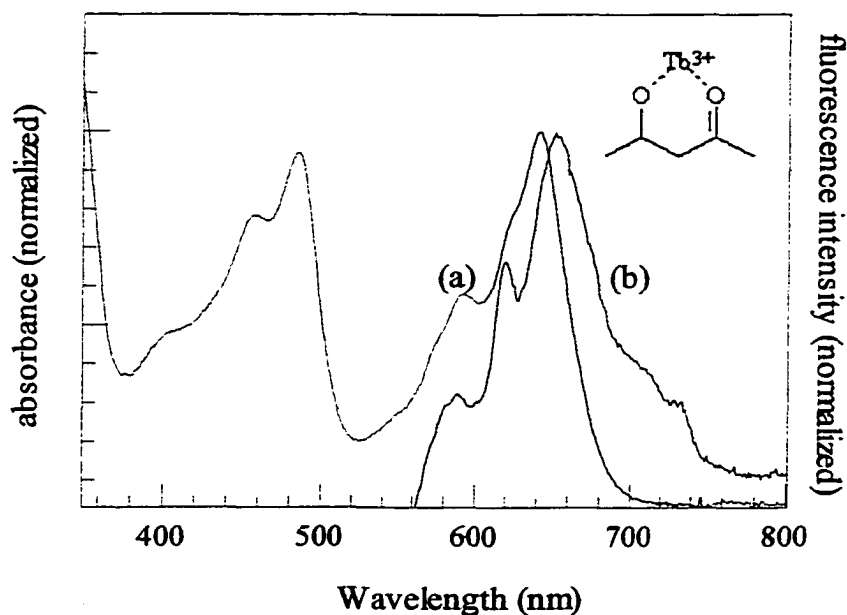


Figure 4.3. Absorption (a) and emission (b) spectra of Hyp/ Tb^{3+} complex in ethanol. The concentrations of hypericin and $\text{TbCl}_3 \cdot 6\text{H}_2\text{O}$ are 1.1×10^{-5} M and 4×10^{-3} M, respectively. The spectra are normalized to the reddest absorption maximum. The excitation wavelength for the emission spectrum is 490 nm.

Table 4.2. Global fitting parameters for the hypericin/Tb³⁺ complex in ethanol*

	a ₁	τ ₁ (ps)	a ₂
520 nm	-0.32	10.2	0.97
530 nm	0.00	10.2	0.97
550 nm	0.00	10.2	0.90
570 nm	0.29	10.2	0.59
580 nm	1.27	10.2	-0.18
600 nm	-0.69	10.2	-0.24
630 nm	-0.76	10.2	-0.36
650 nm	-0.77	10.2	-0.36

*Transient absorption data are fit to the function: $\Delta A(t) = a_1 \exp(-t/\tau_1) + a_2 \exp(-t/\tau_2)$. The preexponential factors are all normalized and should not be interpreted in terms of absolute optical density changes owing to changes in pump intensities and gain settings on data acquisition hardware. In all cases, $\tau_2 = \infty$ since the time scale on which the experiment is performed does not permit its determination.

The rise of the triplet species is evident at 520 nm, the maximum of the triplet-triplet absorption spectrum of free Hyp and the complex (33). The negative-going signals from 630-650 nm are attributed to the ground-state bleaching of the complex. We conclude that any component of stimulated emission with a 10 ps rise time is too weak to be detected. Its presence is obfuscated by the concomitant 10 ps decay of excited-state absorbance, most clearly evident at 580 nm.

CONCLUSIONS

The results presented above indicate that excited-state H-atom transfer occurs in Hyp even when one of the carbonyls is prohibited from accepting a hydrogen. The presence of such a transfer is apparent under very acidic conditions in AOT reverse micelles and cannot be excluded upon chelation of Tb³⁺. There is, thus, no evidence for a concerted hydrogen-atom transfer mechanism in hypericin. We are, however, unable to conclude from the

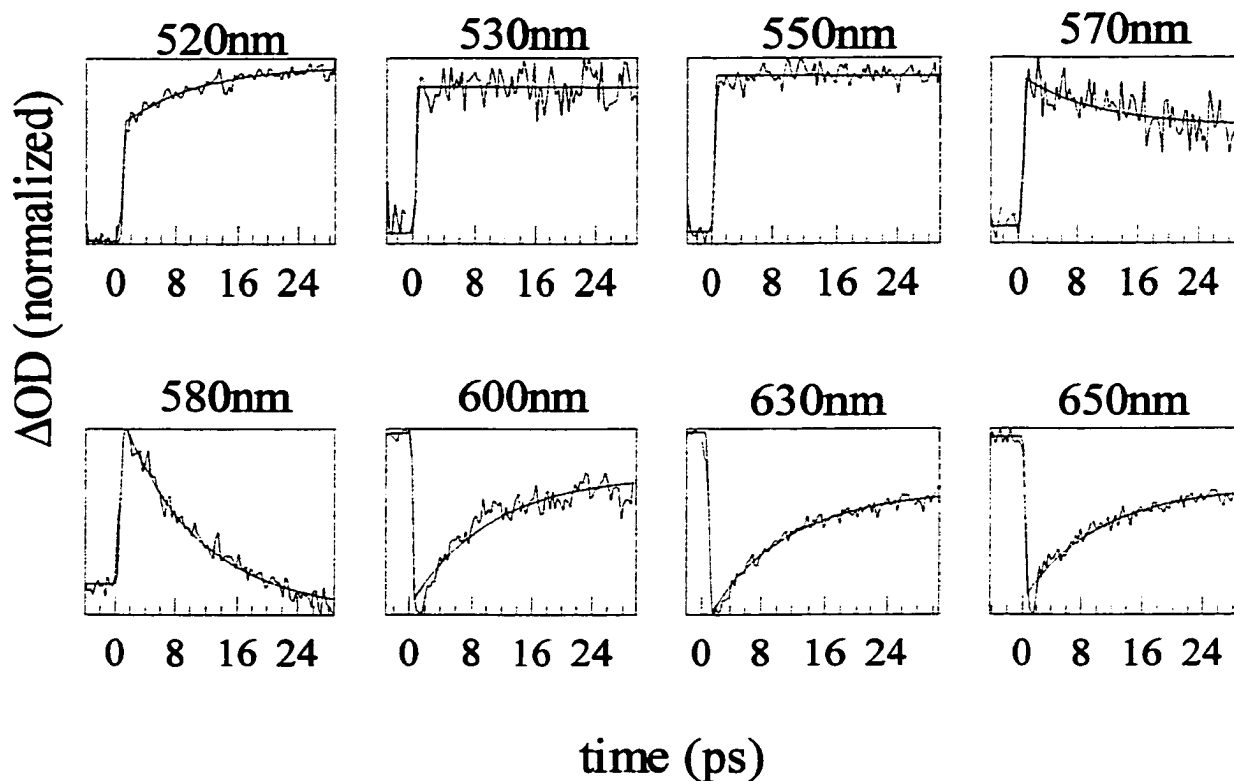


Figure 4.4. Transient absorbance traces of the Hyp/Tb³⁺ complex in ethanol at probe wavelengths of (a) 520 nm, (b) 530 nm, (c) 550 nm, (d) 570 nm, (e) 580 nm, (f) 600 nm, (g) 630 nm and (h) 650 nm. The pump wavelength was 407 nm. The concentrations of Hyp and TbCl₃ were 5×10^{-4} M and 0.2 M, respectively. The global fits to these decays are presented in Table 5.2.

present study if only one hydrogen atom is transferred or if two are transferred in a stepwise fashion. It remains, then, to question why H-atom transfer is completely impeded when hypericin binds to HSA (20). The answer may lie in the requirement for skeletal motion to be coupled to the H-atom transfer (41, 24). Fluorescence anisotropy measurements of the HSA/hypericin complex indicate that the Hyp is rigidly bound and that there is no rapid restricted motion of Hyp relative to the protein. Although this response is plausible, it is not easy to reconcile it with the observation that Hyp undergoes H-atom transfer in a glass at low temperatures (21), where the amplitude of skeletal motion would seem to be less than that in

the HSA matrix. One would need to conclude from the two observations that the protein provides a more constrained environment than the glass. These sorts of problems and questions continue to illustrate the need for further elucidation of the reaction coordinate for the H-atom transfer in Hyp and its analogs (24).

ACKNOWLEDGEMENTS

This work was supported by NSF grant CHE-9613962 to J. W. P. We thank Professor Pierre Jardon for useful discussions.

REFERENCES

1. Duran, N., and P. S. Song. (1986). Hypericin and its photodynamic action. *Photochem. Photobiol.* **43**, 677-680.
2. Lown, J. W. (1997). Photochemistry and photobiology of perylenequinones. *Can. J. Chem.* **75**, 99-119.
3. Diwu, Z. (1995). Novel therapeutic and diagnostic applications of hypocrellins and hypericins. *Photochem. Photobiol.* **61**, 529-539.
4. Kraus, G. A., W. Zhang, M. J. Fehr, J. W. Petrich, Y. Wannemuehler, and S. Carpenter. (1996). Research at the Interface between Chemistry and Virology: Development of a Molecular Flashlight. *Chem. Rev.* **96**, 523-535.
5. Falk, H. (1999). From the Photosensitizer Hypericin to the Photoreceptor Stentorin-- The Chemistry of Phenanthroperylene Quinones. *Angew. Chem. Int. Ed.* **38**, 3116-3136.

6. Meruelo, D., G. Lavie, and D. Lavie. (1988). Therapeutic agents with dramatic antiretroviral activity and little toxicity at effective doses: Aromatic polycyclic diones hypericin and pseudohypericin. *Proc. Natl. Acad. Sci. USA.* **85**, 5230- 5234.
7. Lenard, J., A. Rabson, and R. Vanderoef. (1993). Photodynamic inactivation of infectivity of human immunodeficiency virus and other enveloped viruses using hypericin and rose bengal: inhibition of fusion and syncytia formation. *Proc.Natl.Acad.Sci. USA.* **90**, 158-162.
8. Hudson, J. B., J. Zhou, J. Chen, L. Harris, L. Yip, and G. H. N. Towers. (1994). Hypocrellin, from *Hypocrella bambusae*, is phototoxic to human immunodeficiency virus. *Photochem. Photobiol.* **60**, 253-255.
9. Couldwell, W. T., R. Gopalakrishna, D. R. Hinton, S. He, M. H. Weiss, R. E. Law, and M. L. Apuzzo. (1994). Hypericin: a potential antiglioma therapy. *Neurosurgery.* **35**, 705-710.
10. Anker, L., R. Gopalakrishna, K. D. Jones, R. E. Law, and W. T. Couldwell. (1995). Hypericin in adjuvant brain tumor therapy. *Drugs of the Future.* **20**, 511-517.
11. Zhang, W., R. E. Law, D. R. Hinton, and W. T. Couldwell. (1997). Inhibition of human malignant glioma cell motility and invasion in vitro by hypericin, a potent protein kinase C inhibitor. *Cancer Lett. (Shannon, Irel.)* **120**, 31-38.
12. Gai, F., M. J. Fehr, and J. W. Petrich. (1993). Ultrafast excited-state processes in the antiviral agent hypericin. *J. Am. Chem. Soc.* **115**, 3384-3385.
13. Gai, F., M. J. Fehr, and J. W. Petrich. (1994). Observation of Excited-State Tautomerization in the Antiviral Agent Hypericin and Identification of Its Fluorescent Species. *J. Phys. Chem.* **98**, 5784-5795.

14. Gai, F., M. J. Fehr, and J. W. Petrich. (1994). Role of Solvent in Excited-State Proton Transfer in Hypericin. *J. Phys. Chem.* **98**, 8352-8358.
15. Das, K., D. S. English, M. J. Fehr, A. V. Smirnov, and J. W. Petrich. (1996). Excited-State Processes in Polycyclic Quinones: The Light-Induced Antiviral Agent, Hypocrellin, and a Comparison with Hypericin. *J. Phys. Chem.* **100**, 18275-18281.
16. Das, K., D. S. English, and J. W. Petrich. (1997). Deuterium Isotope Effect on the Excited-State Photophysics of Hypocrellin: Evidence for Proton or Hydrogen Atom Transfer. *J. Phys. Chem. A* **101**, 3241-3245.
17. Das, K., D. S. English, and J. W. Petrich. (1997). Solvent Dependence on the Intramolecular Excited-State Proton or Hydrogen Atom Transfer in Hypocrellin. *J. Am. Chem. Soc.* **119**, 2763-2764.
18. Das, K., A. V. Smirnov, M. D. Snyder, and J. W. Petrich. (1998). Picosecond Linear Dichroism and Absorption Anisotropy of Hypocrellin: Toward a Unified Picture of the Photophysics of Hypericin and Hypocrellin. *J. Phys. Chem. B* **102**, 6098-6106.
19. Das, K., E. Dertz, J. Paterson, W. Zhang, G. A. Kraus, and J. W. Petrich. (1998). Hypericin, hypocrellin, and model compounds: steady-state and time-resolved fluorescence anisotropies. *J. Phys. Chem. B* **102**, 1479-1484.
20. Das, K., A. V. Smirnov, J. Wen, P. Miskovsky, and J. W. Petrich. (1999). Photophysics of hypericin and hypocrellin A in complex with subcellular components: Interactions with human serum albumin. *Photochemistry and Photobiology* **69**, 633-645.

21. Das, K., K. Ashby, J. Wen, and J. W. Petrich. (1999). The temperature dependence of the excited-state intramolecular proton transfer reaction in hypericin and hypocrellin. *A. J. Phys. Chem. B.* **103**, 1581-1585.
22. English, D. S., K. Das, K. D. Ashby, J. Park, J. W. Petrich, and E. W. J. Castner. (1997). Confirmation of Excited-State Proton Transfer and Ground-State Heterogeneity in Hypericin by Fluorescence Upconversion. *J. Am. Chem. Soc.* **119**, 11585-11590.
23. English, D. S., K. Das, J. M. Zenner, W. Zhang, G. A. Kraus, R. C. Larock, and J. W. Petrich. (1997). Hypericin, Hypocrellin, and Model Compounds: Primary Photoprocesses of Light-Induced Antiviral Agents. *J. Phys. Chem. A.* **101**, 3235-3240.
24. Petrich, J. W. (2000). Excited-State Intramolecular H-Atom Transfer in Nearly Symmetrical Perylene Quinones: Hypericin, Hypocrellin, and their Analogs. *Int. Rev. Phys. Chem.*, **19**, 479-500.
25. Dewar, M. J. S. (1984). Multibond reactions cannot normally be synchronous. *J. Am. Chem. Soc.* **106**, 209-219.
26. Chen, Y., F. Gai, and J. W. Petrich. (1993). Solvation of 7-azaindole in alcohols and water: Evidence for concerted, excited-state, double-proton transfer in alcohols. *J. Am. Chem. Soc.* **115**, 10158-10166.
27. Eloy, D., A. Le Pellec, and P. Jardon. (1996). Protonation and deprotonation of hypericin in the ground state and the first excited singlet state in a nonionic micellar medium. *J. Chim. Phys. Phys.-Chim. Biol.* **93**, 442-457.

28. Bouirig, H., D. Eloy, and P. Jardon. (1993). Self-quenching of fluorescence and triplet-triplet absorption of hypericin in liposomes of dipalmitoylphosphatidylcholine. *J. Chim. Phys. Phys.-Chim. Biol.* **90**, 2021-2038.
29. Racinet, H., P. Jardon, and R. Gautron. (1988). Formation d'oxygène sigulet photosensibilisée par l'hypericine étude cinétique en milieu micillaire non ionique. *J. Chim. Phys.* **85**, 971-977.
30. Jardon, P., and R. Gautron. (1989). Photophysical properties of hypericin in solution and in micellar dispersion. *J. Chim. Phys. Phys.-Chim. Biol.* **86**, 2173-2190.
31. Burel, L., P. Jardon, and J.-C. Lepretre. (1997). Electrochemical behavior of hypericin in aqueous liposome and dimethyl sulfoxide media. *New J. Chem.* **21**, 399-403.
32. Bouirig, H., D. Eloy, and P. Jardon. (1992). Formation and reactivity of the singlet oxygen photosensitized by hypericin in the liposomes of dipalmitoylphosphatidylcholine. Evidence of delayed oxidation. *J. Chim. Phys. Phys.-Chim. Biol.* **89**, 1391-1411.
33. Nafis, M., and P. Jardon. (1994). Spectroscopic and photophysical properties of hypericin-metal complexes in relation to their photodynamic activity. *J. Chim. Phys. Phys.-Chim. Biol.* **91**, 99-112.
34. Wong, M., J. K. Thomas and M. Gratzel. (1976). Fluorescence probing of inverted micelles. The state of solubilized water clusters in alkane/AOT solution. *J. Am. Chem. Soc.* **98**, 2391-2397.
35. Silber, J. J., A. Biasuth, E. Abuin, and E. Lissi. (1999). Interactions of small molecules with reverse micelles. *Adv. Coll. Int. Sci.* **82**, 189 – 252.

36. Eastoe, J., G. Fragneto, B. H. Robinson, T. F. Towey, R. K. Henan, and F. J. Leng. (1992). Variation of surfactant counterion and its effect on the structure and properties of aerosol OT-based water-in-oil microemulsions. *J. Chem. Soc. Faraday Trans.* **88**, 461 – 471.
37. English, D. S., W. Zhang, G. A. Kraus, and J. W. Petrich. (1997). Excited-State Photophysics of Hypericin and Its Hexamethoxy Analog: Intramolecular Proton Transfer as a Nonradiative Process in Hypericin. *J. Am. Chem. Soc.* **119**, 2980-2986.
38. Chowdhury, P. K., K. D. Ashby, A. Datta, and J. W. Petrich. (2000). Effect of pH on the fluorescence and absorption spectra of hypericin in reverse micelles. *Photochem. Photobiol.*, **72**, 612-618.
39. Jain, T. J., M. Varshney, and A. Maitra. (1989). Structural Studies of Aerosol-OT reverse micellar aggregates by FT-IR spectroscopy. *J. Phys. Chem.* **93**, 7408-7416.
40. Cho, C. H., M. Chung, J. Lee, T. Nguyen, S. Singh, M. Vedamuthu, S. Yao, S.-B. Zhu, and G. W. Robinson. (1995). Time and space-resolved studies of the physics and chemistry of liquid water near a biologically relevant interface. *J. Phys. Chem.* **99**, 7806 - 7812.
41. Smirnov, A. V., K. Das, D. S. English, Z. Wan, G. A. Kraus, and J. W. Petrich. (1999). Excited-State Intramolecular H-Atom Transfer of Hypericin and Hypocrellin A Investigated by Fluorescence Upconversion. *J. Phys. Chem. A.* **103**, 7949-7957.
42. El Seoud, O. A. (1989) Effects of organized assemblies on acid base equilibria. *Adv. Coll. Int. Sci.* **30**, 1 – 30.

CHAPTER 5: IDENTIFICATION OF A VIBRATIONAL FREQUENCY CORRESPONDING TO H-ATOM TRANSLOCATION IN HYPERICIN

A paper submitted in Photochemistry and Photobiology

B. M. Showalter², A. Datta¹, P. K. Chowdhury¹, J. Park¹, P. Bandyopadhyay¹,
P. K. Choudhury¹, S. Kesavan¹, Y. Zeng¹, G. A. Kraus¹, M. S. Gordon¹, J. P. Toscano^{*2},
and J. W. Petrich^{*1}

ABSTRACT

By means of time-resolved infrared spectroscopy, *ab initio* quantum mechanical calculations, and synthetic organic chemistry, a region in the infrared spectrum, between 1400 and 1500 cm^{-1} , of triplet hypericin has been found corresponding to translocation of the hydrogen atom between the enol and the keto oxygens, $\text{O}\cdots\text{H}\cdots\text{O}$. This result is discussed in the context of the photophysics of hypericin and of eventual measurements to observe directly the excited-state H-atom transfer.

INTRODUCTION

Hypericin (Figure 5.1) is one of many naturally and commonly occurring perylene quinone pigments that have stimulated great interest because of their broad spectrum of light-induced biological activities (1-4), among which are light-induced virucidal activity against several types of viruses, including the human immunodeficiency virus (HIV) (5-7), as well as antiproliferative and cytotoxic effects on tumor cells (8-10). Owing to this important

¹ Department of Chemistry, Iowa State University, Ames, Iowa 50011-3111.

² Department of Chemistry, Johns Hopkins University, Baltimore, Maryland 21218-2685

*Authors to whom correspondence should be addressed.

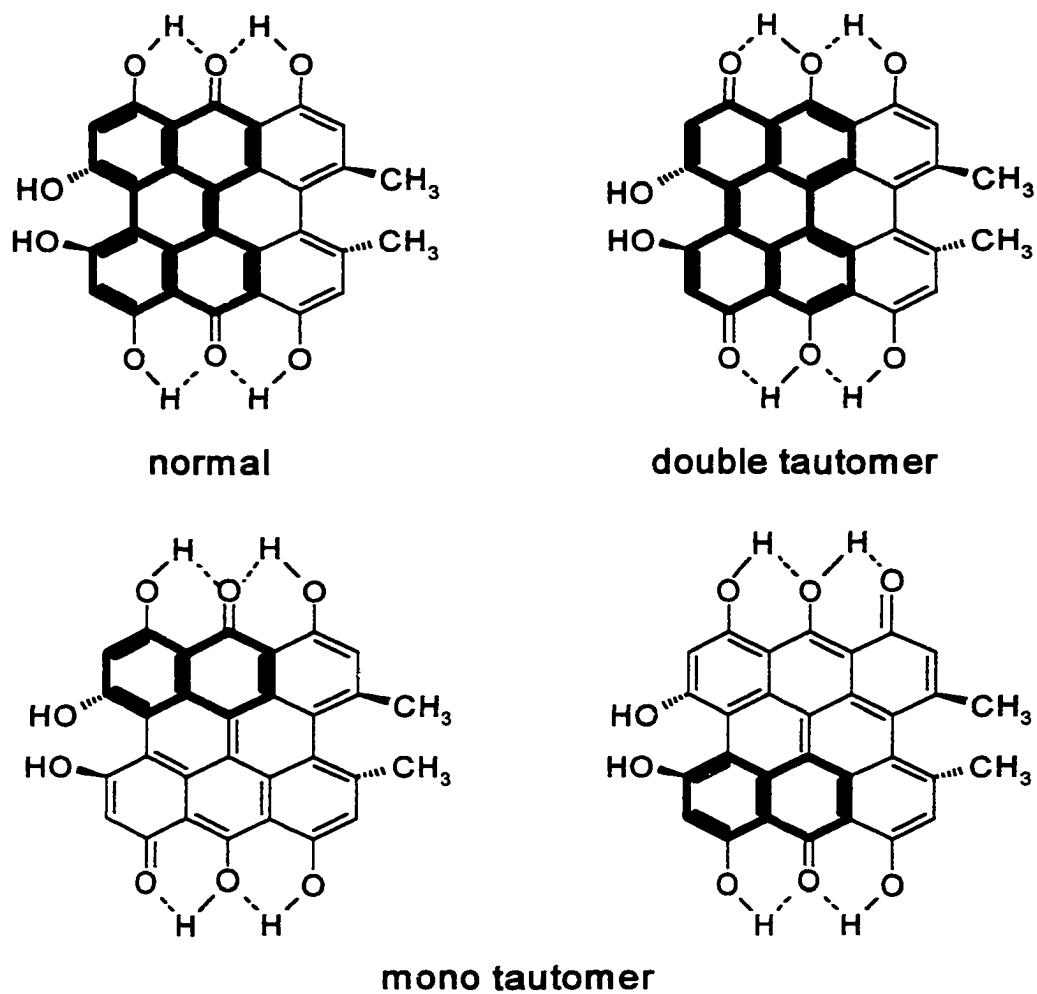


Figure 5.1. Hypericin in several tautomeric forms: upper left, the 7,14-dioxo tautomer (“normal” form); upper right, the 1,6-dioxo tautomer (a double tautomer); bottom left, the 6,14-dioxo monotaotomer; bottom right, the 7,13-dioxo monotaotomer). The portions of the aromatic skeletons highlighted in bold indicate regions that are conserved upon tautomerization (24,50) and that thus contribute to the observed mirror image symmetry between the absorption and fluorescence spectra.

biological activity, over the past few years we have been studying the photophysics of hypericin and its analogs, such as hypocrellin (Figure 5.2) (11-22). By means of H/D substitution, investigation of *O*-methylated analogs, and complementary studies using both transient absorption and fluorescence upconversion spectroscopies, we have argued that the major primary photophysical process is excited-state hydrogen atom transfer.

There are two objections, nevertheless, that are still occasionally raised to this assignment. These are the absence of a deuterium isotope effect for the 10-ps component of hypericin and hypocrellin and the mirror image symmetry between the absorption and emission spectra in hypericin and hypocrellin.

We have extensively discussed the lack of a deuterium isotope effect (23,12,15,17,24). *Its absence is easily attributed to the reaction coordinate not being identified with the proton coordinate.* There is precedent for this in other systems (25-27). Requiring the *absence* of mirror image symmetry between the absorption and emission spectra assumes that the potential energy surface of the emitting species is significantly different from that of the absorbing species. Such a displacement in the coordinate of the emitting species is clearly evident in the most commonly studied proton transfer systems: methyl salicylate (26,28); 7-azaindole dimer (29,30); 2-phenyl-benzotriazole (31); and 3-hydroxyflavone (32-36).

If, however, we consider systems in which the normal and tautomer species are symmetric, or nearly so, this disparity no longer exists or is significantly minimized. 5-Hydroxytropolone (37-39) presents an excellent example of such a case. Other examples are the double H-atom transfer in naphthazarin (40) and in the 4,9-dihydroxyperylene-3,10-quinone subunit of hypocrellin, producing entirely symmetric structures.

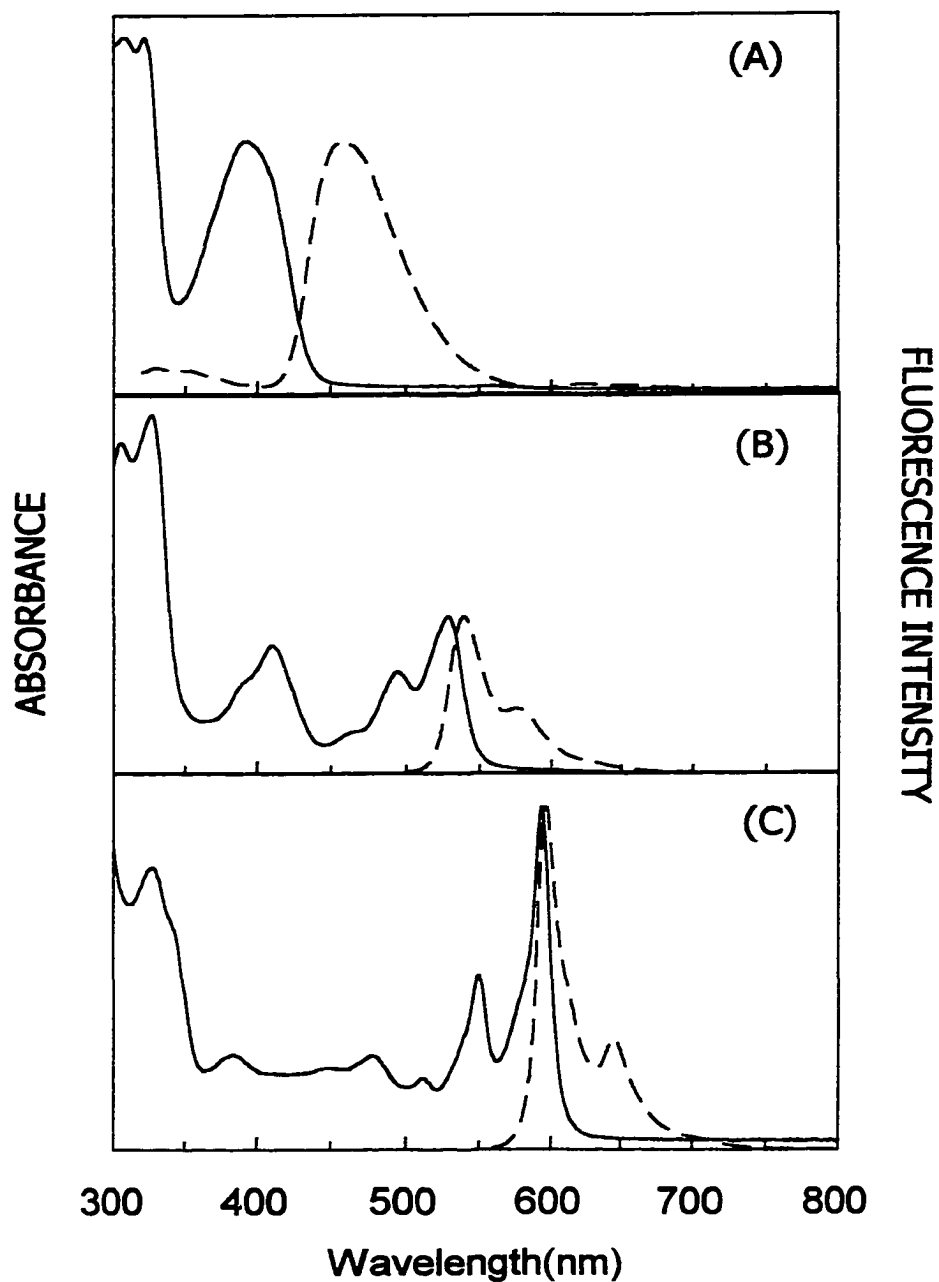


Figure 5.2. Steady-state absorption (—) and emission (---) spectra of. (A) hexacetoxy analog in acetonitrile excited at 270 nm; (B) hexamethoxy hypericin in dimethyl sulfoxide excited at 480 nm; and (C) hypericin in acetonitrile excited at 550 nm.

We argue that hypericin and hypocrellin A have very similarly symmetric normal and tautomeric forms as indicated by the highlighted bond systems in Figure 5.1. That is, regardless of the tautomeric form in which the molecule finds itself, there is always conserved an aromatic core to which is attached a hydroxyl group *peri* to a carbonyl group. Even in the case of the monotaomerized species, it is possible to draw resonance forms that upon superposition restore the aromatic character of the substructure involved in the H-atom transfer reaction. Consequently, we conclude that the mirror image symmetry observed in hypericin and hypocrellin is not at all surprising.

We recognize, however, that no matter how satisfactory one finds the above reasoning, a direct demonstration of an excited-state H-atom transfer requires measurements of the carbonyl or hydroxyl stretching frequency as a function of time subsequent to laser excitation. Such measurements require a tunable infrared probe source coupled to a visible or ultraviolet pump pulse. A first step in this process is the identification of vibrational modes that are indicative of translation of the hydrogen atom between the enol and the keto oxygens.

MATERIALS AND METHODS

Sample Preparation. Hypericin and hypocrellin A were obtained from Molecular Probes and used without further purification. Hexamethoxy hypericin was prepared as previously described (41). Hexaacetoxy-2,2'-dimethylmesonaphodianthren (42) was prepared as follows. A mixture of hypericin (0.07 g) and anhydrous sodium acetate (0.07 g) in acetic anhydride (7 mL) was boiled for 5-10 minutes. Over 30 minutes, small portions of zinc powder (1.9 g) were added to the boiling solution until the color changed to yellow. The

reaction was cooled to room temperature and filtered through a pad of Celite. The filtrate was concentrated in vacuo to obtain a yellow residue which was purified by preparative thin layer chromatography using hexanes: ethyl acetate. The yield of product was 25%. NMR (CDCl₃): 2.02 (s, 3 H), 2.20 (s, 3 H), 2.35 (s, 3 H), 2.37 (s, 3 H), 3.97 (s, 2 H), 4.12 (s, 2 H), 6.77 (s, 1 H), 7.13 (s, 1 H), 7.19 (s, 1 H), 7.24 (s, 1 H). MS m/z 728, 670, 628, 586, 560, 458.

Time-Resolved Infrared Spectroscopy. The solutions were prepared in the dark in acetonitrile-*d*₃, obtained from Cambridge Isotope laboratories and used as received. Sample concentrations were: hypericin, 5×10^{-5} M; hexa *O*-methyl hypericin, 2×10^{-4} M; hexacetoxy analog, 9.2×10^{-4} M. The solutions were purged with a constant flow of argon during the experiments. The TRIR measurements are described in detail elsewhere (43). The broad-band output of a MoSi₂ IR source (JASCO) was overlapped, on the sample contained in a flowing cell, with the excitation pulses from a Quantronix Q-switched Nd:YAG laser (355 nm, 90 ns, 1.5 mJ) operating at 200 Hz. Changes in IR intensity were monitored by a MCT photovoltaic IR detector (Kolmar Technologies, KMPV 11 - 1 - J1), amplified and digitized with a Tektronix TDS520A oscilloscope. The experiment was conducted in the dispersive mode with a JASCO TRIR - 1000 spectrometer. TRIR difference spectra were collected at 16 cm⁻¹ resolution.

Time-resolved Visible Absorption Spectroscopy. The apparatus used for ultrafast kinetic measurements is described in detail elsewhere (22,41).

***Ab initio* Quantum Mechanical Calculations.** Details are given elsewhere (44). Initial structures for all minima were obtained with the semiempirical AM1 (45) molecular orbital method. Using these structures as starting points, the geometries were then optimized

at the restricted Hartree-Fock (RHF) level of theory for closed shell singlet ground states and restricted open shell Hartree-Fock (ROHF) for the excited triplet states, using the 3-21G basis set (46). At each RHF/3-21G stationary point, the Hessian (matrix of energy second derivatives) was calculated using finite double differencing of the analytic gradients. The Hessian is used to determine the nature of each stationary point (positive definite for a local minimum, one negative eigenvalue for a saddle point) and to provide an estimate of the vibrational frequencies and the vibrational zero-point energies. All calculations discussed here were performed with the electronic structure code GAMESS (47).

RESULTS AND DISCUSSION

Figure 5.2 presents a comparison of the steady-state absorption and emission spectra of the hexaacetoxy analog, hexamethoxy hypericin, and hypericin. These data indicate that both the hydroxyls *peri* to the carbonyl groups and the carbonyl groups themselves play significant roles in determining the form of the spectra of hypericin. The presence of the carbonyl groups at the 7 and 14 positions is the more important of the two factors. Figures 5.3 and 5.4 compare the transient absorption kinetics of the hexaacetoxy analog and of hypericin, respectively: the analog clearly lacks the ~10-ps rising component that is the signature of excited H-atom transfer in hypericin. This rising component is also absent in the kinetics of hexamethoxy hypericin (22,41).

Figure 5.5 and Table 5.1 present the time-resolved infrared data for hypericin, hexamethoxy hypericin, and the hexaacetoxy analog lacking the 7,14 carbonyls. These spectra were obtained on the microsecond time scale, and hence they reflect the photophysics of triplet species and any possible photoproducts. Because the transient data are difference

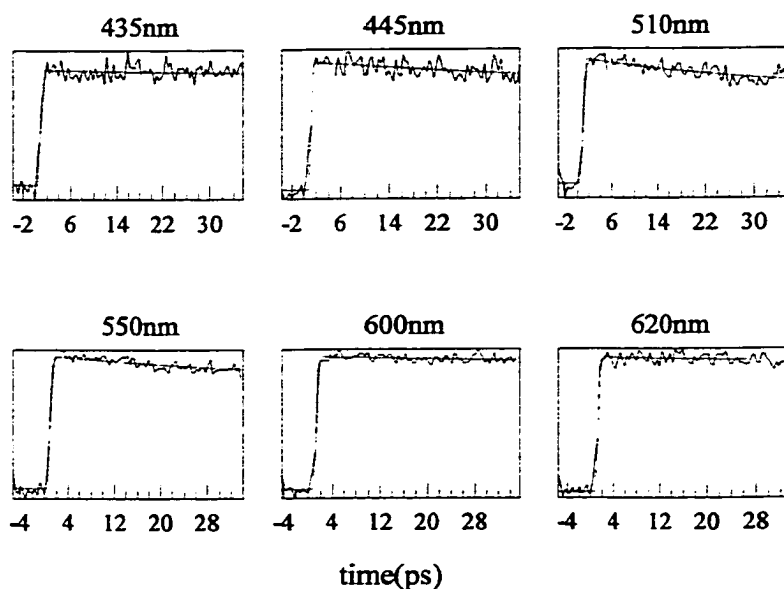


Figure 5.3. Transient absorption traces (ΔA vs. time) of the hexacetoxy analog in acetonitrile, $\lambda_{\text{pump}} = 403 \text{ nm}$. A global fit to the kinetics at the six probe wavelengths presented yields a time constant of 43 ps.

spectra, their features are considerably more pronounced than those of the ground-state spectra.

The hexaacetoxy analog provides the simplest kinetics of the three analogs: only one transient is observed (all the time constants being identical within the experimental error of approximately $\pm 10 \%$). This transient most likely corresponds to the decay of the triplet state. Furthermore, since all the bleaches completely recover (Figure 5.5) on this 3 μs time scale, it can be concluded that no net chemistry is occurring for this analog. For hypericin and the hexamethoxy analog, there are at least two transients (the interpretation and determination of the time constants being more complicated because of the presence of overlapping bands). The shorter transient most likely corresponds to the decay of the triplet,

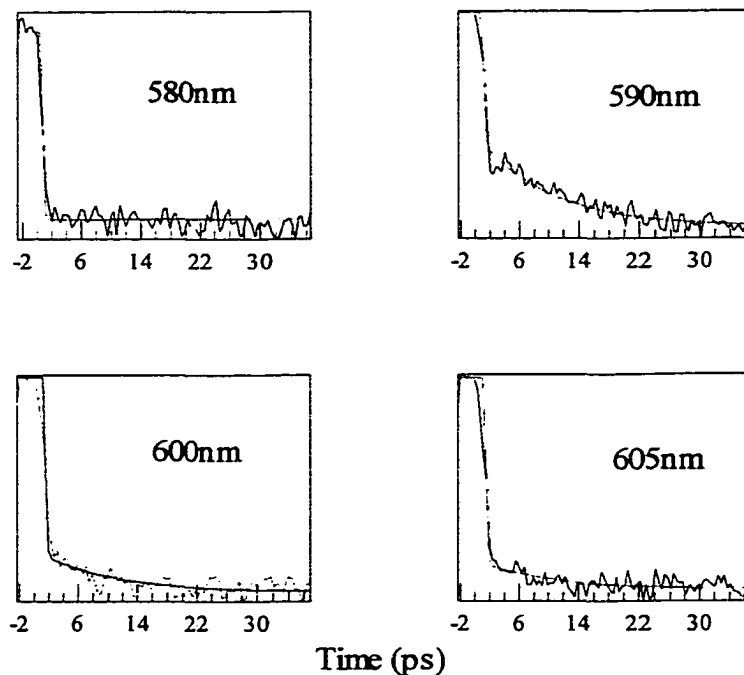


Figure 5.4. Transient absorption traces (ΔA vs. time) of hypericin in acetonitrile, $\lambda_{\text{pump}} = 403$ nm. A global fit to the kinetics at the four probe wavelengths presented yields a time constant of 10 ps.

while the longer corresponds to the presence of a photoproduct, which may be attributed to a radical or anion formed by H-atom or proton abstraction in the case of hypericin (48).

Finally, although oxygen is removed from all of the samples, the triplet decay of the compounds studied here occurs on a time scale of no longer than $\sim 3 \mu\text{s}$. On the other hand, the triplet decay of thoroughly degassed hypericin is 1.1 ms at room temperature in ethanol (49). At least part of the reason for this discrepancy may be attributed to the high solute concentration required for the infrared measurements (see above), which contributes to self quenching by the ground state and to triplet-triplet annihilation.

Figure 5.5. Comparison of the transient infrared spectra on the microsecond time scale of hypericin, *O*-hexamethoxy hypericin, and a hypericin analog that lacks carbonyl groups, the hexaacetoxy analog. The salient feature of the data is that the latter two compounds, which cannot execute excited state H-atom transfer owing to the absence of either labile protons or appropriate carbonyl groups, lack the feature at $\sim 1450\text{ cm}^{-1}$. *Ab initio* calculations at the Hartree-Fock 3-21G level for the normal and two monotautomeric forms of the hypericin triplets indicate normal modes with substantial O...H...O character in the region $\sim 1400\text{-}1460\text{ cm}^{-1}$. While these preliminary results do not demonstrate a time-resolved H-atom transfer, they do clearly point to a region of the spectrum that must be investigated in further studies. For hypericin and hexamethoxy hypericin (solid line, 0-1 μs ; dashed line, 14-18 μs), for the reduced analog (solid line, 0-0.5 μs ; dashed line, 7-9 μs).

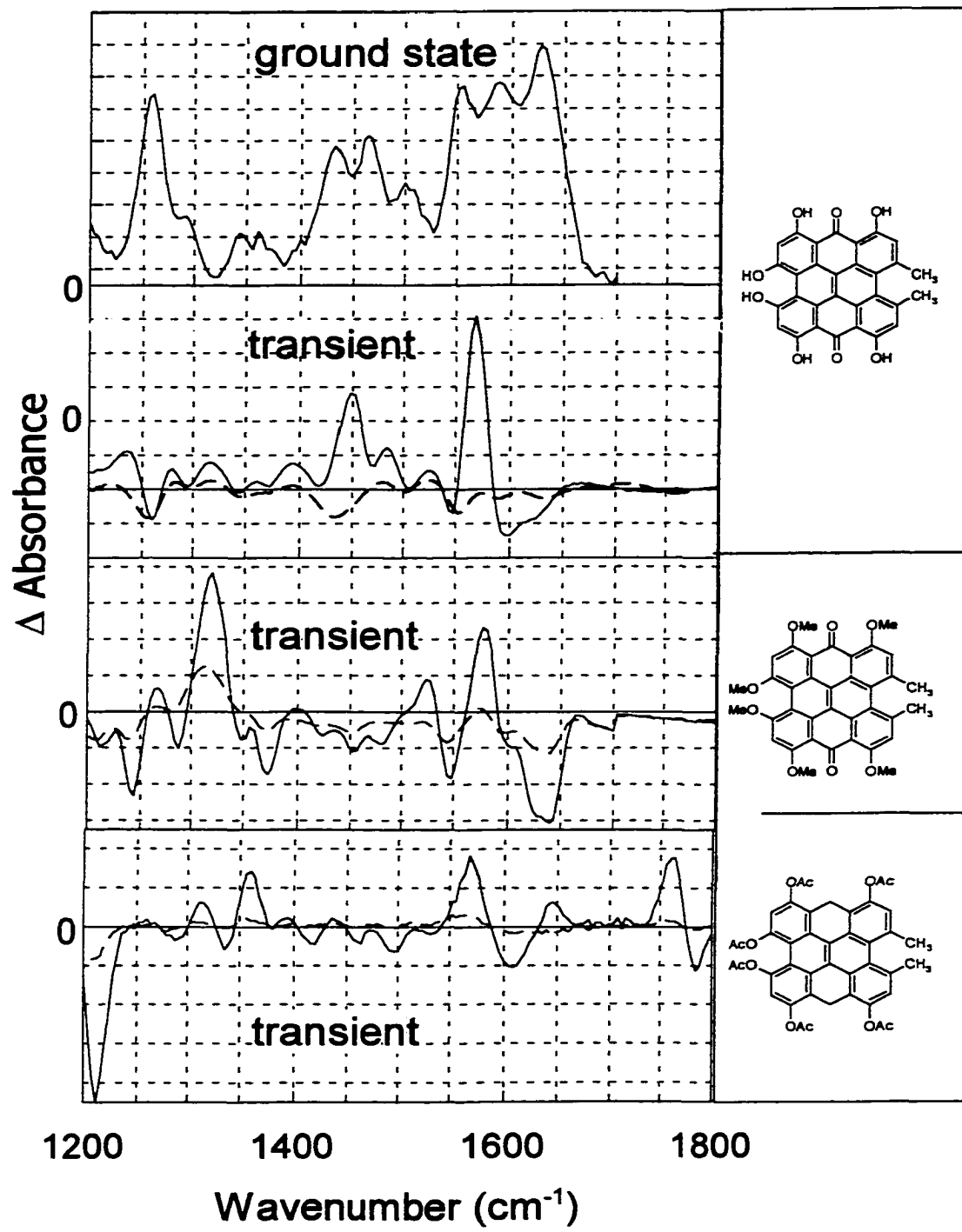


Table 5.1. Infrared Kinetics

Band (cm ⁻¹)	τ (μ sec) ^a	Initial Sign of Signal
Hypericin		
1300-1332	9.1	Absorption
1380-1414	2.9	Absorption
1436-1464	3.3	Absorption
1472-1492	5.9	Absorption
1516-1536	12.5	Absorption
1552-1584	3.0	Absorption
1558-1628	5.6	Bleach
Hexamethoxy Hypericin		
1232-1252	0.4	Bleach
	19.6	Bleach
1260-1276	0.3	Absorption
	3.8	Absorption
1280-1292	6.7	Bleach
1300-1340	10.0	Absorption
1360-1384	10.1	Bleach
1516-1532	0.3	Absorption
	3.8	Absorption
1536-1560	31.3	Bleach
1564-1588	8.3	Absorption
1612-1656	13.9	Bleach
Hexaacetoxy Analog		
1204-1224	3.1	Bleach
1304-1324	2.9	Absorption
1348-1372	2.2	Absorption
1556-1580	2.7	Absorption
1596-1624	2.6	Bleach
1636-1656	2.6	Absorption
1748-1772	2.1	Absorption
1780-1796	2.4	Bleach

^a The time constant indicates the relaxation time for the induced absorption or bleach and not a rise time for the appearance of the signal. Where two time constants are indicated, a biphasic relaxation was observed. Given the spectral bandwidth over which the kinetics were monitored, it cannot be determined with certainty whether the relaxation is itself biphasic or if two species with different time constants are observed.

The salient feature of these spectra is in the region between 1400-1500 cm⁻¹: a strong band is present here for hypericin and is absent in both O-hexamethoxy hypericin, which lacks hydrogen atoms that can coordinate to the carbonyl, and in the reduced analog, which lacks the necessary carbonyls. The ground-state infrared spectrum of hypericin is included at the top of the Figure. Ab initio quantum mechanical calculations (Table 5.2) reveal strong normal modes in this spectral region for the triplet species of the normal form of hypericin and the 6, 14- and 7, 13-dioxo monotautomers (Figure 5.1). Calculations were not performed for the triplet species of the double tautomers (44). Assignments of these modes are given in Table 5.2.

CONCLUSIONS

A vibrational mode corresponding to H-atom translocation has been identified in hypericin by the joint contributions of synthetic, computational, and spectroscopic methods. Identification of this mode is a only a first step in providing a direct demonstration of excited-state intramolecular H-atom transfer in hypericin and its analogs. There is considerable work to be accomplished. As indicated in Table 5.2, *ab initio* calculations predict that the normal modes in this region of the spectrum are very close for the normal and monotautomeric forms. The direct observation of the formation of the tautomer will require both adequate temporal and spectral resolution.

It must be remembered, furthermore, that the identification of the H-atom translocation mode is not equivalent to the identification of the reaction coordinate. We have attributed the absence of a deuterium isotope effect on the excited-state H-atom transfer (for the ~10-ps component in hypericin and hypocrellin A) to the zero-point energy in the

Table 5.2. Calculated Frequencies of Normal Mode Vibrations of Hypericin Species**7,14-dioxo tautomer, ground state singlet ("normal" form)**

frequency (cm ⁻¹)	scaled ^a	oscillator(s)
1238	1102	Ring breathing + C(13)-O and C(1)-O stretches. C(2)-C(3)-OH and C(5)-C(4)-OH motions.
1331	1185	Ring breathing mode + Some C(1)-O and C(6)-O stretches.
1377	1225	Ring breathing + out of phase C(13)-O and C(8)-O + out of phase C(1)-O and C(6)-O stretches.
1489	1325	Ring breathing mode + out of phase C(13)-O and C(8)-O + out of phase C(1)-O and C(6)-O + C(13)-O-H and C(8)-O-H stretches.
1500	1335	Ring breathing mode + in phase C(1)-O and C(13)-O stretches. C-C=O (7,14) bending. H bonding affected.
1558	1387	Ring breathing mode + C(1)-O and C(6)-O in phase stretch + C(13)-O and C(8)-O in phase stretch. C(13)-O-H bend (small).
1723	1533	C-C-O movements (8,13). O-H stretches (8,13) + C-O-H bending. H bonding affected.
1746	1554	C-O-H movements (1, 13, 6 ,8). H bonding affected + mostly ring breathing.
1811	1612	Ring motion + out of phase C(7)=O and C(14)=O stretches. C(1)-O and C(13)-O in phase stretches. H bonding affected.

7,14-dioxo tautomer, lowest triplet ("normal" form)

frequency (cm ⁻¹)	scaled ^a	oscillator(s)
1345	1197	Ring breathing motion + C-O stretches.
1350	1201	C-O in phase stretch (1,6) + Ring breathing.
1399	1245	Out of phase C-O stretch (8,13) + Smaller C=O out of phase stretches. Ring motion.
1424	1267	Ring breathing (C-C=O backbone movements (7,14)) C-O-H bends (1,13,6,8). H bonding affected.
1459	1298	Ring motion. Out of Phase C=O movements. In phase C-O (1,13) H bonding affected.
1504	1339	Out of Phase C-O stretch (8,13) + ring motion. H bonding affected. Small C-O-H bending.
1554	1384	In phase C-O stretch (1,6) + small C=O stretches + Ring motion. H bonding affected
1605	1428	Out of Phase C=O stretch (7,14). Out of phase C-O stretch (1,6 and 8,13). Ring motion. H bonding affected
1707	1520	Small C-O-H movement (8,13). Ring motion. H bonding affected
1712	1524	C-O-H (1,6,13,8). O-H bends. H bonding affected
1727	1537	C-O-H bends (8,13). H bonding affected.
1812	1613	C=O out of phase stretch (7,14). O-H bends (1,6,8,13). H bonding affected strongly.

6, 14 dioxo tautomer, lowest triplet (monotautomer)

frequency (cm ⁻¹)	scaled ^a	oscillator(s)
1268	1128	Ring breathing + In phase C(13)-O and C(8)-O stretches.
1273	1133	Ring breathing + 1 and 7 in-phase C-O stretches + 13 and 8 out of phase C-O stretches. 1, 8 and 13 C-O-H bends (small). (H bonding affected).
1299	1156	Ring breathing + C(1)-O stretch. C(1)-C(14)-C(13) backbone breathing + 13 C-O-H bending. 3 C-O stretch. 3 O-H bend. (H bonding affected).
1388	1236	10-H bending + 3 O-H bending + ring breathing. (H-bonding affected).
1407	1252	Ring motion + In-phase 14 C=O stretch and 7 C-O stretch. 8 C-O stretch. 1 and 8 O-H bending. (H-bonding affected).
1529	1361	1 and 13 out of phase C-O stretches. 7,8 C-O-H bends. C(3)-O stretch + ring motion. (H bonding affected).
1545	1375	7,8 C-O in-phase stretches. 1 C-O stretch. 7 O-H bending. Ring motion. (H bonding affected).
1635	1455	8, 1, 13 O-H bends + ring breathing (C(9)-C(10) stretch).
1714	1525	C12-C13 stretch + C(13)-O-H bend + C(14) = O out of plane motion + 13 O-H bend. (H bonding strongly affected).
1747	1554	Out of phase C=O stretches + C(13)-O stretch. O-H bends (small) + ring breathing (H bonding affected).
1816	1616	14 C=O stretch. C(2)-C(1)-O movement. 1 and 13 C-O-H bends. (H bonding affected).
1829	1627	6 C=O stretch. 7 and 8 C-O-H bends. (H bonding affected).

7, 13 dioxo tautomer, lowest triplet (montautomer)

frequency (cm ⁻¹)	scaled ^a	oscillator(s)
1268	1128	Ring breathing + 1, 7 and 13 C-O stretches.
1311	1166	Ring breathing.
1393	1239	Ring motion. 7 C=O out of plane stretch. 1, 8 C-O stretches.
1413	1258	Ring breathing (mainly C(11)-C(12) stretch). 13, 14 C-O + C=O stretch (In Phase). 7 C=O stretch. 8,2 O-H bends (small). (H-bonding affected).
1473	1311	1,6 out of phase C-O stretch. 8 C-O stretch. Ring breathing.
1529	1361	7 C-O and 14 C=O out of phase stretch. 6 and 8 out of phase C-O stretch. O-H bends. Ring motion. (H bonding affected).
1568	1396	In phase 1 and 14 C-O stretch + Ring motion. 6, 14 C-O-H bends (small). (H-bonding affected)
1653	1471	Ring motion. C(13)-O stretch. C(1)-O-H bend.
1729	1539	6 C-O-H movement. (H bonding affected).
1809	1610	6,8, 14 O-H bends. 7 and 13 out of phase C=O stretch. (H bonding affected)
1820	1619	14, 1 O-H bends. 13 C=O stretch. (H bonding affected).

^a The calculated frequencies are scaled by a factor of 0.89 (52).

proton coordinate lying above the barrier, and the hydrogen atom being effectively delocalized between the two oxygen atoms. Consequently, the reaction coordinate for the excited-state H-atom transfer cannot be identified with the proton coordinate and it must be concluded that other intramolecular motions are in fact responsible for the process. Temperature dependent measurements indicate that these motions are extremely low-amplitude, $E_a = 0.044 \pm 0.008$ kcal/mol for hypericin (20). Because the nature of this motion is not yet identified, we refer to it as the “*skeleton coordinate*” (24,50). We propose that it is the time-scale for this latter conformational change that determines the observed H-atom transfer time. The exact nature of the conformational changes that are coupled to the H-atom transfer reaction in hypericin and hypocrellin has yet to be identified (51).

ACKNOWLEDGMENTS

This work was funded by NSF grant CHE-9613962 (JWP, MSG, GAK), NIH grant R21 GM57351 (JWP, GAK), and NSF grant CHE-9733052 (JPT).

REFERENCE

1. Duran, N., and P. S. Song (1986) Hypericin and its photodynamic action. *Photochem. Photobiol.* **43**, 677-680.
2. Lown, J. W. (1997) Photochemistry and photobiology of perylenequinones. *Can. J. Chem.* **75**, 99-119.
3. Diwu, Z. (1995) Novel therapeutic and diagnostic applications of hypocrellins and hypericins. *Photochem. Photobiol.* **61**, 529-539.

4. Kraus, G. A., W. Zhang, M. J. Fehr, J. W. Petrich, Y. Wannemuehler, and S. Carpenter (1996) Research at the Interface between Chemistry and Virology: Development of a Molecular Flashlight. *Chem. Rev.* **96**, 523-535.
5. Meruelo, D., G. Lavie, and D. Lavie (1988) Therapeutic agents with dramatic antiretroviral activity and little toxicity at effective doses: Aromatic polycyclic diones hypericin and pseudohypericin. *Proc. Natl. Acad. Sci. USA.* **85**, 5230- 5234.
6. Lenard, J., A. Rabson, and R. Vanderoef (1993) Photodynamic inactivation of infectivity of human immunodeficiency virus and other enveloped viruses using hypericin and rose bengal: inhibition of fusion and syncytia formation. *Proc. Natl. Acad. Sci. USA.* **90**, 158-162.
7. Hudson, J. B., J. Zhou, J. Chen, L. Harris, L. Yip, and G. H. N. Towers (1994) Hypocrellin, from *Hypocrella bambusae*, is phototoxic to human immunodeficiency virus. *Photochem. Photobiol.* **60**, 253-255.
8. Couldwell, W. T., R. Gopalakrishna, D. R. Hinton, S. He, M. H. Weiss, R. E. Law, and M. L. Apuzzo (1994) Hypericin: a potential antiglioma therapy. *Neurosurgery.* **35**, 705-710.
9. Anker, L., R. Gopalakrishna, K. D. Jones, R. E. Law, and W. T. Couldwell (1995) Hypericin in adjuvant brain tumor therapy. *Drugs of the Future.* **20**, 511-517.
10. Zhang, W., R. E. Law, D. R. Hinton, and W. T. Couldwell (1997) Inhibition of human malignant glioma cell motility and invasion in vitro by hypericin, a potent protein kinase C inhibitor. *Cancer Lett. (Shannon, Irel.).* **120**, 31-38.
11. Gai, F., M. J. Fehr, and J. W. Petrich (1993) Ultrafast excited-state processes in the antiviral agent hypericin. *J. Am. Chem. Soc.* **115**, 3384-3385.

12. Gai, F., M. J. Fehr, and J. W. Petrich (1994) Observation of Excited-State Tautomerization in the Antiviral Agent Hypericin and Identification of Its Fluorescent Species. *J. Phys. Chem.* **98**, 5784-5795.
13. Gai, F., M. J. Fehr, and J. W. Petrich (1994) Role of Solvent in Excited-State Proton Transfer in Hypericin. *J. Phys. Chem.* **98**, 8352-8358.
14. Das, K., D. S. English, M. J. Fehr, A. V. Smirnov, and J. W. Petrich (1996) Excited-State Processes in Polycyclic Quinones: The Light-Induced Antiviral Agent, Hypocrellin, and a Comparison with Hypericin. *J. Phys. Chem.* **100**, 18275-18281.
15. Das, K., D. S. English, and J. W. Petrich (1997) Deuterium Isotope Effect on the Excited-State Photophysics of Hypocrellin: Evidence for Proton or Hydrogen Atom Transfer. *J. Phys. Chem. A.* **101**, 3241-3245.
16. Das, K., D. S. English, and J. W. Petrich (1997) Solvent Dependence on the Intramolecular Excited-State Proton or Hydrogen Atom Transfer in Hypocrellin. *J. Am. Chem. Soc.* **119**, 2763-2764.
17. Das, K., A. V. Smirnov, M. D. Snyder, and J. W. Petrich (1998) Picosecond Linear Dichroism and Absorption Anisotropy of Hypocrellin: Toward a Unified Picture of the Photophysics of Hypericin and Hypocrellin. *J. Phys. Chem. B.* **102**, 6098-6106.
18. Das, K., E. Dertz, J. Paterson, W. Zhang, G. A. Kraus, and J. W. Petrich (1998) Hypericin, hypocrellin, and model compounds: steady-state and time-resolved fluorescence anisotropies. *J. Phys. Chem. B.* **102**, 1479-1484.
19. Das, K., A. V. Smirnov, J. Wen, P. Miskovsky, and J. W. Petrich (1999) Photophysics of hypericin and hypocrellin A in complex with subcellular

- components: Interactions with human serum albumin. *Photochem. and Photobiol.* **69**, 633-645.
20. Das, K., K. Ashby, J. Wen, and J. W. Petrich (1999) The temperature dependence of the excited-state intramolecular proton transfer reaction in hypericin and hypocrellin A. *J. Phys. Chem. B.* **103**, 1581-1585.
 21. English, D. S., K. Das, K. D. Ashby, J. Park, J. W. Petrich, and E. W. J. Castner (1997) Confirmation of Excited-State Proton Transfer and Ground-State Heterogeneity in Hypericin by Fluorescence Upconversion. *J. Am. Chem. Soc.* **119**, 11585-11590.
 22. English, D. S., K. Das, J. M. Zenner, W. Zhang, G. A. Kraus, R. C. Larock, and J. W. Petrich (1997) Hypericin, Hypocrellin, and Model Compounds: Primary Photoprocesses of Light-Induced Antiviral Agents. *J. Phys. Chem. A.* **101**, 3235-3240.
 23. Chen, Y., F. Gai, and J. W. Petrich (1994) Solvation and excited-state proton transfer of 7-azaindole in alcohols. *Chem. Phys. Lett.* **222**, 329-334.
 24. Smirnov, A. V., K. Das, D. S. English, Z. Wan, G. A. Kraus, and J. W. Petrich (1999) Excited-State Intramolecular H-Atom Transfer of Hypericin and Hypocrellin A Investigated by Fluorescence Upconversion. *J. Phys. Chem. A.* **103**, 7949-7957.
 25. Frey, W., F. Laermer, and T. Elsaesser (1991) Femtosecond studies of excited-state proton and deuterium transfer in benzothiazole compounds. *J. Phys. Chem.* **95**, 10391-10395.
 26. Herek, J. L., S. Pedersen, L. Banares, and A. H. Zewail (1992) Femtosecond real-time probing of reactions. IX. Hydrogen-atom transfer. *J. Chem. Phys.* **97**, 9046-9061.

27. Peteanu, L., and R. A. Mathies (1992) Resonance Raman Intensity Analysis of the Excited-State Proton Transfer in 2-Hydroxyacetophenone. *Journal of Physical Chemistry*. **96**, 6910-6916.
28. Goodman, J., and L. E. Brus (1978) Proton Transfer and Tautomerism in an excited state of methyl salicylate. *J. Am. Chem. Soc.* **100**, 7472-7474.
29. Taylor, C. A., M. A. El-Bayoumi, and M. Kasha (1969) Excited-State Two-Proton Tautomerism in Hydrogen-Bonded N-Heterocyclic Base Pairs. *Proc. Natl. Acad. Sci. USA*. **63**, 253-260.
30. Takeuchi, S., and T. Tahara (1998) Femtosecond Ultraviolet-Visible Fluorescence Study of the Excited-State Proton-Transfer Reaction of 7-Azaindole Dimer. *J. Phys. Chem. A*. **102**, 7740-7753.
31. Kim, Y. R., J. T. Yardley, and R. M. Hochstrasser (1989) Solvent Effects on Intramolecular Proton Transfer. *Chem. Phys.* **136**, 311-319.
32. Swinney, T. C., and D. F. Kelley (1991) Proton-transfer and solvent polarization dynamics in 3-hydroxyflavone. 2. Mixed Solvents. *J. Phys. Chem.* **95**, 10369-10373.
33. Strandjord, A. J. G., and P. F. Barbara (1985) Proton transfer kinetics of 3-hydroxyflavone: Solvent effects. *J. Phys. Chem.* **89**, 2355-2361.
34. Schwartz, B. J., L. A. Peteanu, and C. B. Harris (1992) Direct observation of fast proton transfer: Femtosecond photophysics of 3-hydroxyflavone. *J. Phys. Chem.* **96**, 3591-3598.
35. McMorro, D., and M. Kasha (1984) Intramolecular excited-state proton transfer in 3-hydroxyflavone. Hydrogen-bonding solvent perturbations. *J. Phys. Chem.* **88**, 2235-2243.

36. Brucker, G. A., T. C. Swinney, and D. F. Kelley (1991) Proton-transfer and solvent polarization dynamics in 3-hydroxyflavone. *J. Phys. Chem.* **95**, 3190-3195.
37. Croteau, R., and R. M. Leblanc (1978) Photophysical Processes in Tropolone, alpha-Methoxy-Tropone and Colchicine. *Photochem. and Photobiol.* **28**, 33-38.
38. Ensminger, F. A., J. Plassard, T. S. Zwier, and S. Hardinger (1993) Vibronically state-selective photoisomerization in 5-hydroxytropolone. *J. Chem. Phys.* **99**, 8341-8344.
39. Ensminger, F. A., J. Plassard, T. S. Zwier, and S. Hardinger (1995) Mode-selective photoisomerization in 5-hydroxytropolone. I. Experiment. *J. Chem. Phys.* **10**, 5246-5259.
40. Mazzini, S., L. Merlini, R. Mondelli, G. Nasini, E. Ragg, and L. Scalioni (1997) Deuterium isotope effect on ¹H and ¹³C chemical shifts of intramolecularly hydrogen bonded perylenequinones. *J. Chem. Soc., Perkin Trans. 2.* 2013-2021.
41. English, D. S., W. Zhang, G. A. Kraus, and J. W. Petrich (1997) Excited-State Photophysics of Hypericin and Its Hexamethoxy Analog: Intramolecular Proton Transfer as a Nonradiative Process in Hypericin. *J. Am. Chem. Soc.* **119**, 2980-2986.
42. Brockman, H., and W. Sanne (1957) Zur Kenntnis Des Hypericins Und Pseudo-Hypericins. *Chem. Ber.* **90**, 2480-2491.
43. Falk, H. (1999) From the Photosensitizer Hypericin to the Photoreceptor Stentorin--The Chemistry of Phenanthroperylene Quinones. *Angew. Chem. Int. Ed.* **38**, 3116-3136.

44. Wang, Y., T. Yuzawa, H. Hamaguchi, and J. P. Toscano (1999) Time-Resolved IR Studies of 2-Naphthyl(carbomethoxy)carbene: Reactivity and Direct Experimental Estimate of the Singlet/Triplet Energy Gap. *J. Am. Chem. Soc.* **121**, 2875-2882.
45. Petrich, J. W., M. S. Gordon, and M. Cagle (1998) Structure and Energetics of Ground-State Hypericin: Comparison of Experiment and Theory. *J. Phys. Chem. A.* **102**, 1647-1651.
46. Stewart, J. J. P. (1990) MOPAC : A semiempirical molecular orbital program. *J. Comput.-Aided Mol. Des.* **4**, 1-105.
47. Binkley, J. S., J. A. Pople, and W. J. Hehre (1980) Self-Consistent Molecular Orbital Methods. 21 . Small Split-Valence Basis Sets for First-Row Elements. *J. Am. Chem. Soc.* **102**, 939-947.
48. Hehre, W. J., R. Ditchfield, and J. A. Pople (1972) Self-Consistent Molecular Orbital Methods. XII. Further Extensions of Gaussian-Type Basis Sets for Use in Molecular Orbital Studies of Organic Molecules *J. Chem. Phys.* **56**, 2257-2261.
49. Pople, J. A., and J. S. Binkley (1976) Theoretical Models Incorporating Electron Correlation. *Int. J. Quantum Chem. Symp.* **10**, 1-19.
50. Schmidt, M. W., K. K. Baldrige, J. A. Boatz, S. T. Elbert, M. S. Gordon, J. H. Jensen, S. Koseki, N. Matsunaga, K. A. Nguyen, S. Su, T. L. Windus, M. Dupuis, and J. A. Montgomery, Jr (1993) The General Atomic and Molecular Electronic Structure System. *J. Comp. Chem.* **14**, 1347-1363.
51. Fehr, M. J., M. A. McCloskey, and J. W. Petrich (1995) Light-Induced Acidification by the Antiviral Agent Hypericin. *J. Am. Chem. Soc.* **117**, 1833-18366.

52. Dumas, S (2000) *Reactivite des etats photoexcites de l'hypericine. Etude comparative avec des derives analogues. Thesis. Universite Joseph Fourier--Grenoble 1.*
53. Petrich, J. W (2000) *Excited-State Intramolecular H-Atom Transfer in Nearly Symmetrical Perylene Quinones: Hypericin, Hypocrellin, and their Analogs. International Reviews in Physical Chemistry. 19, 479-500.*
54. Datta, A., P. Bandyopadhyay, J. Wen, J. W. Petrich, and M. S. Gordon (2001) *Coupling of Large-Amplitude Side Chain Motions to the Excited-State H-Atom Transfer of Perylene Quinones: Application of Theory and Experiment to Calphostin C. J. Phys. Chem. A 105, 1057-1060.*
55. Scott, A. P., and L. Radom (1996) *Harmonic Vibrational Frequencies: An Evaluation of Hartree-Fock, Moller-Plesset, Quadratic Configuration Interaction, Density Functional theory, and Semiempirical Scale Factors. J. Phys. Chem. 100, 16502-16513.*

CHAPTER 6: THE ROLE OF OXYGEN IN THE ANTIVIRAL ACTIVITY OF HYPERICIN AND HYPOCRELLIN

A paper published in *Photochemistry and Photobiology*¹

Jaehun Park¹, Doug S. English¹, Yvonne Wannemuehler², Susan Carpenter^{*2},
and Jacob W. Petrich^{*1}

ABSTRACT

The light-induced antiviral activity of hypericin and hypocrellin in the presence and absence of oxygen was examined under experimental conditions where the effect of oxygen depletion could be quantified. There was a significant reduction of light-induced antiviral activity of hypericin and hypocrellin under hypoxic conditions. Interestingly, antiviral activity of hypocrellin was not observed at low oxygen levels at which hypericin retained measurable virucidal activity. This suggests that additional pathways, such as the generation of protons from excited states of hypericin, may enhance the biological activity of activated oxygen species.

INTRODUCTION

The naturally occurring polycyclic quinones hypericin and hypocrellin are of current interest because of their light-induced (1) antiviral and antitumor activity (2-11). In addition,

¹Reprinted with permission from *Photochemistry and photobiology*, 1998, **68**, 593.

²Department of Chemistry, Iowa State University, Ames, Iowa 50011-3111.

³Department of Microbiology, Immunology, and Preventive Medicine, Iowa State University, Ames, IA 50011-1250

*Authors to whom correspondence should be addressed.

hypericin has attracted attention for its antidepressant activity (12-15). We have discussed elsewhere several aspects of the excited-state photophysics of hypocrellin and hypericin (16-25) and have proposed means of exploiting these properties (26,27). These molecules have been the subject of several reviews (27-30).

It has been shown that the antiviral and antitumor activities of hypericin can be dependent on oxygen (9,10). However, the mechanism of action of hypericin at the cellular level still remains unclear. Usually photosensitization processes involve molecules having a high triplet yield (31). The triplet state of a photosensitizer, such as hypericin, may induce two different kinds of common and well known photoreactions. The first and perhaps most common is the so-called Type II, oxygen-dependent, mechanism. Singlet oxygen formation occurs via energy transfer from the triplet state of the photosensitizer to the ground triplet state of molecular oxygen. The second is the Type I radical mechanism. This complex mechanism may involve any of several reactive species such as singlet oxygen, $^1\text{O}_2$ (31,32), superoxide radical anion, $\text{O}_2^{\bullet-}$ (33,34), hydroxyl radical, $^{\bullet}\text{OH}$ (33,34), as well as hypericin radicals and radical ions (33).

Comparative studies for nine perylenequinones, including hypocrellin and hypericin, provide evidence, however, that the quantum yield of singlet oxygen formation is not sufficient to explain the reported antiviral activities of these molecules, and that other structural features of perylenequinones are involved (36). In fact, the quantum yield of singlet oxygen from hypericin is much less than had initially been presumed. Recently, Jardon and coworkers have revised their earlier estimation of a singlet oxygen quantum yield of 0.73 (32), essentially equal to the triplet yield, to 0.36 in ethanol and less than 0.02 in water (37). Based on this result, mechanisms involving *only oxygen* clearly cannot explain

all the activity of hypericin.

We had previously reported that hypericin does not require oxygen for its antiviral activity (24,27,38,39). In those studies, however, we were not able to estimate accurately low oxygen levels in our virus samples. In the present study, we reexamine the importance of oxygen using experimental conditions where the effect of oxygen depletion could be quantified. The results indicate that while antiviral pathways independent of oxygen may exist, the role of oxygen in this activity is significant. The ability of photogenerated protons to enhance the activity of activated oxygen species (40) is considered to be of importance.

MATERIALS AND METHODS

A. Titration of infectious virus. Antiviral assays were done in low light conditions. Cell-free stocks of the MA-1 isolate of EIAV containing approximately 10^7 focus-forming units/ml (FFU/mL) of EIAV, were diluted 1:10 in phosphate-buffered saline (PBS). Hypericin or hypocrellin A (Molecular Probes) were added to a final concentration of $10\mu\text{g/ml}$, and samples were deoxygenated and/or illuminated as described below. Following treatment, serial ten-fold dilutions of *samples* were inoculated onto equine dermal cells in the presence of $8\mu\text{g/mL}$ polybrene which is for increasing viral effectivity. Cells were incubated five days, fixed in ice cold methanol, and virus-infected cells were detected by immunocytochemistry as described elsewhere (1,41). Foci of infected cells were counted and results are expressed as \log_{10} reduction in virus titer as compared to an untreated control sample.

B. Quantitative measurement of oxygen levels. What is meant by “hypoxic” depends on the sensitivity and precision of the oxygen-detection technique. Under our

experimental conditions, it is unwieldy to control accurately the amount of oxygen dissolved in our samples before and after deoxygenation, which is necessary in order to know the lowest oxygen concentration that we can detect. We have chosen, therefore, an indirect measurement of oxygen levels, as a function of ATP concentration, in terms of the generation of chemiluminescence by the reaction of luciferase and luciferin.

The ATP assay is based on the requirement for ATP in the production of chemiluminescent emission (emission maximum $\sim 560\text{nm}$ at pH 7.8) (26,27). The reaction is pseudo first-order in ATP when all reactant concentrations except that of ATP are in excess. Similarly, under hypoxic conditions all reactant concentrations except that of oxygen are in excess; and the reaction is pseudo first-order in oxygen. *Because the chemiluminescent reaction requires a one-to-one ratio of ATP to oxygen*, all other things being equal, if the rate of chemiluminescent emission produced is the same for a reaction that is pseudo first-order in oxygen or ATP, we can assume that the concentrations of ATP and oxygen are the same in both reactions.

To measure the limit of oxygen detection using the ATP assay, 1.8 mg/mL of luciferase-luciferin in glycine buffer (Sigma, L0633 ATP standard assay kit, $3 \times 10^{-15}\text{M}$ sensitivity) was prepared in PBS buffer. The chemiluminescent reaction was initiated by adding 5 μL of ATP to 1 mL of the luciferase/luciferin solution. After the samples were injected with 5 μL of ATP, chemiluminescence was monitored at 614 nm in a SPEX Fluoromax with the excitation beam blocked. The detection wavelength of 614 nm was chosen because here the chemiluminescence is not obscured by hypericin or hypocrellin absorption. A 1-mm emission slitwidth, corresponding to a 4-nm bandpass, was employed. Chemiluminescence was collected from 500-750 nm with scan rate (integration time) of 0.3

sec/nm and is reported here in arbitrary units of counts per second (cps).

C. Illumination and deoxygenation. Samples were prepared by adding an aliquot of hypericin or hypocrellin to a final concentration of 2.0×10^{-5} M and 1.8×10^{-5} M, respectively, to 1 mL of the EIAV containing 1.8 mg/mL of luciferase-luciferin in glycine buffer (Sigma, L0633 ATP standard assay kit, 3×10^{-15} M sensitivity). Preliminary experiments indicated these conditions had no background antiviral activity as compared to untreated controls (data not shown). Samples were deoxygenated with argon in glass vials fitted with rubber septa and kept on ice. Other methods of deoxygenation such as freeze-pump-thaw cycles were prohibited because multiple cycles result in decreased virus infectivity. After stirring and/or deoxygenating, the samples were injected with 5 μ L of 0.1 M ATP and monitored for chemiluminescence *as described above*. In order to activate hypericin or hypocrellin, the samples were illuminated for 10 minutes, while stirring, with a 300-W projector bulb fitted with a 530-nm long-pass filter. Following illumination, samples were kept on ice in the dark and assayed for infectious virus as described above.

D. Singlet oxygen assays. Singlet oxygen assays were performed using a liquid nitrogen cooled CCD (North Coast model E0-817). A Q-switched Nd:YAG (Laser Photonics KYD300) was used for excitation producing 10 kHz 50 ns pulses. Fluorescence and scattered light were blocked using 1.3 μ m bandpass filter fitted with a silicon slab to block wavelengths shorter than 960 nm. The excitation beam was chopped at 400 Hz and the output of the detector was fed to a lock-in amplifier (Stanford Research SR830). Two samples from the same solution were prepared for each experiment *and* each was stirred in a cuvette fitted with a septum for 20-25 minutes. One sample was kept under flowing argon and the other was kept under flowing oxygen. Unless otherwise indicated,

tetraphenylporphine (TPP) in benzene was used as the standard for the singlet oxygen yield, $\Phi = 0.62$ (42). To calculate the quantum yield of singlet oxygen, the method below was used.

The background signal from a deoxygenated sample, S_{deox} , was subtracted from the signal obtained from an oxygenated sample, S_{ox} .

$$S^{\text{sample}} = S_{\text{ox}} - S_{\text{deox}} \frac{\text{OD (532 nm)}_{\text{ox}}}{\text{OD (532 nm)}_{\text{deox}}} \quad (1)$$

The signal difference between oxygenated samples and deoxygenated samples was usually more than a factor of 10. The signal from the standard, TPP, was calculated in the same way and the quantum yield of the singlet oxygen sample was calculated, relative to that of TPP, as:

$$\Phi_{\text{rel}} = \frac{S^{\text{sample}}}{S^{\text{TPP}}} \frac{\text{OD (532 nm)}^{\text{TPP}}}{\text{OD (532 nm)}^{\text{sample}}} \quad (2)$$

Where the optical density, OD, is measured at the excitation wavelength of 532 nm. The measured Φ values reported in Table 6.1 are the average of four experiments.

RESULTS AND DISCUSSION

Previous studies in our laboratory had suggested that significant antiviral activity of hypericin could be observed in hypoxic conditions. In the present study, we reexamined the importance of oxygen using experimental conditions where the effect of oxygen depletion could be better quantified. The detection limit of the ATP assay was 8.50×10^{-7} M with 70 cps (Figure 6.1). Based on our above argument, we conclude that the detection limit of oxygen is 8.50×10^{-7} M at 70 cps of chemiluminescence measured at 614 nm using a scan

Table 6.1. Quantum yield of singlet oxygen, Φ

compound	solvent	Φ_{rel}	Φ
hypericin	benzene	$0.55 \pm 0.07^{\dagger}$	$0.34 \pm 0.05^{\dagger}$
hypocrellin	benzene	$1.08 \pm 0.11^{\dagger}$	$0.67 \pm 0.07^{\dagger}$
hypocrellin	ethanol	$2.03 \pm 0.33^{\ddagger}$	$0.73 \pm 0.12^{\ddagger}$
hexamethoxyhypericin [*]	ethanol	$3.04 \pm 0.27^{\ddagger}$	$1.09 \pm 0.10^{\ddagger}$

[†]TPP in benzene used as standard, $\Phi = 0.62$ (42).

[‡]Hypericin in ethanol used as standard, $\Phi = 0.36$ (37)

^{*}Prepared as described in English *et al.* (19).

rate of 0.3 sec/nm. Our previous work used an oxygen detection kit that was only sensitive to levels of 6.25×10^{-6} M (38). With the more sensitive assay conditions employed here, samples contained under a normal atmosphere of air had typical levels of oxygen providing 15,000-32,000 counts per second whereas samples which had been stirred under a steady flow of argon for 20 minutes or more had typical levels of oxygen providing 280-7,000 counts per second.

The antiviral activity of hypericin and hypocrellin was markedly reduced by deoxygenation (Figure 6.2). Both hypericin and hypocrellin decreased infectious virus titers by more than 1,000 fold in the presence of oxygen and light. In low oxygen conditions, however, hypericin gave only a 10-fold reduction in virus titer and hypocrellin had no detectable antiviral activity. In fact, no antiviral activity of hypocrellin was detected at oxygen levels three to four times higher than that in which hypericin retained some measurable activity, indicating that deoxygenation had a much more drastic effect on

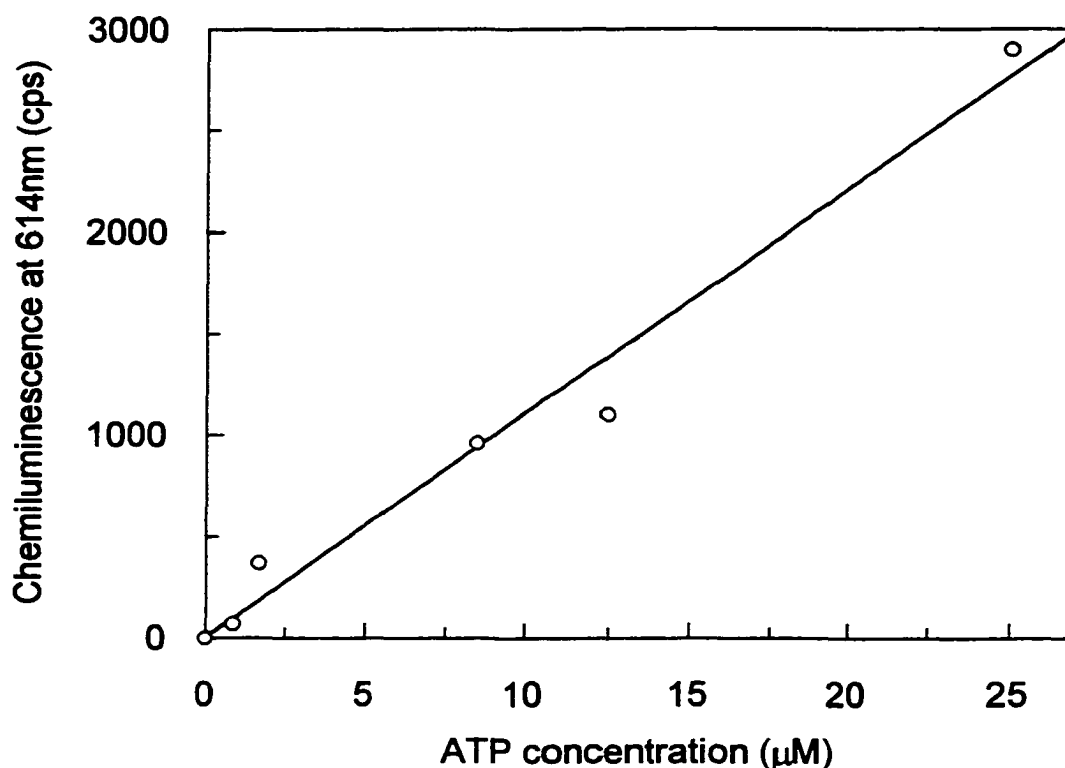


Figure 6.1. A log-log plot illustrating the effect of deoxygenation on the virucidal activity of hypericin and hypocrellin. Samples containing approximately 10^6 FFU were treated with hypericin or hypocrellin, deoxygenated by argon, and assayed for infectious virus as described in the text. Results are reported as \log_{10} reduction in virus titer in test samples as compared to an untreated control sample. Oxygen concentrations are quantified in terms of the chemiluminescent assay described in the text.

hypocrellin-activity than on hypericin activity. This is of interest because the singlet oxygen yield of hypocrellin is roughly twice that of hypericin (Table 6.1). Together, these results suggest that hypericin and hypocrellin differ in the levels of oxygen required for optimal antiviral activity. We had previously taken these differences to indicate that oxygen was not necessary for antiviral activity in hypericin (39). The present results clearly demonstrate that oxygen plays a critical role in virus killing by both hypericin and hypocrellin; however, additional processes may contribute to the enhanced biological activity of hypericin at low oxygen levels.

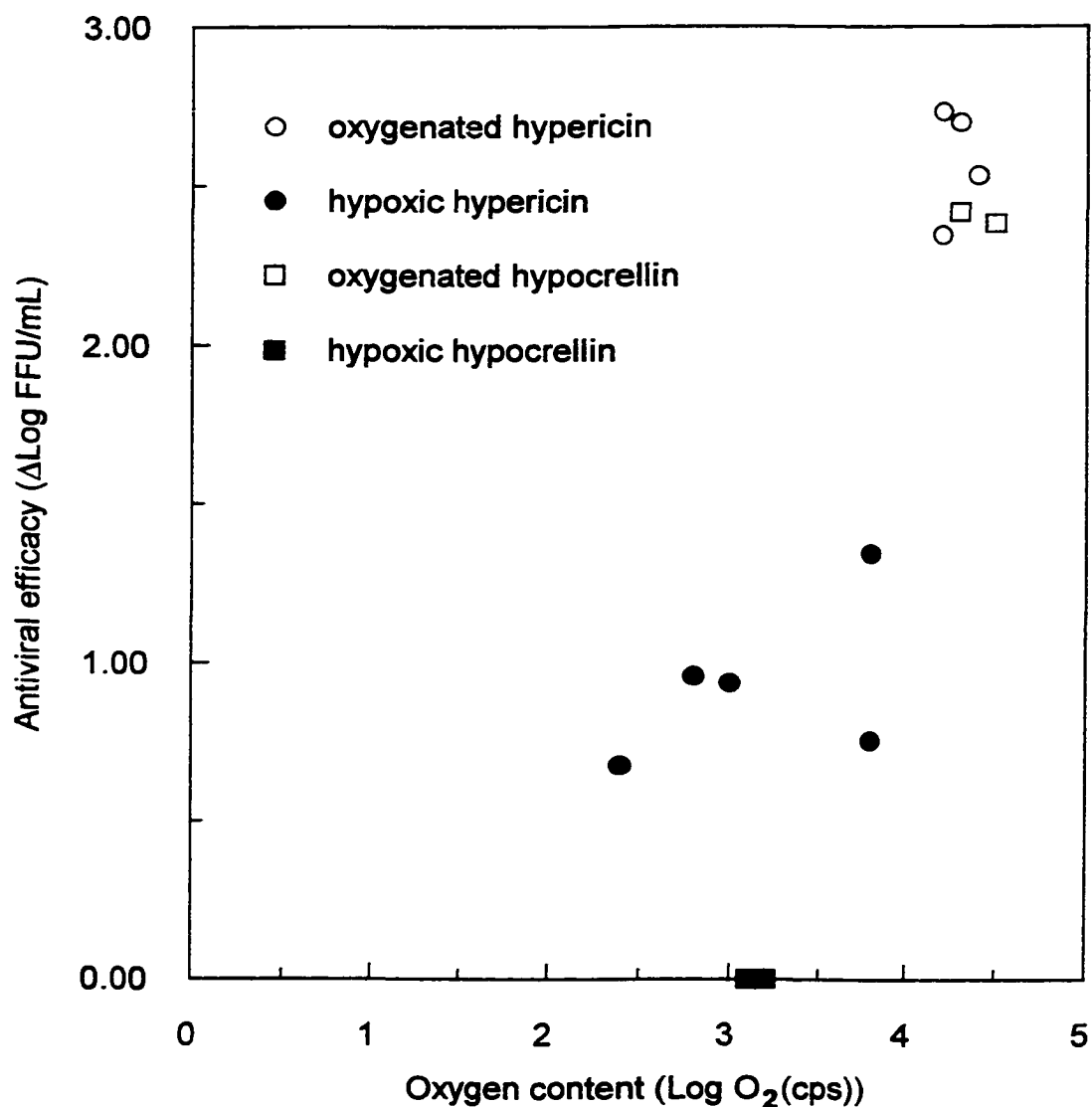


Figure 6.2. Dependence of the chemiluminescence signal at 614 nm on ATP concentration. Each point represents data from a reaction that is pseudo first-order with respect to ATP. Because the stoichiometry for the chemiluminescent reaction is the same for ATP as for oxygen, the intensity of chemiluminescence, as measured in counts per second (cps) is taken as a quantitative measure of oxygen concentration under “hypoxic” conditions, when the reaction is expected to be pseudo first-order with respect to oxygen. See text for details.

A significant nonradiative process in hypericin and its analogs is intramolecular proton (or atom) transfer (16-25). Of special relevance to the role of labile protons for the light-induced biological activity of hypericin is the observation that hypericin acidifies its surroundings upon light absorption (40, 43, 44). The role of photogenerated protons takes on significance in the context of the growing body of literature implicating changes in pH with inhibition of virus replication (45), antitumor activity (46,47), and apoptosis (48-51).

Recently we have employed a confocal laser microspectrofluorometric analysis to monitor intracellular pH changes during photosensitization of cells by hypocrellin A using the ratiometric fluorescent pH probe, C-Snarf-1 (40). Under 0.1 μ W of excitation power, this pH decrease is *larger and faster* for cells treated with hypocrellin A than for those treated with hypericin. Thus, hypocrellin appears to be more efficient than hypericin in producing photoinduced pH decreases. This interpretation is supported by the observation that the initial value of the pH is already very low when cells are not protected from ambient light before the microspectrofluorometric measurements. Such high sensitivity of hypericin to light is not observed. Because acidification occurs so rapidly with hypocrellin, it may be that the transferred protons do not effectively potentiate the activity of oxygen species. An example of such acid-induced potentiation is the following. It has been shown that while superoxide radical, $O_2^{\bullet-}$, does not react with linoleic acid, its conjugate acid, the hydroperoxyl radical, HO_2^{\bullet} , does so at a biologically significant rate (52-54).

CONCLUSIONS

Hypericin is a more effective antiviral agent at low oxygen concentrations than is hypocrellin (Figure 6.2). Photogenerated protons from hypericin and hypocrellin

(39,40,43,44) are suggested to contribute to this antiviral activity. One possible mechanism by which these protons may enhance antiviral activity is by potentiation of activated oxygen species. The light-induced pH drop is more rapid for hypocrellin than for hypericin.

Consequently, it is possible that for hypocrellin at low oxygen levels, under experimental conditions identical to those used for hypericin, the light-induced pH drop is too rapid to be effective in activating the oxygen species. It is, of course, possible that the enhanced antiviral activity in hypericin arises from direct interaction of hypericin itself or reactive hypericin species in a classical type I mechanism.

Our previous work has indicated that antiviral activity of hypericin is dependent on the hypericin concentration (26). The present study has demonstrated the sensitivity of the antiviral activity of hypericin and hypocrellin to the concentration of oxygen. A comprehensive investigation of the biological activities of hypericin, hypocrellin, and their analogs will necessarily consider the roles of the photosensitizer concentration, the oxygen concentration, and the intensity and duration of the light exposure.

ACKNOWLEDGMENTS—J.W.P. was supported by NSF grant CHE-9613962. Support was also provided through the Carver Trust. We thank Professor Peter de Witte for communicating his results on the oxygen requirement for hypericin activity while this manuscript was in preparation, Dr. F. Sureau for helpful conversations, and Dr. A. Darmany for useful discussions and technical assistance with the singlet oxygen measurements.

REFERENCES

1. Carpenter, S. and G. A. Kraus (1991) Photosensitization is required for inactivation of equine infectious anemia virus by hypericin. *Photochem. Photobiol.* **53**,169-174.
2. Meruelo, D., G. Lavie and D. Lavie (1988) Therapeutic agents with dramatic antiretroviral activity and little toxicity at effective doses: aromatic polycyclic diones hypericin and pseudohypericin. *Proc. Natl. Acad. Sci. USA* **85**, 5230-5234.
3. Lavie, G., F. Valentine, B. Levin, Y. Mazur, G. Gallo, D. Lavie, D. Weiner and D. Meruelo (1989) Studies of the mechanisms of action of the antiretroviral agents hypericin and pseudohypericin. *Proc. Natl. Acad. Sci. USA* **86**, 5963-5967.
4. Hudson, J. B., J. Zhou, J. Chen, L. Harris, L. Yip and G. H. N. Towers (1994) Hypocrellin, from *Hypocrella bambuse*, is phototoxic to human immunodeficiency virus. *Photochem. Photobiol.* **60**, 253-255.
5. Lopez-Bazzocchi, I., J. B. Hudson and G. H. N. Towers (1991) Antiviral activity of the photoactive plant pigment hypericin. *Photochem. Photobiol.* **54**, 95-98.
6. Degar, S., A. M. Prince, D. Pascaul, G. Lavie, B. Levin, Y. Mazur, D. Lavie, L. S. Ehrlich, C. Carter and D. Meruelo (1992) Inactivation of the human immunodeficiency virus by hypericin: evidence for photochemical alterations of p24 and a block in uncoating. *AIDS Res. Hum. Retroviruses* **8**, 1929-1936.
7. Meruelo, D., S. Degar, N. Amari, Y. Mazur, D. Lavie, B. Levin and G. Lavie (1992) Mode of action of hypericin as an antiretroviral agent and other relevant findings. In *Natural Products as Antiviral Agents*. (Edited by C. K. Chu and H. G. Cutler), pp. 91-119. Plenum Press, New York.
8. (1991) Treating AIDS with worts. *Science* **254**, 522.

9. Thomas, C. and R. S. Pardini (1992) Oxygen dependence of hypericin-induced phototoxicity to EMT6 mouse mammary carcinoma cells. *Photochem. Photobiol.* **55**, 831-837.
10. Thomas, C., R. S. MacGill, G. C. Miller and R. S. Pardini (1992) Photoactivation of hypericin generates singlet oxygen in mitochondria and inhibits succinoxidase. *Photochem. Photobiol.* **55**, 47-53.
11. Lenard, J., A. Rabson and R. Vanderoef (1993) Photodynamic inactivation of infectivity of human immunodeficiency virus and other enveloped viruses using hypericin and rose bengal: inhibition of fusion and syncytia formation. *Proc. Natl. Acad. Sci. USA* **90**, 158-162.
12. Kreitmair, H. (1950) *Hypericum perforatum*—das Johanniskraut. *Pharmazie* **5**, 556-557.
13. Linde, K., G. Ramirez, C. D. Mulrow, A. Pauls, W. Weidenhammer and D. Melchart (1996) St John's wort for depression—an overview and meta-analysis of randomised clinical trials. *Br. Med. J.* **313**, 253-258.
14. Suzuki, O., Y. Katsumata, M. Oya, S. Bladt and H. Wagner (1984) Inhibition of monoamine oxidase by hypericin. *Planta Medica* **50**, 272-274.
15. Anker, L., R. Gopalakrishna, K. D. Jones, R. E. Law and W. T. Couldwell (1995) Hypericin in adjuvant brain tumor therapy. *Drugs of the Future* **20**, 511-517.
16. Gai, F., M. J. Fehr and J. W. Petrich (1993) Ultrafast excited-state processes in the antiviral agent hypericin. *J. Am. Chem. Soc.* **115**, 3384-3385.
17. Gai, F., M. J. Fehr and J. W. Petrich (1994) Observation of excited-state tautomerization in the antiviral agent hypericin and identification of its fluorescent

- species. *J. Phys. Chem.* **98**, 5784-5795.
18. Gai, F., M. J. Fehr and J. W. Petrich (1994) Role of solvent in excited-state proton transfer in hypericin. *J. Phys. Chem.* **98**, 8352-8358.
 19. English, D. S., W. Zhang, G. A. Kraus and J. W. Petrich (1997) Excited-state photophysics of hypericin and its hexamethoxy analog, intramolecular proton transfer as a nonradiative process in hypericin. *J. Am. Chem. Soc.* **119**, 2980-2986.
 20. English, D. S., K. Das, J. M. Zenner, W. Zhang, G. A. Kraus, R. C. Larock and J. W. Petrich (1997) Hypericin, hypocrellin, and model compounds, primary photoprocesses of light-induced antiviral agent. *J. Phys. Chem. A.* **101**, 3235-3240.
 21. Das, K., D. S. English, M. J. Fehr, A. V. Smirnov and J. W. Petrich (1996) Excited-state processes in polycyclic quinones: the light induced antiviral agent, hypocrellin, and comparison with hypericin. *J. Phys. Chem.* **100**, 18275-18281.
 22. Das, K., D. S. English and J. W. Petrich (1997) Solvent dependence on the intracellular excited-state proton or hydrogen atom transfer in hypocrellin. *J. Am. Chem. Soc.* **119**, 2763-2764.
 23. Das, K., D. S. English and J. W. Petrich (1997) Deuterium isotope effect on the excited-state photophysics of hypocrellin, evidence for proton or hydrogen atom transfer. *J. Phys. Chem. A.* **101**, 3241-3245.
 24. English, D., K. Das, K. D. Ashby, J. Park, J. W. Petrich and E. W. Castner, Jr. (1997) Confirmation of excited-state proton transfer and ground-state heterogeneity in hypericin by fluorescence upconversion. *J. Am. Chem. Soc.* **119**, 11585-11590.
 25. Das, K., E. Dertz, J. Paterson, W. Zhang, G. A. Kraus and J. W. Petrich (1998) Hypericin, hypocrellin, and model compounds: steady-state and time-resolved

- fluorescence anisotropies. *J. Phys. Chem. B* **102**, 1479-1484.
26. Carpenter, S., M. J. Fehr, G. A. Kraus and J. W. Petrich (1994) Chemiluminescent activation of the antiviral activity of hypericin: a molecular flashlight. *Proc. Natl. Acad. Sci. USA* **91**, 12273-12277.
27. Kraus, G. A., W. Zhang, M. J. Fehr, J. W. Petrich, Y. Wannemuehler and S. Carpenter (1996) Research at the interface between chemistry and virology, development of a molecular flashlight. *Chem. Rev.* **96**, 523-535.
28. Duran, N. and P.-S. Song (1986) Hypericin and its photodynamic action. *Photochem. Photobiol.* **43**, 677-680.
29. Diwu, Z. (1995) Novel therapeutic and diagnostic applications of hypocrellins and hypericins. *Photochem. Photobiol.* **61**, 529-539.
30. Lown, J. W. (1997) Photochemistry and photobiology of perylenequinones. *Can. J. Chem.* **75**, 99-119.
31. Jardon, P., N. Lazorchak and R. Gautron (1986) Propriétés du premier état triplet de l'hypericine étude par spectroscopie laser. *J. Chim. Phys.* **83**, 311-315.
32. Racinet, H., P. Jardon and R. Gautron (1988) Formation D'oxygène singulet $^1\Delta_g$ photosensibilisée par l'hypericine étude cinétique en milieu micellaire non ionique. *J. Chim. Phys.* **85**, 971-977.
33. Weiner, L. and Y. Mazur (1992) EPR studies of hypericin. Photogeneration of free radicals and superoxide. *J. Chem. Soc. Perkin Trans.* **2**, 1439-1442.
34. Diwu, Z. and J. W. Lowen (1993) Photosensitization with anticancer agents. 17. EPR studies of photodynamic action of hypericin: formation of semiquinone radical and activated oxygen species on illumination. *Free Rad. Biol. Med.* **14**, 209-215.

35. Malkin, J. and Y. Mazur (1993) Hypericin derived triplet states and transients in alcohols and water. *Photochem. Photobiol.* **57**, 929-933.
36. Hudson, J. B., V. Imperial, R. P. Haugland and Z. Diwu (1997) Antiviral activities of photoreactive perylenequinones. *Photochem. Photobiol.* **65**, 352-354.
37. Darmanyan, A., L. Burel, D. Eloy and P. Jardon (1994) Singlet oxygen production by hypericin in various solvents. *J. Chim. Phys.* **91**, 1774-1785.
38. Fehr, M. J., S. L. Carpenter and J. W. Petrich (1994) The role of oxygen in the photoinduced antiviral activity of hypericin. *Bioorg. Med. Chem. Lett.* **4**, 1339-1344.
39. Fehr, M. J., S. L. Carpenter, Y. Wannemuehler and J. W. Petrich (1995) Roles of oxygen and photoinduced acidification in the light-dependent antiviral activity of hypocrellin A. *Biochemistry* **34**, 15845-15848.
40. Chaloupka, R., F. Sureau, E. Kocisova and J. W. Petrich (1998) Hypocrellin A photosensitization involves an intracellular pH decrease in 3T3 cells. *Photochem. Photobiol.* **68**, 44-50.
41. Carpenter, S., L. H. Evans, M. Sevoian and B. Chesebro. (1987) Role of the host immune response in selection of equine infectious anemia virus variants. *J. Virol.* **61**, 3783-3789.
42. Schmidt, R. And E. Afshari (1990) Effect of solvent on the phosphorescence rate constant of singlet molecular oxygen ($^1\Delta_g$). *J. Phys. Chem.* **94**, 4377-4378.
43. Fehr, M. J., M. A. McCloskey and J. W. Petrich (1995) Light-induced acidification by the antiviral agent hypericin. *J. Am. Chem. Soc.* **117**, 1833-1836.
44. Sureau, F., P. Miskovsky, L. Chinsky and P. Y. Turpin (1996) Hypericin-induced cell photosensitization involves an intracellular pH decrease. *J. Am. Chem. Soc.* **118**,

- 9484-9487.
45. Pinto, L. H., L. J. Holsinger and R. A. Lamb (1992) Influenza virus M₂ protein has ion channel activity. *Cell* **69**, 517-528.
 46. Newell, K. J. and I. F. Tannock, I. F. (1989) Reduction of intracellular pH as a possible mechanism for killing cell in acidic region of solid tumor, effects of carbonylcyanine-3-chlorophenylhydrazone. *Cancer Res.* **49**, 4447-4482.
 47. Newell, K. J., P. Wood, I. Stratford and I. Tannock (1992) Effect of agents which inhibit the regulation of intracellular pH on murine solid tumours. *Br. J. Cancer* **66**, 311-317.
 48. Barry, M. A., J. E. Reynold and A. Eastman (1993) Etoposide-induced apoptosis in human HL-60 cells is associated with intracellular acidification. *Cancer Res.* **53**, 2349-2357.
 49. Li, J. and A. Eastman (1995) Apoptosis in an interleukin-2-dependent cytotoxic lymphocyte cell line is associated with intracellular acidification. *J. Biol. Chem.* **270**, 3203-3211.
 50. Gottlieb, R. A., J. Nordberg, E. Skowronski and B. M. Babior (1996) Apoptosis induced in Jurkat cells by several agents is preceded by intracellular acidification. *Proc. Natl. Acad. Sci. USA* **93**, 654-658.
 51. Weller, M., M. Trepel, C. Grimm, M. Schabet, D. Bremen, S. Krajewski and J. C. Reed (1997) Hypericin-induced apoptosis of human malignant glioma cells is light-dependent, independent of bcl-2 expression, and does not require wild-type p53. *Neurological Res.* **19**, 459-470.
 52. Gebicki, J. M. and B. H. J. Bielski (1981) Comparison of the capacities of the

- perhydroxyl and the superoxide radicals to initiate chain oxidation of linoleic acid. *J. Am. Chem. Soc.* **103**, 7020-7022.
53. Ferradini, C. (1986) Espèces activées radicalaires de l'oxygène. *Biochimie* **68**, 779-785.
54. Bielski, B. H. J., R. L. Arudi and M. W. Sutherland. (1983) A study of the reactivity of HO_2/O_2^- with unsaturated fatty acids. *J. Biol. Chem.* **258**, 4759-4761.

CHAPTER 7: TUMOR CELL TOXICITY OF HYPERICIN AND RELATED ANALOGS

A paper submitted in Photochemistry and Photobiology

Nick J. Wills¹, Jaehun Park², Jin Wen², Sarathy Kesavan², George A. Kraus²,
Jacob W. Petrich², and Susan Carpenter^{1*}

ABSTRACT

A series of hypericin analogs were found to differ in their cytotoxic activity induced by ambient light levels. These analogs vary in their ability to partition into cells, to generate singlet oxygen as well as in other photophysical properties. The data suggest that the biological activity of hypericin is due to a combination of factors whose roles may vary under different circumstances.

INTRODUCTION

Hypericin and pseudohypericin (Figure 7.1) are members of the phenanthroperylene quinone family and are major constituents of the plant *Hypericum perforatum*, commonly known as St. John's wort. Hypericin has demonstrated light-induced anti-tumor and antiviral (1-5) activities and has attracted interest as a possible treatment for various cancers and viral infections (3,4,6). While the biological activities of hypericin have been well documented, the molecular and cellular events that mediate those activities are less well characterized.

¹ Department of Veterinary Microbiology and Preventive Medicine, Iowa State University, Ames, IA 50011

² Department of Chemistry, Iowa State University, Ames, IA 50011

*Authors to whom correspondence should be addressed.

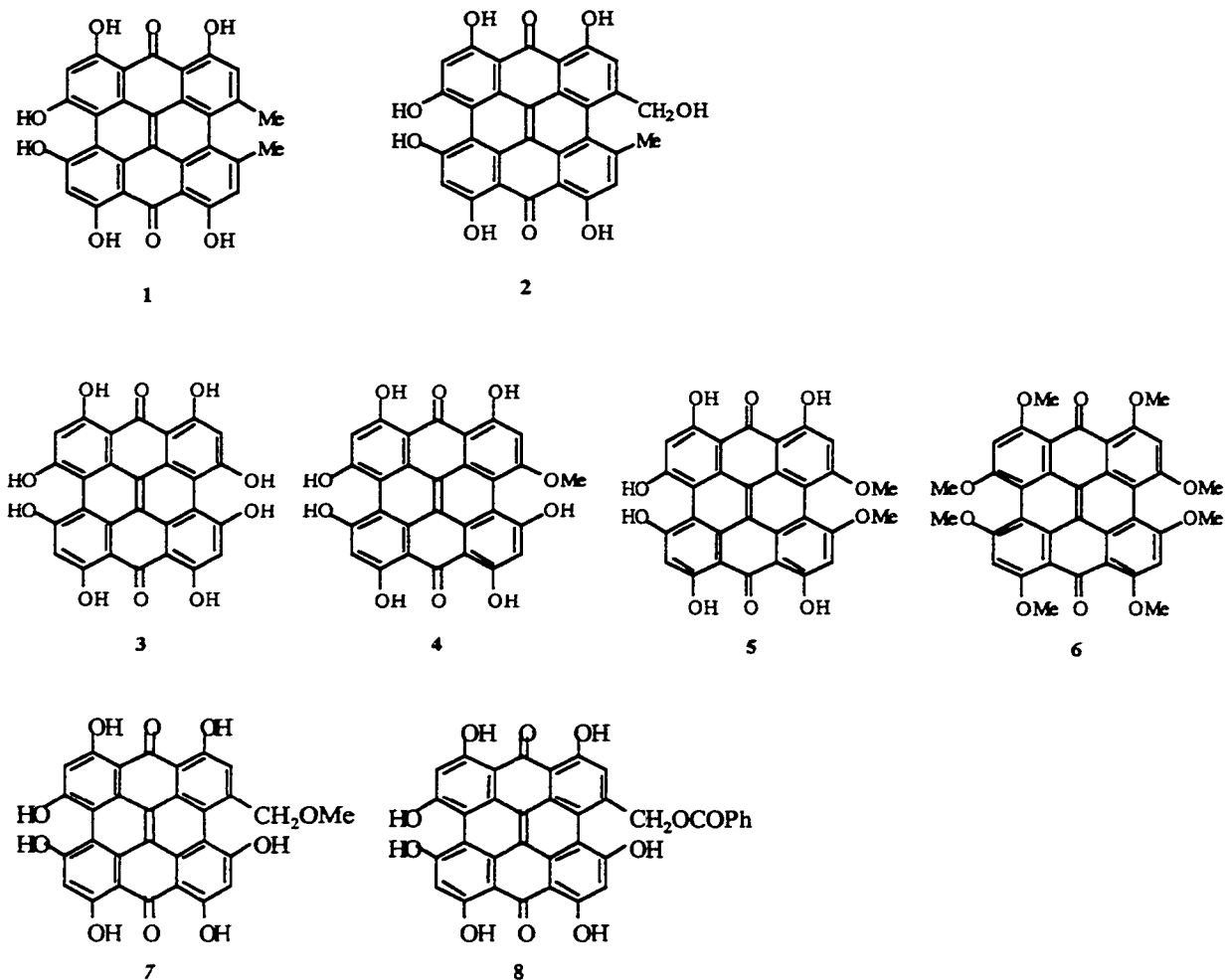


Figure 7.1. Structure of hypericin (1), pseudohypericin (2), and analogs 3-8.

Light-induced production of singlet oxygen is thought to be the primary mechanism of tumor cell toxicity (7). Singlet oxygen production results in lipid peroxidation and membrane damage in the cell, leading to disruption of the cell membrane and a necrotic phenotype (8,9). Lower levels of singlet oxygen may lead to leakage of the mitochondrial membrane with subsequent release of cytochrome c and activation of a pro-apoptotic enzymatic cascade (8). Light activation of hypericin can induce an intracellular pH drop (10), and it has been

suggested that intermolecular proton transfer contributes to the antiviral and cytotoxic effects of hypericin-related compounds, even in relatively hypoxic conditions (11). In addition, hypericin interferes with cellular transcription factors and a number of cell signaling pathways (12-15). Although it is not known how interactions with cell signaling pathways contribute to hypericin-mediated cytotoxicity, inhibition of these pathways may be an important component of any therapeutic application of hypericin-related compounds.

Hypericin is a more effective antiviral agent than pseudohypericin (16,17); however, the molecular basis for the differences in activity is not well understood. Insight into the molecular rationale for the differences in biological activity among related hypericin analogs may enable researchers to design more effective therapeutics. Previous studies from our group showed that minor changes in substituents resulted in dramatic differences in antiviral activity (18,19). In this paper, we extend our previous analyses of hypericin analogs to examine their level and mode of cytotoxic activity. These studies suggest that cytotoxic activity depends on a combination of factors, including photophysical properties, membrane solubility, and singlet oxygen production.

MATERIALS AND METHODS

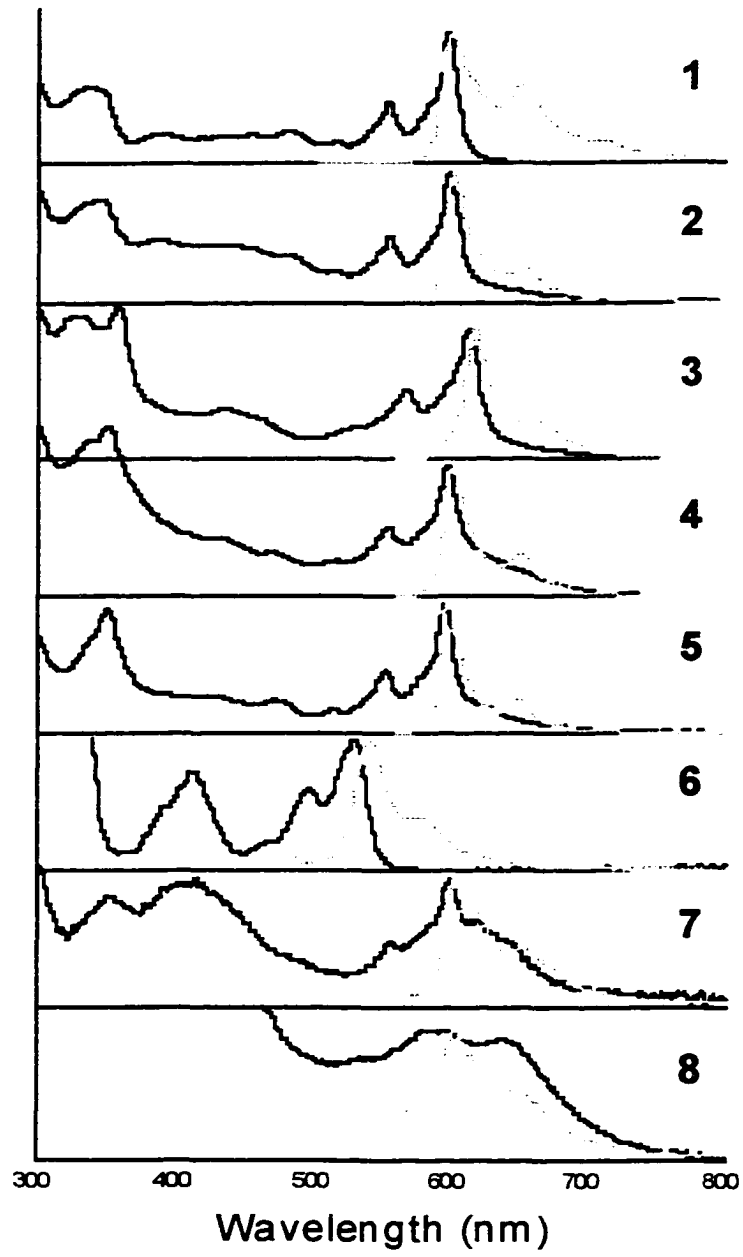
Cell lines. The human colon adenocarcinoma cell line SW480 (ATCC# CCL 228) was grown in Dulbecco's modified Eagle medium (DMEM) supplemented with 10% fetal calf serum and penicillin/streptomycin. The cells were incubated at 37°C with 7% CO₂.

Synthesis of analogs. Hypericin (Molecular Probes, Eugene, OR) and pseudohypericin (Calbiochem, La Jolla, CA) were purchased from commercial sources. The synthesis of analogs 3-6 was previously described (18,19). To synthesize the methyl ether

of pseudohypericin (**7**) a catalytic amount of sulfuric acid was added to a solution of 10 mg of pseudohypericin in 2 mL of methanol. This solution was stirred at ambient temperature for four hours and heated at 45 °C for four hours. The solution was then cooled, concentrated in vacuo and the product purified using a silica gel preparative layer plate. The benzoate of pseudohypericin (**8**) was synthesized by adding N-methylmorpholine (5 mg, 0.049 mmol) to a solution of benzoic acid (0.0214 mmol) in anhydrous methylene chloride (2 mL) at -15 °C. The solution was stirred for 5 minutes at this temperature, after which benzylchloroformate (8 mg, 0.046 mmol) was added to get a yellow solution. The yellow solution was stirred at -15 °C for 15 minutes before 1-hydroxybenzotriazole (3 mg, 0.022 mmol) was added. The reaction mixture was stirred for an additional 20 minutes before pseudohypericin (11 mg, 0.0213 mmol) dissolved in DMF (0.2 mL) was added, resulting in a deep red solution. The solution was allowed to warm to room temperature and was stirred at room temperature for an additional 12 h. After 12 h, the solvent was evaporated and the crude mixture was purified by preparative thin layer chromatography using a mixture of ethyl acetate and methanol. The steady state absorption and emission spectra of all analogs are given in Figure 7.2.

Cytotoxicity assay. SW480 cells were seeded in 6-well plates at a concentration of 1×10^6 cells/well, and allowed to adhere overnight. The next day, the media was replaced with prewarmed media, and hypericin or related analogs were added to a final concentration of 20 μ M. Cells were incubated at room temperature for 30 minutes in the dark, or were illuminated under standard overhead fluorescent bulbs (Philips, 34W) at a distance of 1.8 m from the light source. Cell viability was assayed using the MTT metabolic activity assay (R&D Systems, Minneapolis, MN), and the percent cytotoxicity was calculated from a

Figure 7.2. Steady-state absorption (black line) and emission (gray line) of hypericin and analogs. Absorption measurements were obtained with a Perkin Elmer Lambda18 double beam UV-Vis spectrophotometer with 1-nm band pass. A 1-cm pathlength cuvette was employed. Fluorescence measurements are obtained with a Spex Fluoromax fluorometer. The individual spectra (indicated by analog number) are normalized to the peak of maximum absorbance in the visible range. The extinction coefficients shown in Table 7.1 are: 1, $44,000 \text{ M}^{-1} \text{ cm}^{-1} \pm 5\%$ at 599nm; 2, $9,000 \text{ M}^{-1} \text{ cm}^{-1} \pm 10\%$ at 599nm; 3, $21,000 \text{ M}^{-1} \text{ cm}^{-1} \pm 10\%$ at 612nm; 4, $23,000 \text{ M}^{-1} \text{ cm}^{-1} \pm 10\%$ at 596nm; 5, $6,000 \text{ M}^{-1} \text{ cm}^{-1} \pm >50\%$ at 594nm; 6, $8,100 \text{ M}^{-1} \text{ cm}^{-1} \pm 50\%$ at 528nm; 7, $640 \text{ M}^{-1} \text{ cm}^{-1} \pm 20\%$ at 600nm; 8, $450 \text{ M}^{-1} \text{ cm}^{-1} \pm 15\%$ at 585nm. Extinction coefficients were determined as usual by plotting absorbance against concentration and taking the slope. Errors in extinction coefficient arise from uncertainty in the initial concentration of stock solution, owing to solubility problems or perhaps to sample degradation over time.



standard curve derived from serial dilutions of known cell numbers. Each analog was assayed in triplicate, and each experiment was repeated at least two times.

Cell Association. SW480 cells were aliquoted in a standard Eppendorf tube at 5×10^5 cells in 500 μ l phosphate buffered saline (PBS) containing 20 μ M of each analog. The tubes were gently rocked for 30 min in the dark, and the cells were pelleted by centrifugation. The supernatant fraction was collected (F_{sup}), the cells were extracted with 95% ethanol (F_{ext}) as previously reported (3). To determine the amount of analog in each fraction, 30 μ l of the undiluted analog (F_{start}), F_{sup} , or F_{ext} were added to 1.5ml DMSO and the steady state absorbance spectrum of the samples was measured using a Perkin Elmer Lambda18 double beam UV-Vis spectrophotometer with 1 nm band pass. The absorbance readings were collected at the wavelength of peak visible absorption for each analog and were used to calculate the amount of analog that was cell associated as follows. The percent recovered (R) was calculated as: $R = (A_{F_{ext}} + A_{F_{sup}}) / A_{F_{start}} * 100$; the percent of the compound that was cell associated was determined as: $CA = A_{F_{ext}} / (A_{F_{ext}} + A_{F_{sup}}) * 100$. For comparisons among the analogs, the percent cell-associated was corrected for the percent recovered as: Corrected Cell Associated = $(CA/R) * 100$. All assays were done in duplicate and repeated two to three times.

Measurement of Singlet Oxygen Yield. A 1-kHz Nd: YAG (Quantronix) was used to excite samples at 527 nm. The excitation irradiance at most of the samples was 13 mW/cm^2 , except for 6, where it was 5 mW/cm^2 . A laser pointer (B & W Tex Inc., Newark, DE) was initially tried as an excitation source, but its lower power, providing 2 mW/cm^2 at 532nm, was insufficient to produce measurable quantities of singlet oxygen under the conditions of our experiment. Fluorescence and scattered light were blocked by a 1270 ± 40

nm bandpass filter fastened to a liquid nitrogen cooled charge-coupled device (North Coast model E0-817). The excitation beam was chopped at 400 Hz and the output of the detector was fed to a lock-in amplifier (Stanford Research SR510), which provided the signal, S , proportional to the intensity of the singlet oxygen luminescence. Rose bengal in DMSO was used as the standard for the singlet oxygen yield, $\Phi=0.162$ (20). All analogs were measured in DMSO. The relative quantum yield and the quantum yield of singlet oxygen were calculated as below: where the optical density, OD, was measured at the excitation wavelength of 527nm.

$$\Phi = \Phi_{rel} \times 0.162 \qquad \Phi_{rel} = \frac{S_{sample}}{S_{standard}} \frac{OD_{527nm}^{standard}}{OD_{527nm}^{sample}}$$

The OD of most of the compounds was ~ 0.2 , except for analogs **7** and **8**, for which it was ~ 0.08 . The measured Φ values reported in Table 7.1 represent the average of three experiments.

RESULTS

Cytotoxic activity of hypericin analogs

Previous studies had determined that hypericin analogs with minor alterations in substituents showed dramatic differences in antiviral activity (18). Initial experiments were done to determine if these analogs also differed in cytotoxic activity. SW480 cells were treated with 20 μM of each analog and cytotoxic activity was quantified using an MTT assay (Figure 7.3). The cytotoxicity of hypericin (**1**) approached 100%, and exceeded the maximum sensitivity of the assay, which was determined to be 94% (data not shown). Pseudohypericin (**2**) and the other analogs displayed a range of cytotoxic activity in the light,

Table 7.1. Biological and photophysical properties of hypericin (1), pseudohypericin (2), and analogs 3-8.

Analog	Cytotoxicity ¹	Cell Association ²			¹ O ₂ Yield ^{3,4}	ϵ (M ⁻¹ cm ⁻¹) ⁵
		Recovered	Cell Associated	Corrected Cell Associated		
1	94± 2	96.2	67.9	70.5	0.34±0.04	44,000
2	21±16	93.3	65.2	70.0	0.46±0.02	9,000
3	0± 4	81.5	23.8	29.2	0.41±0.04	21,000
4	37± 3	73.5	50.5	68.5	0.15±0.01	23,000
5	88± 5	117.0	72.6	62.1	0.25±0.01	6,000
6	19±12	55.0	14.8	26.8	0.21±0.02	8,100
7	0±15	172.4	135.8	78.7	0.56±0.03	640
8	0± 8	100.0	64.7	64.7	0.76±0.11	450

¹Cytotoxicity determined by MTT assay and reported as percentages.

²All values were calculated as described in Materials and Methods and are reported as percentages.

³As determined in DMSO, relative to rose bengal in DMSO used as standard. $\Phi = 0.162$.

⁴An extensive compilation of singlet oxygen yields is given in (20).

⁵Wavelengths used for calculations and standard errors of mean values are given in the legend to Figure 7.2.

whereas no compound tested had activity in the absence of light. The biological activity of hypericin analogs 3-6 was highly sensitive to changes in the number of hydroxyl groups on the phenanthroperylene ring. Analog 3, which was substituted with eight hydroxyl groups, showed no cytotoxic activity. Increased cytotoxic activity was observed when the bay hydroxyl groups (that is, those not involved in intramolecular hydrogen bonding with the carbonyl groups) were converted into methoxy groups (compare the relative activity of analogs 3, 4 and 5), with the cytotoxicity of 5 nearly that of hypericin. However, analog 6, where all of the hydroxyl groups were converted into methoxy groups, showed markedly reduced cytotoxic activity. This result is consistent with the hypothesis that the biological activity involves light induced acidification mediated by labile proton transfer (21).

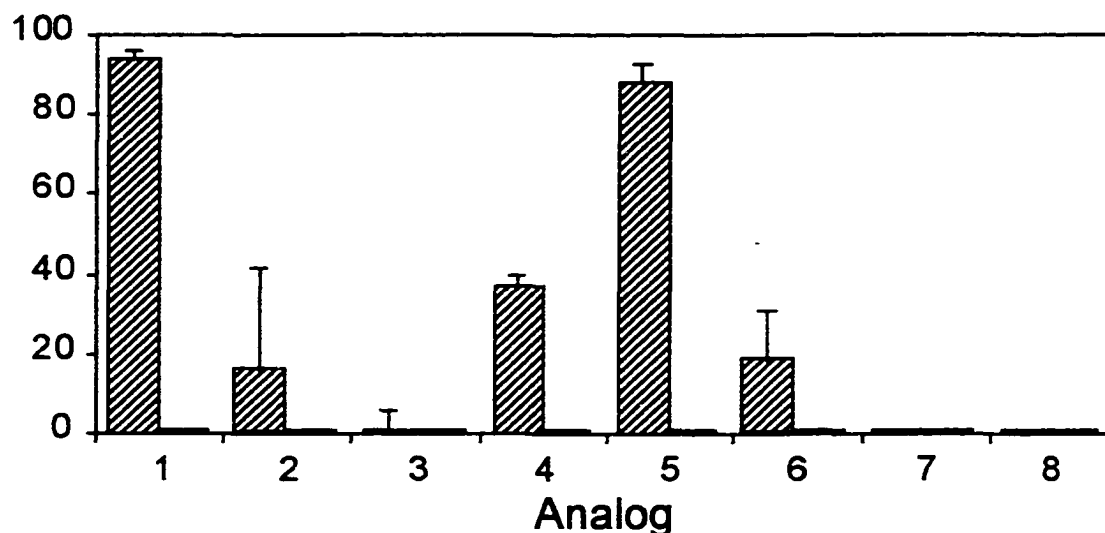


Figure 7.3. Cytotoxic activity of hypericin (1), pseudohypericin (2), and analogs 3-8 on SW480 cells. Hashed bars represent experiments done in light, black bars represent experiments done in dark. The percent cytotoxicity was calculated relative to the number of viable cells in samples treated with DMSO alone. Values are the mean of at least four independent treatments, each assayed in triplicate. Error bars represent the standard deviation.

Pseudohypericin (2) consistently showed lower levels of cytotoxicity as compared to hypericin. In the majority of assays, pseudohypericin killed approximately 30% of the cells, although activity ranged from 0 to 50% across all experiments. Analogs 7 and 8, which contained additional modifications to the methanol side group, showed no cytotoxic activity. Overall, the analogs displayed similar patterns of tumor cell cytotoxicity as was previously reported for their antiviral activity (18), suggesting a similar mechanism may be involved for the antiviral and anti-tumor activity of hypericin and related analogs.

Cell association studies

The cytotoxic activity of the hypericin analogs is likely dependent on the amount of analog that associates with the cell. Therefore, we calculated the amount of each analog that partitioned with SW480 cells after a 30 minute incubation at room temperature in the dark. Following incubation, cells were centrifuged and the amount of analog in the supernatant and the cell extract fractions was calculated based upon their absorbance. In most cases, using the corrected cell association values, 62-70% of each analog partitioned with the cell fraction. The exceptions were analogs **3** and **6**, where less than 30% of the analog was cell associated. The cytotoxicity of **3** and **6** was significantly less than that of hypericin, suggesting that the reduced level of cell association may contribute to the reduced cytotoxicity of these analogs. However, there was a range of cytotoxic activity among the analogs with similar values of cell association. When all analogs were considered, there was no correlation between cell association and cytotoxic activity (Figure 7.4a). Therefore, partitioning of the molecule into the cell may be necessary for the cytotoxic activity of the analog, but this factor alone is not sufficient to explain all of the differences seen in cytotoxic activity.

Singlet oxygen generation

Singlet oxygen is considered to be important in cytotoxic activity of photoactivated hypericin, and we measured the singlet oxygen yield for analogs **1-8** (Table 7.1). Among the analogs in our study, we found some with high singlet oxygen yields and low cytotoxic activity, whereas other analogs showed lower singlet oxygen yields and high cytotoxic activity.

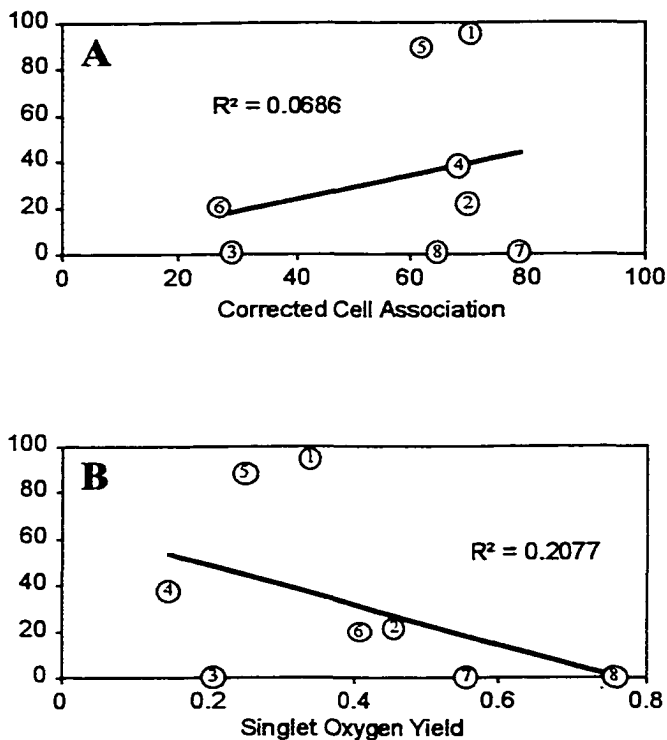


Figure 7.4. Correlation between cytotoxic activity and a) corrected cell association or b) singlet oxygen yield. The location of each analog is indicated by 1-8. The R^2 value was calculated by linear regression analysis using Microsoft Excel.

Notably, 7 and 8, which have the highest yields, were essentially non-toxic to the SW480 cells under ambient light conditions. Also, 5 had lower singlet oxygen yields and higher cytotoxic activity than 2, yet both showed comparable cell association levels. Overall, we found a very poor correlation between cytotoxicity and singlet oxygen yield (Figure 7.4b).

The singlet oxygen yields were, by necessity (see Materials and Methods), measured using a high intensity excitation source. In contrast the light-induced cytotoxicity of the analogs was measured using fluorescent room light. Therefore, we included the maximum extinction coefficients of all compounds in our comparative analysis (Table 7.1). The maximum extinction coefficients of 7 and 8 in the visible region of the spectrum were on the order of 100 times less

than that of hypericin; those of analogs 2, 5 and 6 were approximately 5 fold lower than hypericin. These differences in absorbance may provide a partial explanation for the low cytotoxicity of 7 and 8 in ambient light conditions, despite efficient singlet oxygen production under high intensity excitation. However, comparative analysis within sub-groups of analogs having relatively similar extinction coefficients (i.e. 1, 3, 4 or 2, 5, 6), or singlet oxygen yields (2 and 3), failed to find a correlation between either of these parameters and cytotoxicity. These results indicate that the photophysical properties of the analogs are an important component of cytotoxicity, but cannot account for all of the observed differences in cytotoxic activity shown in Figure 7.3.

DISCUSSION

Hypericin exhibits potent and diverse biological activities and has received wide attention as a potential therapeutic drug. However, the molecular mechanisms of biological activity are not well understood. We previously suggested that differences in the antiviral activity among hypericin and several synthetic analogs were due to differences in the ability of the molecules to partition between water and the cell membrane (18,19). Here, we used tumor cell toxicity to examine the importance of membrane association and photophysical properties to the cytotoxic activity of hypericin and related analogs. The analogs differed in their ability to partition into cells, to generate singlet oxygen, and in their maximum extinction coefficient. Each of these parameters was suggested to contribute to the biological activity of the analogs; however, no one parameter was found to correlate directly with cytotoxic activity. Optimal biological activity of photoactivated hypericin may therefore

depend on the interaction of a number of factors. Moreover, the relative contribution of each factor may vary, depending on the experimental conditions.

It is not clear how minor modifications to hypericin side groups can result in dramatic differences in biological activity. Benzylic substituents exert an inductive (electron-withdrawing) effect based on the electronegativity of the substituent. Such an effect influences the reactivity of the quinone. Wegner and co-workers (22) have shown that the greater the inductive effect of the benzylic substituent, the easier the quinone is to reduce. Once the quinone is reduced, the corresponding hydroquinone is harder to oxidize. If the biological activity of a bioactive quinone depends on the rate of regeneration of the quinone by *in vivo* oxidizing agents, a significant inductive effect will reduce activity. This is seen where the inductive effect of benzylic substituents (OBz > OH > H) inversely paralleled the cytotoxicity of the analogs (**8** < **2** < **1**). Further studies of hypericin analogs with benzylic substituents of lower electronegativity will be conducted to better understand this effect. Studies comparing hypericin analogs that differ in inductive effect may provide useful insight into the mechanism of hypericin cytotoxicity and will influence the design of “tethered molecules” composed of hypericin and bioactive molecules (19). A caveat in assessing these effects is to take into account the significance of the inductive effect on the absorption spectrum of the analogs: the seemingly innocuous presence of the –OH group in **2** diminishes the maximum extinction coefficient by nearly a factor of 5 with respect to that of hypericin. This effect is even more pronounced in analogs **7** and **8**, where it is reduced by nearly a factor of 100.

CONCLUSIONS

For eight compounds, we have measured their cytotoxicity under ambient light conditions, their capacity to associate with SW480 tumor cells, and their singlet oxygen yield. There is no clear correlation among these three parameters, indicating that other factors are likely to be important for biological activity. More work is required to better understand the relationships among the parameters tested here, as well as those of incident light intensity and of photophysical properties such as light-induced pK_a changes and redox chemistry. Other factors, such as interactions with specific subcellular organelles or cell signaling pathways, may also play a significant role in hypericin mediated cytotoxicity. The results presented here highlight the need for additional studies to elucidate the mechanisms of hypericin cytotoxicity.

ACKNOWLEDGMENTS--We thank Yvonne Wannemuehler and Pramit Chowdhury for valuable assistance on this project. This work supported by NIH grant R21 GM57351.

REFERENCES

1. Cohen, P. A., J. B. Hudson, and G. H. Towers (1996) Antiviral activities of anthraquinones, bianthrone and hypericin derivatives from lichens. *Experientia* **52**, 180-183.
2. Alecu, M., C. Ursaciuc, F. Halalau, G. Coman, W. Merlevede, E. Waelkens, and P. de Witte (1998) Photodynamic treatment of basal cell carcinoma and squamous cell carcinoma with hypericin. *Anticancer Res.* **18**, 4651-4.
3. Chung, P. S., C. K. Rhee, K. H. Kim, W. Paek, J. Chung, M. B. Paiva, A. A.

- Eshraghi, D. J. Castro, and R. E. Saxton (2000) Intratumoral hypericin and KTP laser therapy for transplanted squamous cell carcinoma. *Laryngoscope* **110**, 1312-1316.
4. Martens, A., A. De Moor, E. Waelkens, W. Merlevede, and P. de Witte (2000) In vitro and in vivo evaluation of hypericin for photodynamic therapy of equine sarcoids. *Vet. J.* **159**, 77-84.
 5. Vandebogaerde, A. L., E. M. Delaey, A. M. Vantieghem, B. E. Himpens, W. J. Merlevede, and P. A. de Witte (1998) Cytotoxicity and antiproliferative effect of hypericin and derivatives after photosensitization. *Photochem. Photobiol.* **67**, 119-125.
 6. Lavie, G., Y. Mazur, D. Lavie, and D. Meruelo (1995) The chemical and biological properties of hypericin--a compound with a broad spectrum of biological activities. *Med. Res. Rev.* **15**, 111-119.
 7. Johnson, S. A. S., A. E. Dalton, and R. S. Pardini (1998) Time-course of hypericin phototoxicity and effect on mitochondrial energies in EMT6 mouse mammary carcinoma cells. *Free Rad. Biol. Med.* **25**, 144-152.
 8. Vantieghem, A., Z. Assefa, P. Vandenaabeele, W. Declercq, S. Courtois, J. R. Vandenneede, W. Merlevede, P. de Witte, and P. Agostinis (1998) Hypericin-induced photosensitization of HeLa cells leads to apoptosis or necrosis. *FEBS Lett.* **440**, 19-24.
 9. Ryter, S. W. and R. M. Tyrrell (1998) Singlet molecular oxygen (O₂): A possible effector of eukaryotic gene expression. *Free Radic. Biol. Med.* **24**, 1520-1534.
 10. Sureau, F., P. Miskovsky, L. Chinsky, and P. Turpin (1996) Hypericin-induced cell photosensitization involves an intracellular pH decrease. *J. Am. Chem. Soc.* **118**,

- 9484-9487.
11. Chaloupka, R., F. Sureau, E. Kocisova, and J. W. Petrich (1998) Hypocrellin A photosensitization involves an intracellular pH decrease in 3T3 cells. *Photochem. Photobiol.* **68**, 44-50.
 12. Bork, P. M., S. Bacher, M. L. Schmitz, U. Kaspers, and M. Heinrich (1999) Hypericin as a non-antioxidant inhibitor of NF-kB. *Planta Medica* **65**, 297-300.
 13. Takahashi, I., S. Nakanishi, E. Kobayashi, H. Nakano, K. Suzuki, and T. Tamaoki (1989) Hypericin and pseudohypericin specifically inhibit protein kinase C: possible relation to their antiretroviral activity. *Biochem. Biophys. Res. Commun.* **165**, 1207-1212.
 14. Agostinis, P., Z. Assefa, A. Vantieghem, J. R. Vandenheede, W. Merlevede, and P. de Witte (2000) Apoptotic and anti-apoptotic signaling pathways induced by photodynamic therapy with hypericin. *Advan. Enzyme Regul.* **40**, 157-182.
 15. Assefa, Z., A. Vantieghem, W. Declercq, P. Vandenabeele, J. K. Vandenableele, W. Merlevede, P. de Witte, and P. Agostinis (1999) The activation of the c-Jun N-terminal kinase and p38 mitogen-activated protein kinase signaling pathways protects HeLa cells from apoptosis following photodynamic therapy with hypericin. *J. Biol. Chem.* **274**, 8788-8796.
 16. Lavie, G., F. Valentine, B. Levin, Y. Mazur, G. Gallo, D. Lavie, D. Weiner, and D. Meruelo (1989) Studies of the mechanisms of action of the antiretroviral agents hypericin and pseudohypericin. *Proc. Natl. Acad. Sci. USA* **86**, 5963-5967.
 17. Meruelo, D., G. Lavie, and D. Lavie (1988) Therapeutic agents with dramatic antiretroviral activity and little toxicity at effective doses: aromatic polycyclic diones

- hypericin and pseudohypericin. *Proc. Natl. Acad. Sci. USA* **85**, 5230-5234.
18. Kraus, G. A., W. Zhang, S. Carpenter, and Y. Wannemuehler (1995) The synthesis and biological evaluation of hypericin analogs. *Bioorg. Med. Chem. Lett.* **5**, 2633-2636.
 19. Kraus, G. A., W. Zhang, M. J. Fehr, J. W. Petrich, Y. Wannemuehler, and S. Carpenter (1996) Research at the interface between chemistry and virology: the development of a molecular flashlight. *Chem.Rev.* **96**, 523-535
 20. Redmond, R. W. and J. N. Gamlin (1999) A compilation of singlet oxygen yields from biologically relevant molecules. *Photochem. Photobio.* **70**, 391-475.
 21. Park, J., D. S. English, Y. Wannemuehler, S. Carpenter, and J. W. Petrich (1998) The role of oxygen in the antiviral activity of hypericin and hypocrellin. *Photochem. Photobiol.* **68**, 593-597.
 22. Wegner, G., T. F. Keyes, N. Nakabayashi, and H. G. Cassidy (1969) Inductive effects of substituents upon spectral and redox properties of p-benzoquinones. *J. Org. Chem.* **34**, 2822-6.

CHAPTER 8. CONCLUSIONS

The preceding chapters have shown the excited state photophysics of hypericin (chapter 3, 4, 5) and light induced biological activity of hypericin and its analogs (Chapter 6, 7). Femtosecond laser technology has provided the opportunity to investigate the rapid dynamics of these molecules. Our previous studies [1-6] suggested some evidence for the excited state H-atom transfer in hypericin. However, hypericin analog which has no labile protons does not show stimulated emission, which means no excited state H-atom transfer.

Chapter 3 gives more clear evidence for the excited state H-atom transfer.

Fluorescence upconversion measurements, which monitor only emission from the fluorescent singlet state, demonstrate that hexamethoxy hypericin, which possesses no labile protons, has an instantaneous rise time for its transient response. On the other hand, hypericin shows a clear 10-ps rise time. This confirms excited-state H-atom transfer as the primary photophysical process in hypericin. More direct demonstration of an excited state H-atom transfer can be done by observing the bleaching of the carbonyl or hydroxyl stretching frequency directly as a function of time following the laser excitation. A tunable infrared probe pulse with a visible or ultraviolet pump light source is required for this experiment.

Ab initio calculations [7] and NMR experiments [8] suggest only one hypericin species, the normal form, is populated in the ground state. Since the NMR time scale might be slower than interconverting ground species, work should be done with higher time resolution and a tunable excitation source to reveal ground state heterogeneity.

In Chapter 4, a femtosecond transient absorption spectroscopy technique is used to determine if excited state H-atom transfer is concerted. Previous studies using human serum albumin (HSA) and hypericin [9] suggested that excited state H-atom transfer is concerted, but the results from the hypericin in reverse micelles show no evidence for a concerted hydrogen atom transfer mechanism. We are, however, unable to conclude if only one hydrogen atom is transferred or if two are transferred in a stepwise fashion.

In Chapter 5, by means of time-resolved infrared spectroscopy, *ab initio* quantum mechanical calculations, and synthetic organic chemistry, a region in the infrared spectrum, between 1400 and 1500 cm^{-1} , of triplet hypericin has been found corresponding to translocation of the hydrogen atom between the enol and the keto oxygens, $\text{O}\cdots\text{H}\cdots\text{O}$. This result is discussed in the context of the photophysics of hypericin and of eventual measurements to observe directly the excited-state H-atom transfer.

In Chapter 6, light induced antiviral activity of hypericin and hypocrellin is compared in normoxic and hypoxic conditions. Although both molecules require oxygen to show full virucidal effects, hypericin is still effective at low oxygen level where hypocrellin is not. Since the singlet oxygen yield of hypericin is about half of that of hypocrellin, this result can not be explained by traditional Type II mechanism. We propose that the ejected proton upon illumination might enhance the activity of activated oxygen species.

In Chapter 7, a series of hypericin analogs were found to differ in their cytotoxic activity induced by ambient light levels. These analogs vary in their ability to partition into cells, to generate singlet oxygen as well as in other photophysical properties. The percent distribution of hypericin and its analogs in cells are measured using a steady state absorption

technique. We attempt to find a relationship between those results and the exact localization of the drug at subcellular level.

REFERENCES

1. Gai, F., M. J. Fehr and J. W. Petrich *J. Am. Chem. Soc.* **115**, 3384 (1993)
2. Gai, F., M. J. Fehr and J. W. Petrich *J. Phys. Chem.*, **98**, 8352 (1994)
3. Gai, F., M. J. Fehr and J. W. Petrich *J. Phys. Chem.* **98**, 5784 (1994)
4. Fehr, M. J., M. A McCloskey and J. W. Petrich. *J. Am. Chem. Soc.* **117**, 1833 (1995)
5. English, D. S., W Zhang, G. A. Kraus and J. W. Petrich *J. Am. Chem. Soc.* **119**, 2980 (1997)
6. English, D. S.; K. Das, J. M. Zenner, W. Zhang, G. A. Kraus, R. C Larock and J. W. Petrich *J. Phys. Chem. A*, **101**, 3235 (1997)
7. Petrich, J. W., M. S. Gordon, M. Cagle *J. Phys. Chem. A*, **102**, 1647 (1998)
8. Smirnov, A. V., D. B. Fulton, A. Andreotti and J. W. Petrich *J. Am. Chem. Soc.* **121**, 7979 (1999)
9. Das, K., A. V. Smirnov, J. Wen, P. Miskovsky, and J. W. Petrich *Photochem. Photobiol.*, **69**, 633.(1999)